Assessment of Effectiveness and Design Procedure of Gravel Drains as Liquefaction Countermeasure

A Dissertation submitted

to

The Graduate School of Science and Engineering

EHIME UNIVERSITY

In partial fulfilment

of the requirements for the degree of

Doctor of Engineering

Advisor: Professor Mitsu Okamura

By

Utari Sriwijaya Minaka

December 2020

Certificate

This is to certify that the dissertation entitled, “Assessment of Effectiveness and Design Procedure of Gravel Drains as Liquefaction Countermeasure” presented by Utari Sriwijaya Minaka in partial fulfillment of the academic requirement of the Doctor of Engineering has been examined and accepted by the evaluation committee at Graduate School of Science and Engineering of Ehime University.

…….

Mitsu Okamura

Professor of Civil and Environmental Engineering

Thesis Advisor / Examiner 1

…….

Hideaki Yasuhara

Professor of Civil and Environmental Engineering

Examiner 2

…….

Netra Prakash Bhandary

Professor of Civil and Environmental Engineering

Examiner 3

Acknowledgement

This dissertation was completed with support and advice from individuals and groups who proved help and their valuable assistance during the study. This acknowledgement is my deepest sincere to thank for those whom I do really want to express for their collaboration.

I want to thank God, Allah SWT for giving me the strength to stay all the way to the end, and for sending all these wonderful and helping people to guide me during this unforgettable experience.

First and foremost, I would like to express my deepest gratitude to my supervisor Professor Mitsu Okamura, for his teachings, guidance, and encouragement during all these years. His supervision and discussion brought me to have new insights and ideas in the field of not only geotechnical engineering particularly soil improvement but science in general as well. His overly enthusiasm and integral view on research, his emphasis on dedication and high quality of work has made a deep impression on my development as a researcher. His expert supervision encouraged me to keep enthusiasm on innovation and helped me to overcome my weakness on writing. I will always be grateful for all your help.

Special thanks to my dissertation committee, Professor Hideaki Yasuhara and Assoc. Professor Netra Prakash Bhandary for their guidance and helpful suggestions. Their comment has served me well and I owe them my heartfelt appreciation. Also, I am thankful to Dr. Kohei Ono for his willingness to always help with nice discussion and to all valuable guidance throughout my studies so I can complete my dissertation.

Thanks also go to Mrs. Naoko Jinnouchi for every kind supports in administrative processes of the Faculty of Engineering Ehime University. I would like to thank Mr. Ryoichi Tamaoka

for his help during the experiments. I am thankful to all my seniors and friends for their supports and togetherness in joy and in sorrow during the years in Ehime University.

I would also like to thank all the colleagues of the Geotechnical Engineering Laboratory for their help and friendship, especially to Asri Nurani Sjafruddin, Imamura Mamoru, Inoue Tadahiro, and Inaba Yuji for all of good memories, thank you.

My gratefully acknowledge should sent to my Mom, Yetti Fendri, for the unconditional support, whose love, patience, encouragement, and prayer has kept me strong and inspired. To Meri Wardana, thank you for your encouragement and sincere support.

Finally, I would like to thanks to my wonderful family; for always being there for me, for being so patience and supportive and for all their help and love. This dissertation is the outcome of their sacrifice and their kind of support in many ways.

Abstract

Vertical drains have been extensively used as a liquefaction countermeasure and seismic case histories have shown the effectiveness of this technique. However, it has often been observed that excessive settlement and deformation of ground occurred despite the fact that dissipation of excess pore water pressure is expedited by this technique. The current design practice of gravel drains as a liquefaction countermeasure involves selection of drain spacing and diameter to keep the peak excess pore water pressure ratio low, which was verified mostly with small scale 1g shaking tests; its validity for field scale prototype is yet to be well investigated.

In this study, a series of centrifuge tests was conducted to gain insight into the stress-dependent behavior of loose sand deposits with the level surface improved by gravel drains. Effects of permeability, drain diameter/spacing ratio, and groundwater level on the pore water pressure response of soil were systematically investigated. The experimental data were then used to validate current design procedure which was originally proposed by Seed and Booker (1977).

One of the important features of strength properties of soils involved in the design of gravel drains was examined by using triaxial cyclic test. The influence of excess pore water pressure and confining pressure on the volumetric strain characteristics of the soil under cyclic loading were investigated. It was found through laboratory tests that the coefficient of volumetric compressibility, m_v, is highly dependent of the stress level, while m_v is assumed to be fixed in the design procedure. Settlement occurrence on the sand surface was measured in several locations, and the data used to examine the liquefaction depth.

The results revealed that the effects of gravel drains to suppress the excess pore pressures depend significantly on depth. The discrepancy of excess pore pressure prediction and the centrifuge test results indicated that the current design procedure failed to elucidate the depth-dependent behavior of the sands. It was also revealed that water flow regime in the gravel drains can be a turbulent flow. The Reynolds number in drains increases from bottom to top, and the permeability coefficient decreased accordingly, resulting in more significant well resistance than expectation based on the current design procedure. When the stress level-dependent m_v and Reynolds number-dependent k_w were used as input soil parameters, the axisymmetric diffusion equation with consideration of well resistance satisfactorily predicted the excess pore pressures in sand with gravel drains. Settlement of ground surface was found increased with the depth of liquefied layer.

Table of Content

List of Figures

List of Tables

Chapter 1

Introduction

1.1 Background

Soil liquefaction is a phenomenon that soil losses its stiffness and strength due to the earthquake shaking. Damage of soil and infrastructure system often induced by liquefaction occurrence such as sink of overlying ground that can caused tilting of the building, lateral spreading, sand boiling, and floating of underground structures. Liquefaction phenomena usually occurs on loose saturated sand during earthquake, due to large excess pore water pressure generation when it unable to drain corresponding to reduction of initial effective stress of the soil (Seed & Idriss, 1982).

Liquefaction studies initiated for the first time after Niigata Earthquake in 1964 and Great Alaska Earthquake in 1964. Several methods have been developed since then for liquefaction mitigation, including the technique to reinforce the soil and the drainage works to dissipate the excess pore water pressure. Vertical drains including gravel drains and stone columns were introduced in the 1970s and have been extensively used since then as a liquefaction remedial measure. Vertical drains installed in a liquefaction prone soil at a small interval provide short drainage paths, typically of the order of a few meters, and higher hydraulic gradient and associated water flow toward the drains are expected when excess pore pressure is generated in the soil during earthquakes. Time for the diffusion process of the excess pore pressure is dramatically reduced and accumulating pore pressures dissipates ideally before

the soil reaches a state of the initial liquefaction. Current design practice involves selecting drain spacing (b) and drain diameter (d_w) that will keep the peak excess pore water pressure ratio below a specified threshold level for a design earthquake. The threshold level of 0.5 – 0.6 originally proposed by Seed and Booker is common in the U.S. (Adalier and Elgamal, 2004), whereas 0.25 – 0.5 is used in Japan (JGS, 1998).

The design of vertical drain in the current practice uses the procedure originally developed by Seed and Booker (1977). They showed that excess pore pressure in sand around a drain can be analyzed with the axisymmetric diffusion equation incorporated with generation of the excess pore pressures owing to earthquake shaking, as indicated in Eq. (1.1),

$$\frac{\partial \Delta u}{\partial t} = \frac{\partial \Delta u_g}{\partial t} + \frac{k}{m_v \gamma_w}\left(\frac{\partial^2 \Delta u}{\partial r^2} + \frac{1}{r}\frac{\partial \Delta u}{\partial r} + \frac{\partial^2 \Delta u}{\partial z^2}\right) \qquad (1.1)$$

where $\partial \Delta u_g / \partial t$ stands for generation rate of the excess pore pressure due to the earthquake cyclic shearing in undrained condition, determined by a cyclic shear stress time history induced by the design earthquake and the liquefaction resistance of the sand. The second term in the right-hand-side of the equation expresses the dissipation of the excess pore pressure in radial direction, r, as well as vertical direction, z, with two dominant soil parameters of the coefficient of permeability, k, and the coefficient of volumetric compressibility, m_v. The latter coefficient is defined as $m_v = \varepsilon_v / \Delta u$ where Δu is the excess pore pressure and ε_v is volumetric strain produced by dissipation of Δu. Hence, m_v exhibits dependency on the stress level (Lee and Albaisa, 1974; Malvick et al., 2008).

The equation is commonly solved in a finite difference scheme with a boundary condition at the interface between the soil and the drain. Seed and Booker (1977) assumed that excess pore pressure in the drains could be negligible and suggested to set $\Delta u = 0$ at the boundary

when the permeability of drains (k_w) is on the order of 200 times or higher than that of soil (k_s). Thereafter, this infinite permeability assumption was subjected to modification. Onoue (1988) claimed importance of the capacity of drain to flow water squeezed out from the surrounding soil. He showed that the infinite permeable drain is not appropriate assumption even for the case of a k_w/k_s ratio larger than 200 and developed diagrams to determine the drain spacing with the well resistance taking into account.

Regarding estimates of soil parameters, Seed and Booker (1977) suggested to use a constant value of m_v irrespective of the excess pore pressure ratios and confining pressures, since the most influential soil parameter in the diffusion process was k_s, which potentially varies in much wider range of values than m_v. This assumption that m_v is a stress independent parameter have been handed over to design procedures in the current practice (JGS, 2004). However, variation of m_v can be more than several times depending on the confining stress level, it may not be reasonable to regard m_v as a constant value irrespective of stress level or depth.

Attempts were made to verify the design procedures using experimental results of tests including relatively large 1g shaking table tests (Sasaki and Taniguchi, 1982; Iai et al., 1988), in-situ tests (Onoue et al, 1987) and small scale 1g tests (Tanaka, 1987). However, many of their results were somewhat ambiguous since the stress level in small 1g models was low. More recently, centrifuge tests have been carried out, which have an incontrovertible advantage to study behavior of foundation soils of which mechanical properties are stress level dependent. Considerable research efforts have been devoted to study the effectiveness of vertical drains to remediate particular soil/structure configurations, including oil tanks (Kimura et al., 1996), gentle slopes (Howell et al., 2012), shallow foundations (Garcia-Torres and Madabhushi, 2018) and embankments (Tomizawa et al., 2018; Kajitori et al.,

2020). Most of them focused on the reduction in deformation rather than pore pressure dissipation effects to prevent triggering the liquefaction. All of these experimental researches using centrifuge modeling showed effectiveness of vertical drains, however, limited attempt has been made to clarify the validity of conventional design procedures that have been being used in practice (Brennan and Madabhushi, 2002, 2006).

In Japan, gravel drains and stone columns had been extensively used as a liquefaction countermeasure technique by 1990s (JGS, 1988), however, they lost the position of a major countermeasure technique after the 1995 Kobe earthquake (JGS, 2004; Rasouli et al., 2016). Rasouli et al. (2016) pointed out two possible reasons for this: one is that arisen from the design procedure in the current practice. After the Kobe earthquake stronger design earthquakes (Level 2 earthquakes) are commonly invoked in Japan and the spacing ration (d_w/b) determined from the design procedures tends to be very small, which results in degradation of their cost competitiveness and thus practicality. On this issue, there are case histories which challenge the appropriateness of the design. There are sites where liquefaction countermeasure with gravel drains had been implemented, hit by an earthquake of ground motions stronger than the design earthquake, but did not cause soil liquefaction (Yasuda et al, 1996; Unno et al., 2014). These facts show clear needs of further research for better understanding the behavior of drains and surrounding soils. The other reason in disfavor of the technique is relatively large subsidence that occurs in the area remediated with vertical drains.

This dissertation is an attempt to explain the effects of soil permeability, drain diameter, and coefficient of volume compressibility of the soil to the effectiveness of gravel drain as liquefaction countermeasures through a series of triaxial testing and centrifuge testing. It is

also the interest of this study to provide a broader of understanding of the settlement behavior on the soil improved with gravel drain.

1.2 Objective of the study

The main objective of this dissertation is divided into two, to examine the behavior of loose sand deposits remediated with gravel drain from the aspects of soil permeability, drain diameter, and stress dependency; along with the settlement behavior.

In term of pore pressure behavior, the objectives are:

1. To examine the pore pressure behavior of loose sand deposits improved with gravel drains using full-scale experiment through a series of centrifuge tests.
2. To investigate the mechanical properties of the soil that controlling the pore pressure behavior, coefficient of volume compressibility (m_v) and permeability coefficient (k) through a series of triaxial cyclic test and laboratory tests, respectively.
3. To validate the current design procedures of gravel drain using full-scale experimental data.

For the settlement examination, the objectives are:

1. To investigate the settlement occurrence of the remediated ground based on centrifuge test results.
2. To predict the settlement potential due to the ground shaking through a series of drained triaxial cyclic testing.

1.3 Dissertation organization

This dissertation consists of seven chapters. Chapter 1 give a brief description of the research background, objectives of the research, and organization of this dissertation. In chapter 2 of this research presents introduction of liquefaction phenomenon, factors affecting

liquefaction susceptibility, which depicted the causes and the results of liquefaction hazard. An overview of literature regarding liquefaction remediation techniques is also presented. A brief review on the mechanism of liquefaction prevention using the dissipation of excess pore water pressure method, ground improvement as a remedial measure against soil liquefaction on sandy soils, and the current state of knowledge on how the dissipation of pore water pressure method is valuable against liquefaction. The previous study on the vertical drain as one of the ground improvement methods were discussed in order to understand the development of this method to prevent liquefaction. Several factors affecting the performance of the vertical drain literature were also presented to understand in which aspects the further research is needed.

Chapter 3 explains the permeability characteristics of the sand and gravel through a series of laboratory test considering vertical and horizontal permeability for the sand and flow in the pipe aspects for the gravel permeability, respectively. It discusses the details of the laboratory testing performed to obtain the permeability characteristic of sand material when the deposition arrangement is considered as an important factor. Further, this chapter explains the permeability test conducted to achieve the appropriate conditions that resemble the behavior of flow in the specific vertical drain shape for the gravel material. Finally, the results of each material permeability coefficient are presented.

Chapter 4 describes the characteristics of volume compressibility of the sand investigated through cyclic triaxial test. As mentioned in chapter 2, there are factors that affect the performance of vertical drains against liquefaction, one of these factors is the volume compressibility of the soil. In this chapter, the details of the laboratory testing using triaxial cyclic to obtain the coefficient of soil volume compressibility and the results are presented.

Chapter 5 presents the analysis of the centrifuge test results. A series of centrifuge test on soil deposits without drain and improved with gravel drain were performed. The tests were conducted with variation of soil permeability, drain diameter, and lowering groundwater level and the results are obtained. Pore pressure behavior of each test is analyzed. Numerical simulations were performed based on the current design procedure of gravel drain. The mechanical properties of the soils used in the tests were examined and used in the numerical simulations to predict the excess pore pressure. Finally, the experimental data were used to validate the current design procedure.

Chapter 6 presents the settlement behavior of the ground improved with gravel drain observed on centrifuge test results and predictions of ground subsidence through a series of triaxial test. Finally, the conclusions of this study are described in the Chapter 7.

Chapter 2

Literature Review

2.1 Introduction

The literature review of the topics regarding this dissertation is presented in this chapter. The fundamental focus is concerning to the development of the gravel drain study as liquefaction remediation. Literature review will consist of liquefaction assessments, liquefaction countermeasures techniques, and volumetric strain characteristics under cyclic loading.

Liquefaction phenomena have become an interest for researcher since 1964 after the Alaska earthquake ($M_w = 9.2$) and Niigata earthquake in Japan ($M_s = 7.5$). These earthquakes have caused major damage due to soil liquefaction such as buildings settlement and tilted, large ground lateral spreading, and infrastructures damage. Research on liquefaction mechanism, predictions, and countermeasures commenced since then.

The liquefaction term has been defined as the condition when saturated sandy soil lose the strength during an earthquake, effective stress of the soil is decreased as the result of increased pore water pressure and lead to deformation of the ground (Kramer, 1996; Seed and Idriss, 1971). In general, based on Kramer (1996), liquefaction phenomenon can be divided into two types depend on the occurrence, flow liquefaction and cyclic mobility. Flow liquefaction occurred in loose sand as the results of contractive response under cyclic loading. Cyclic mobility can occur on dense sand which more likely have dilative response due to cyclic shearing. During cyclic loading, cyclic mobility occurred when shear resistance starts

to pick up at some strains in every cycle due to the positive dilatancy of soil skeleton. Both of these failure mechanisms may occur simultaneously in the soil under one occurrence of earthquake loading.

2.2 Undrained behavior of saturated sand

The behavior of the sand in undrained condition can be divided towards its response under monotonic loading and cyclic loading. The stress-strain response of sand to monotonic or cyclic loading is dependent on several factors, such as relative density of the sand, confining stress, stress history, and sand deposition mode (Seed and Idriss, 1982). Study on soil response to monotonic loading revealed that loose sand most likely to reduce its volume, dense sand tends to increase in volume (dilates) and finally reach the critical state condition (Casagrande, (1975), Castro et al., (1983)). Critical state condition is the state when the sand continuing under shearing until no further change in volume or stress is occurring.

Figure 2.1 illustrates the stress path of saturated sand in undrained and drained condition under monotonic loading. As previously mentioned, the response of sand under monotonic loading is vary depend on relative density. There is loose of critical state when the effective stress of the soil tends to decrease due to the tendency of contraction, and dense of critical when the effective stress of the sand increases due to dilation accordingly. Typical responses of the soils due to shearing force are also presented in Figure 2.2. Shear strain is gradually increasing along with the increase of shear stress for loose sands, meanwhile, for dense sand, shear stress is significantly increase while strain increase accordingly. Then, when shear stress reaches the peak value, its gradually decrease as shear strain increase until reach the constant value (Figure 2.2 (a)). Compression and expansion phase shown in Figure 2.2 (b), loose sands tend to compressed and void ratio is decreasing as a result of densification.

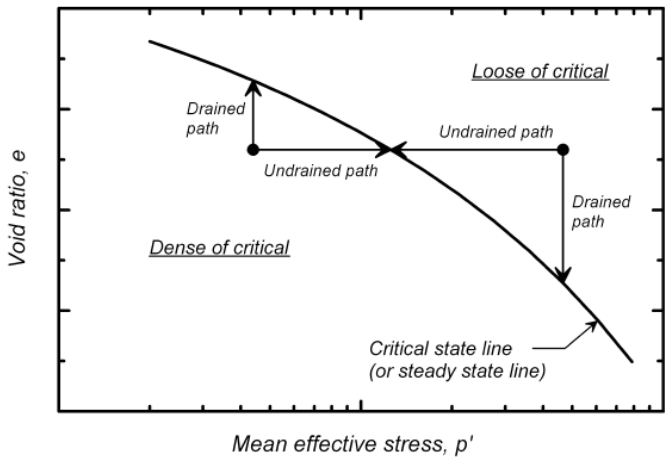

Figure 2.1 The stress path of saturated sand in undrained and drained condition under monotonic loading (Seed and Idriss, 1982)

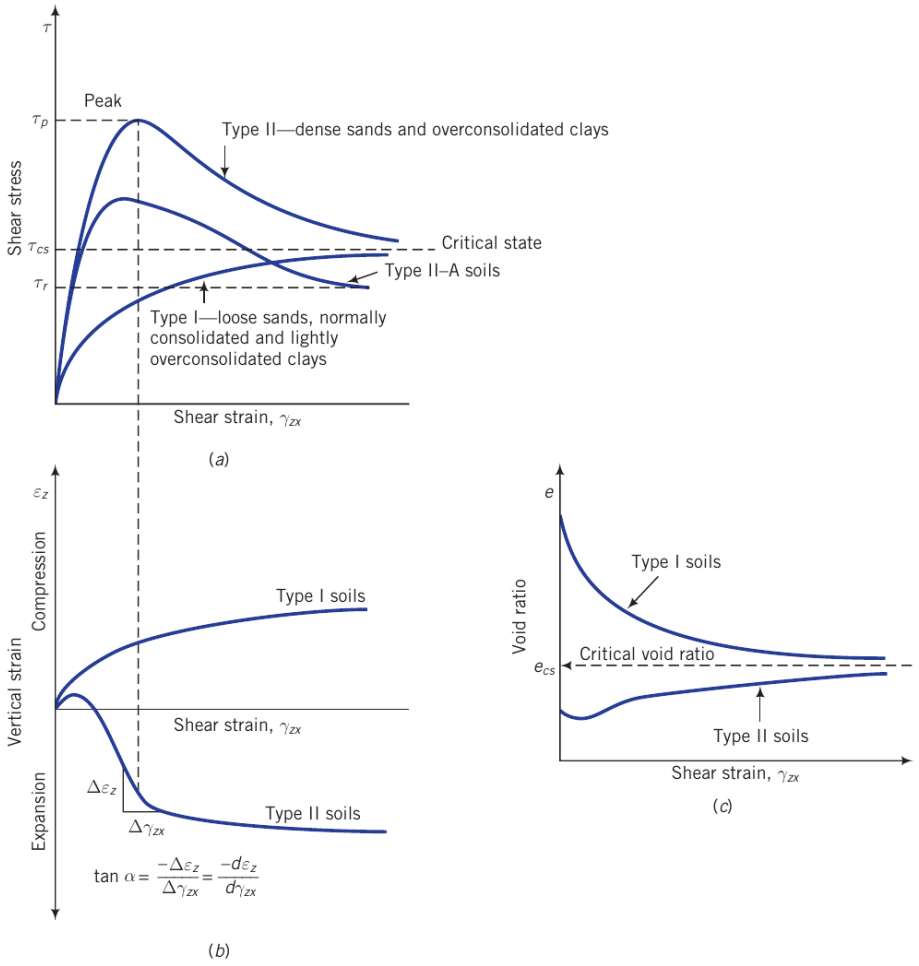

Figure 2.2 Responses of soil to shearing: (a) Stress-strain relationship; (b) vertical strain and shear strain relationship; (c) change in void ratio versus shear strain (Budhu, 2015)

In contrary, dense sand is compressed in the beginning, then significantly expand until reach the peak of shear stress and continuously expand. In this condition, the void ratio behavior is showing the similar pattern with the void ratio of soil in compression-expansion state. The critical state is reached when no volume change occurs during the loading.

In undrained condition under cyclic loading, the sand skeleton tend to contract leading to rearrangement of soil grain and build up the pore pressure. Schematic process of cyclic loading in the sand is shown in Figure 2.3. During drained condition, if the cyclic loading applied to the sand, plastic volumetric contraction will occur in the soil skeleton (from point A to point B). In undrained condition, the effective stress of the soil will reduce since the volume change is not allowed (B to C).

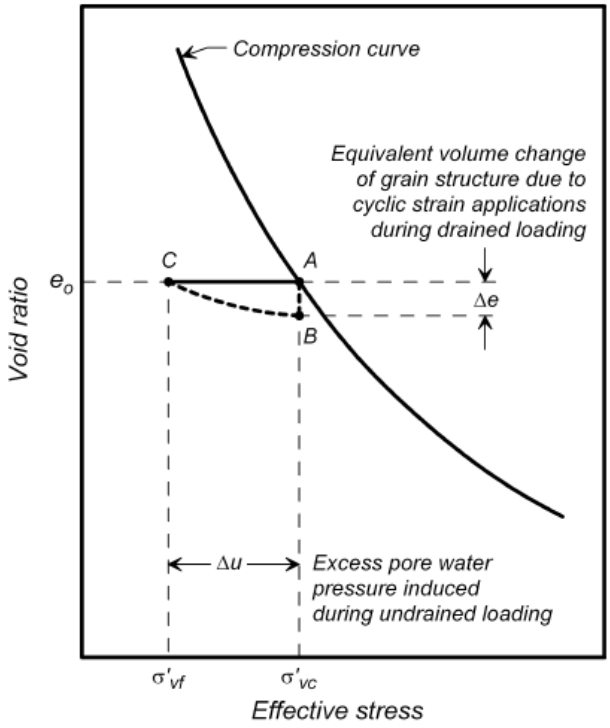

Figure 2.3 Pore pressure mechanism in the soil during cyclic loading (Seed and Idriss, 1982)

If the cyclic loading keeps applying to the sand, the effective stress of the soil will completely reduce to zero due to the pore water pressure increment. The typical of sand response under cyclic loading in undrained condition is also presented in Figure 2.4. It shows the results of triaxial cyclic test of Sacramento river sand (Boulanger and Truman, 1996). Figure 2.4 contains the relationship between number of sinusoidal stress loading with excess pore pressure ratio (r_u) and axial strain (ε_a), and the stress path of the soils. Excess pore water pressure (Δu) generated during the cyclic loading is normalized with the effective consolidation stress (σ'_c) and called excess pore pressure ratio. In the standard of triaxial cyclic test, the confining pressure keeps constant during the test so the maximum value of pore water pressure is 100% which occurs when $\Delta u = \sigma'_c$. The pore pressure keeps

increasing during the cyclic loading and the condition when r_u equal to 1.0 is called the initial liquefaction.

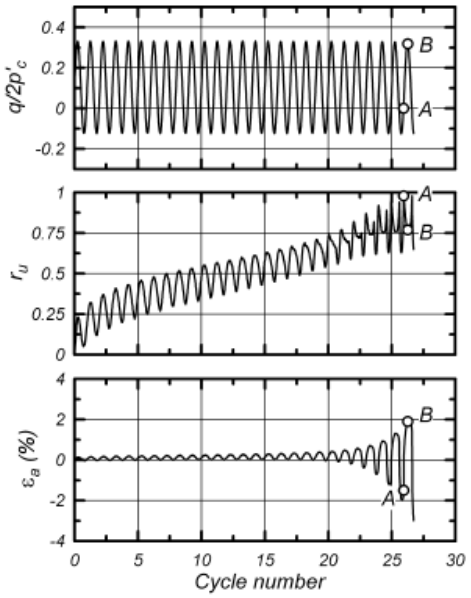

Figure 2.4 Typical results of triaxial cyclic test of sand in undrained condition (Boulanger and Truman, 1996)

Axial strains remained small until the effective stress of the soil approached zero and excess pore pressure ratio approach 100%, and the increment of the axial strains is in the order of 2% after two additional cycles of loading. Point A in the specimen corresponds to the time when excess pore pressure ratio is reached 100% and the load is in zero position, which means the specimens stiffness is very small, the axial strain is follow accordingly. When the applied loading is increase to point B, the stiffness of the specimen is also increase. This is can be seen from the response of excess pore pressure ratio, it is decreasing meanwhile soil is gaining the effective stress. The axial strain is in the largest position the same direction of the loading (positive direction). The soil is gaining strength and stable under the peak of applied shear stress, and reflect the condition dense of critical. The accumulations of strain

after the soil actually reach 100% of pore pressure ratio is called cyclic mobility behavior (Casagrande, 1975).

2.3 Liquefaction effects in the soil

Liquefaction occurs due to sand is distinct material whose behaviour is ruled by the principle effective stress and by dilatancy (Japanese Geotechnical Society, 1998). Loose saturated sand deposits tend to contract under undrained condition due to cyclic loads resulted from that earthquake. Since reduce in volume of sand is not allowed during undrained condition, pore water pressure (u) will increase and the effective stress (σ') will decrease as long as the total stress (σ) is constant during the loading. Based on the effective stress principles, at a certain depth of soil deposit, can be written as:

$$\sigma' = \sigma - u \qquad 2.1$$

When increase in excess pore water pressure is exceedingly large due to the intensity of the cyclic loading, it can approach the initial confining pressure (total stress) of the soil resulting in zero effective stress. This state is referred as the initial liquefaction condition. Decreasing in effective stress of the soils associated with loss of strength and stiffness of soils that contributes to the deformation. For example, after Niigata earthquake in 1964, the liquefied sand caused tilting and bearing failure of buildings (Figure 2.5 (a)). Large deformation of the road due to earthquake-induced liquefaction was found in Christchurch after the earthquake hit in 2011.

(a) (b)

Figure 2.5 (a) Tilting of buildings due to Niigata Earthquake (1964), (b) Extensive damage of the road in Christchurch caused by earthquake (2011)

2.4 Laboratory experiment for simulating liquefaction

Laboratory testing to simulate the liquefaction condition proposed first by Ishihara et al., (1975) using a hollow cylindrical torsional shear device that could reproduced the real field stress condition of the soil. Since the stress state between the real field condition and the specimen in the laboratory test is different, Ishihara et al., (1975) found that the test conducted in the laboratory need to adjust to the ground condition by using the coefficient of lateral earth pressure at rest (k_0). To approximate the real field condition, the cyclic triaxial test has been conducted as shown in Figure 2.6. In the beginning, the confining pressure, σ_0 was applied to the specimen followed by deviatoric stress, σ_d in vertical direction. An assumption has been made that duration of earthquake in the real field is very short, there is no time for pore water pressure to dissipate. The soil will behave like in the undrained condition. Shear stress and normal stress generates in the specimen due to the deviatoric stress applied. The stress acting on the 45° plane in the specimen as $\sigma_d/2$. Normal stress acting on the specimen is compressive component which can be ignored due to it diffused to

the pore water pressure and did not make any change in the effective confining stress (Ishihara, 1996).

Initial liquefaction is reached when the pore water pressure keep increases during applying the deviatoric stress and equal to the initial confining pressure as well as the axial strain is around 5% in double amplitude. Many researchers used this threshold to identify initial liquefaction state (Ishihara, 1996; Okamura and Soga, 2006; Okamura and Noguchi, 2009)

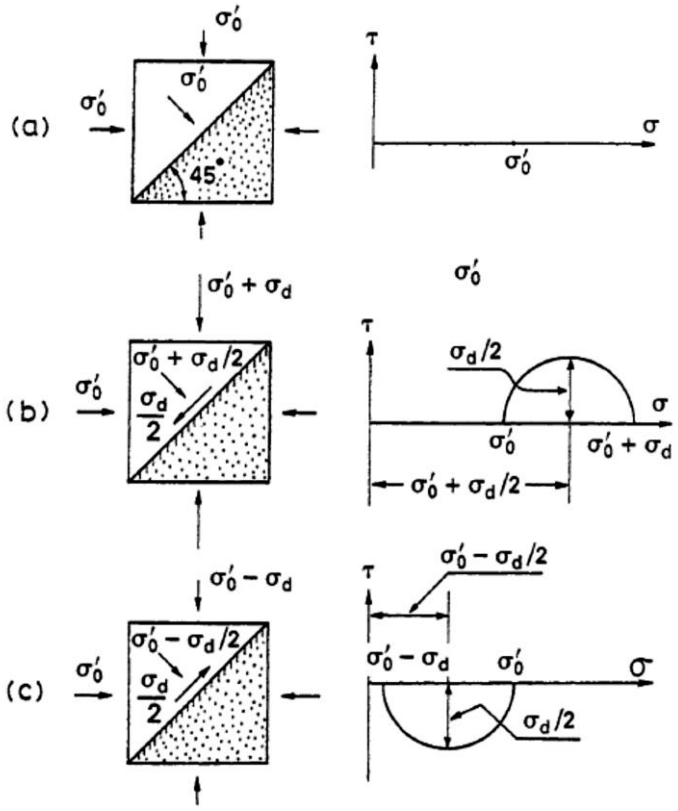

Figure 2.6 Schematic figure of stress condition in the specimen of triaxial cyclic test (Ishihara, 1996)

2.5 Liquefaction remediation techniques

Various soil improvement methods such as densification, reinforcement, solidification, lowering ground water table, dissipation of excess pore pressure, and shear strain restrain

methods are commonly used as liquefaction remediation (Adalier and Elgamal, 2004; Baez and Martin, 1995; Japanese Geotechnical Society, 1998; Mitchell, 2008). These techniques can mitigate the risk of liquefaction through several mechanisms, including increasing the soil density, increasing lateral effective confining pressure of the soil, and providing drainage which reducing the excess pore water pressure generation to avoid liquefaction.

2.5.1 Vertical drain as liquefaction countermeasure

Vertical drains have been extensively used as a liquefaction countermeasure and seismic case histories showed the effectiveness of the technique. The design chart originally produced by Seed and Booker (1977) is commonly employed in the design practice to determine a spacing of drain to keep the seismically induced excess pore pressure below a certain level. Excess pore water pressure is expected to dissipate and keep low by the technique.

Gravel drains and stone columns were used first from 1970s, and more recently drains of artificial materials such as prefabricated vertical drains have been introduced. However, in recent years in particular after 1995 Kobe earthquake in Japan, vertical drains have become obsolete while such other techniques as the soil densification and the solidification have been preferably used (Towhata, 2008; JGS, 2004). One of the major reasons for this is that the currently used design procedure often provides an unrealistically small spacing between drains for stronger design earthquake motions which have been introduced after the Kobe earthquake. Another reason is a concern for excessive settlement that might occur due to dissipation of excess pore pressure generated during earthquakes through vertical drains. In fact, it was reported that excessive settlement and deformation of ground occurred although vertical drains were implemented and worked well (Unno et al., 2014; Yasuda et al., 1996).

Drainage installation to prevent liquefaction is shown in the Figure 2.7. Drainage supposed to increase the dissipation rate of pore water pressure generation and maintain the excess pore pressure in the lower levels throughout the shaking event.

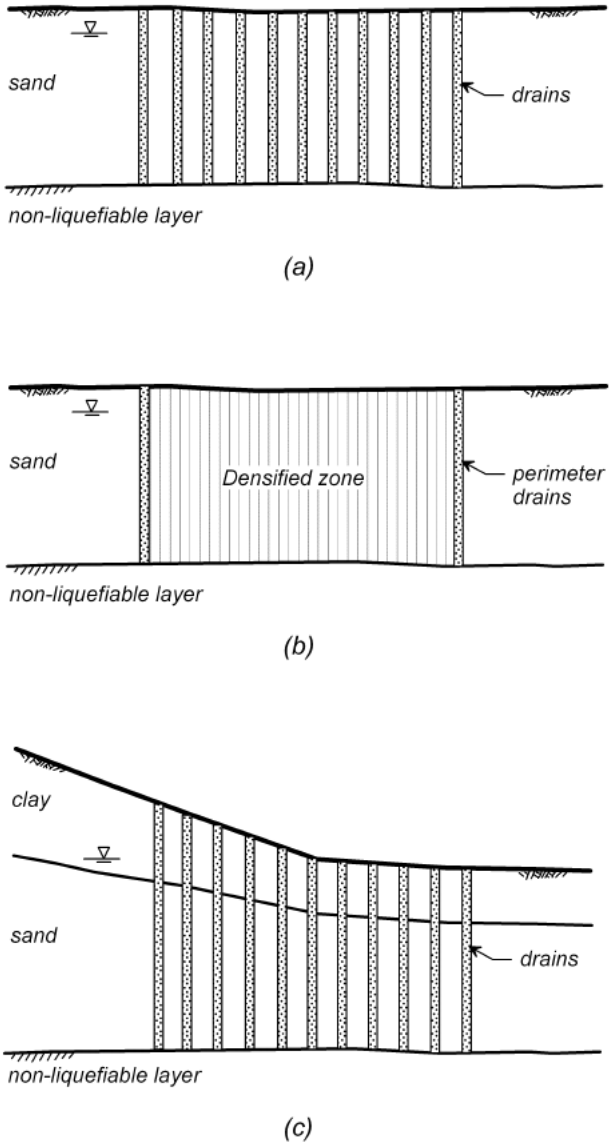

Figure 2.7 Gravel drain installation for liquefaction mitigation

Figure 2.7 (a) illustrates the gravel drain installed in a grid pattern which means to changes the dissipation pattern from vertical to horizontal and reducing the time to dissipate. The

other technique is combining the densification and gravel drain installation as perimeter drain (Figure 2.7 (b)). The drainage means to accommodate the pore pressure from untreated liquefied zones into a treated zone when the pore pressure already in a lower level. The migration of pore pressure into a treated zone reduce the ground or foundation settlement. Figure 2.7 (c) shows the installation of the drain to prevent void redistribution or water film generation beneath a lower permeability soil layer. In this case, the seepage which flow toward surface can be trapped below the impermeable layer and have a risk of very high pore water pressure at the soil interface. The drainage prevents the water film that might develop under the impermeable layer.

2.5.2 Vertical drain design procedure

Seed and Booker (1977) were originally proposed a design procedure of the gravel drain by assuming an infinitely permeable column as a drain material. Basic equation of the design procedure based on the flow of pore water governed by Darcy's Law as follows:

$$\frac{\partial}{\partial x}\left(\frac{k_h}{\gamma_w}\frac{\partial u}{\partial x}\right)+\frac{\partial}{\partial y}\left(\frac{k_h}{\gamma_w}\frac{\partial u}{\partial y}\right)+\frac{\partial}{\partial z}\left(\frac{k_v}{\gamma_w}\frac{\partial u}{\partial z}\right)=\frac{\partial \varepsilon}{\partial t} \tag{2.2}$$

where u is the excess pore water pressure, k_h and k_v is the coefficient of permeability in vertical and horizontal direction, respectively, γ_w is the unit weight of water, ε and is the volumetric change (positive). During the interval time dt, pore water pressure will change, and due to the element subjected to a shear stress that caused additional increase in pore pressure, considering the volume change of the soil, the design procedure to predict the pore pressure is concluded in Equation 1.1.

Seed and Booker (1977) assumed that the dissipation of excess pore pressures is based on purely axisymmetric flow towards the drain, the drainage did not increase the overall

stiffness of the improved soil and has infinite permeability, and the rate of excess pore pressure build up is fitted to the data from large number of element test. Further, there are several factors that affecting the performance of the drainage studied by Onoue (1988); Iai and Koizumi (1986); Pestana et al (2000). They concluded that the effectiveness of drains under shaking events decreases with decreasing soil permeability, increasing soil compressibility, longer drainage length, and longer earthquake shaking. Onoue (1988) worked shows that the drainage resistance has the effect of reducing its capacity to dissipate the pore water pressure especially if the permeability of the drainage is not significantly larger than the soil permeability.

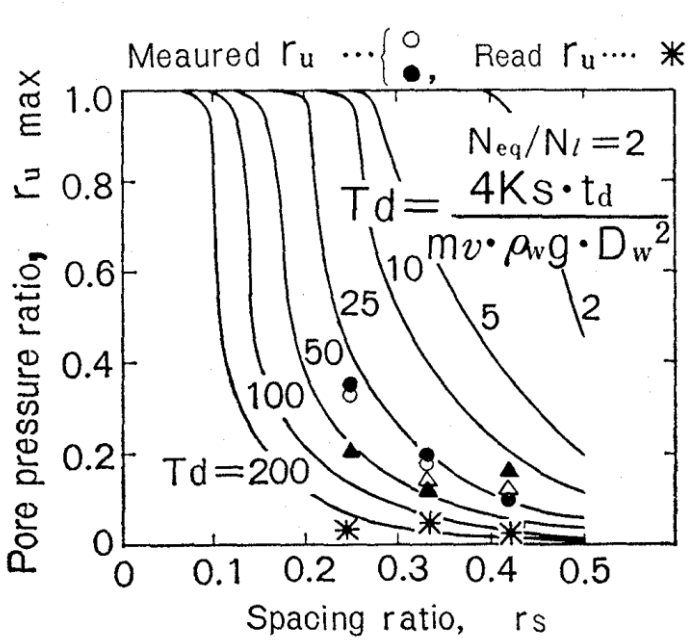

Figure 2.8 Diagram of excess pore pressure ratio design value based on spacing ratio (Onoue et al., 1987)

Seed and Booker design chart has been analyzed by Onoue et al (1987) and compared the results of the design pore pressure ratio in the design chart with measured in-situ data of soil layer improved with gravel drain. The comparison reading value and measured value of

excess pore pressure ration is shown in Figure 2.8. Read value of Seed and Booker (1977) design chart (mark by asterisk) obtained from the curve based on the spacing ratio, then compared with the experimental results obtained by Onoue et al (1987) in a similar spacing ratio. The results showed that excess pore pressure ratio (r_u) read from the chart is considerably smaller than the measured value. It has to be noted that Seed and Booker chart disregarded the well resistance coefficient. Onoue (1988) suggested the improved design chart for gravel drain design procedure by considering well resistance as shown in Figure 2.9.

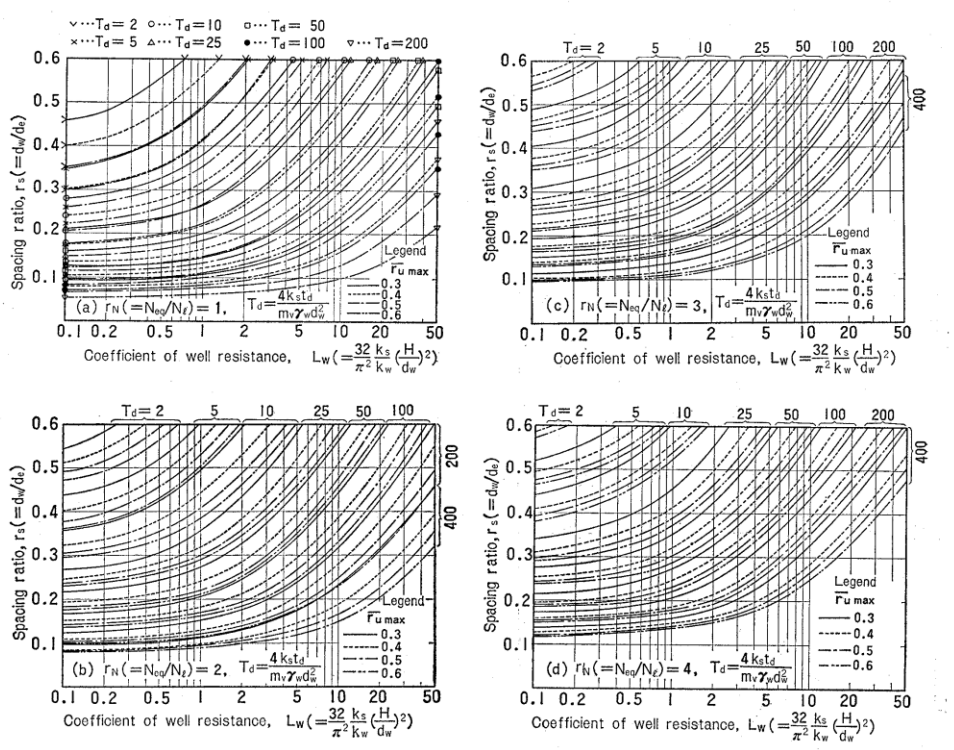

Figure 2.9 Relationship between spacing ratio and well resistance coefficient based on Onoue (1988)

The new design chart by Onoue (1988) provided the coefficient of well resistance relationship with spacing ratio. Design spacing ratio can be obtained through the chart, first

determined the coefficient of well resistance based on the permeability of the soil and gravel, then choosing the earthquake intensity in relation to the liquefaction characteristics of the sand, and determined the design pore pressure ratio.

2.6 Volumetric strain characteristics of the soil under cyclic loading

As mentioned earlier, there are several factors affecting the effectiveness of drain performance. Seed and Booker (1977) mentioned that in the design procedure, value of coefficient of soil volume compressibility can be assumed constant as the excess pore pressure ratio is keep reasonably low. However, in fact, the value is not constant but varies with the pore pressure ratio. Lee and Albaisa (1974) described that the coefficient of soil volume compressibility can be obtained through a triaxial cyclic test (compression). The coefficient of soil volume compressibility, m_v should be estimated on the basis of cyclic triaxial liquefaction tests where the excess pore pressure ($\Delta u_{\max}$) is generated under undrained condition until reached an aimed value, and allow the pore pressure to dissipate while measuring the resulting volumetric strain, $\Delta\varepsilon$ (Bouckovalas et al. 2011):

$$m_v = \frac{\Delta\varepsilon}{\Delta u_{max}} \tag{2.3}$$

Bouckovalas et al (2011) found that m_v is actually varies through the excess pore pressure ratio and could affected the replacement ratio of the gravel drain if the realistic m_v value is being considered.

Volumetric strain characteristic of the sand in undrained and drain condition has been studied by several researchers. Lee and Albaisa (1974) established that in undrained condition, within the soil in the same density and confining pressure, volume change is dependent on the pore pressure build up and independent of the cyclic loading type. Figure 2.10 shows the

coefficient of soil volume compressibility based on triaxial cyclic test results and analytical results relationship with pore pressure generation (Gianella et al., 2017). It illustrates that the dominant factor affecting the m_v value is generation of excess pore pressure before reached the liquefaction state.

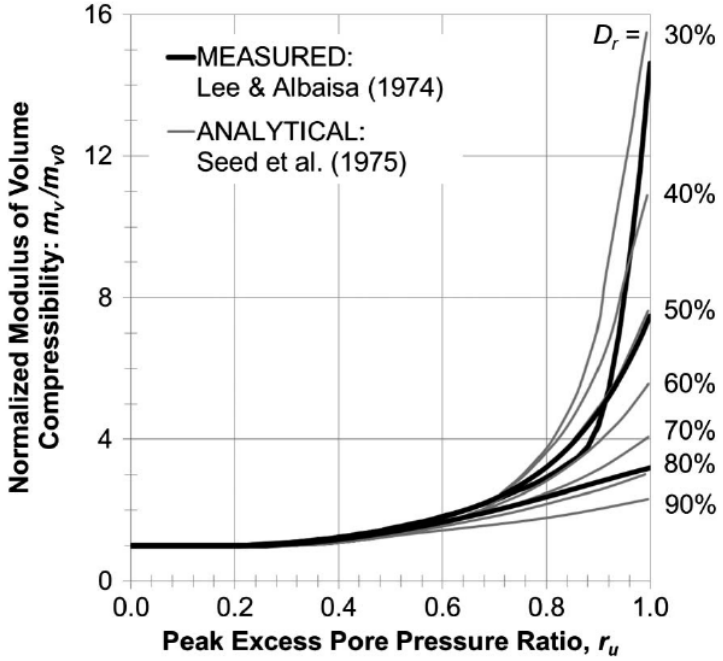

Figure 2.10 Excess pore pressure ratio relationship with coefficient of volume compressibility based on experimental results (Lee and Albaisa, 1974) and analytical results (Seed et al., 1975) (Gianella et al., 2017)

Finn (1981) found a relationship of volumetric contraction and excess pore pressure generation based on cyclic shear stress. Excess pore pressure ratio of a medium dense sand, have a unique correlation with volumetric strain that obtained in drained conditions, it is also required to reach the liquefaction state in undrained condition. Okamura and Soga (2006) found that volumetric strain of the soil relationship with liquefaction resistance is basically independent from confining pressure.

2.7 Flow in the pipe

Flow in the pipe in the engineering practice most likely found out as turbulent flow. Turbulent flow is characterized by rapid fluctuations of swirling regions of fluid. This rapid fluctuation often associated with higher friction which caused higher possibility of particle mixing during the flow (Figure 2.11)

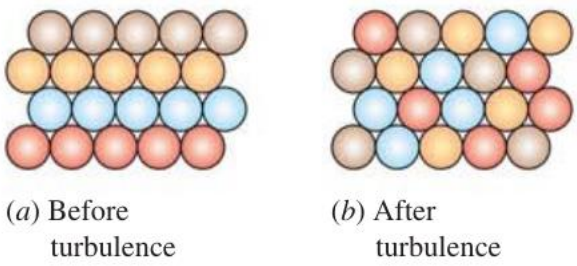

Figure 2.11 Fluid particles condition comparison during flow (a) before turbulence, (b) after turbulence.

Typical velocity profiles for fully developed laminar and turbulent flows are shown in Figure 2.12. Note that the velocity profile in laminar flow is parabolic and fuller in turbulent flow. The velocity in the turbulent flow consists of several layer which shows there is reduction of flow velocity.

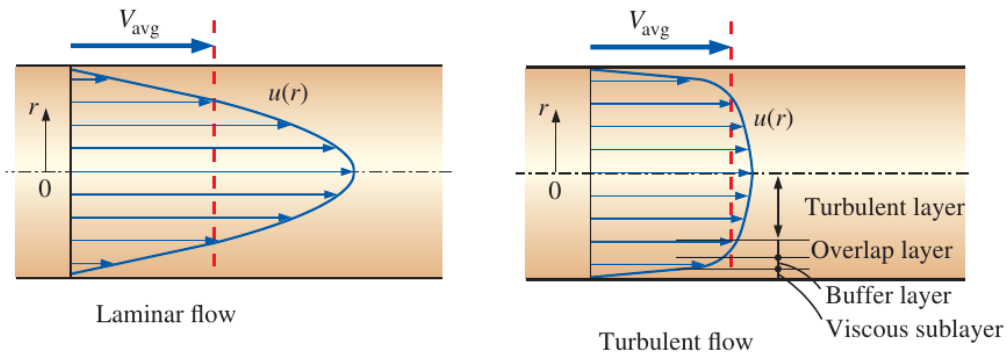

Figure 2.12 The velocity profile in laminar and turbulent flow

2.8 Liquefaction-induced ground settlement

Several methods have been established to predict the settlement behavior of the soil due to liquefaction. Volumetric strain profiles have been used to propose the estimation of the settlement under shaking event. Silver and Seed (1971) conducted simple shear stress to study volume change behavior which control the stability of saturated material and predict the settlement potential due to the ground shaking. It is found that for a given density and number of cycles, the volumetric strains are independent of the vertical stress. Ishihara and Yoshimine (1992) concluded that liquefaction induced volume change is depend not only on relative density of the soil but also on maximum shear strain. The relationship between maximum shear strain amplitude and volumetric strain due to liquefaction is shown in Figure 2.13.

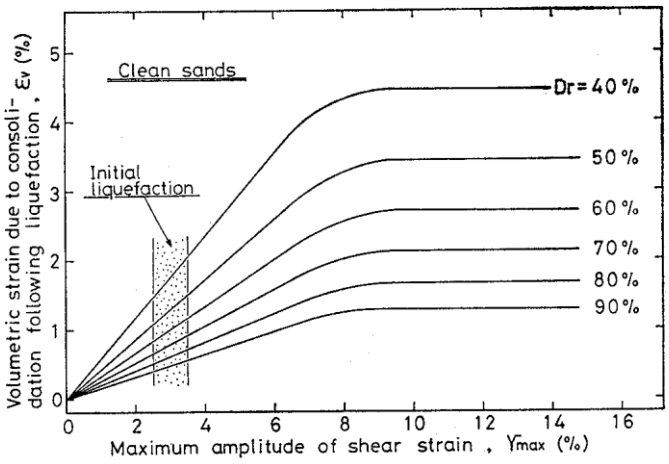

Figure 2.13 Post-liquefaction volumetric strain plotted against maximum shear strain (Ishihara and Yoshimine, 1992)

Tokimatsu and Seed (1987) proposed a simplified method to predict the settlement due to the earthquake shaking based on cyclic shear ratio of saturated sand and N-SPT data. The experimental data obtained from laboratory using triaxial test then calibrated with the case history data. The chart shown in Figure 2.14 is proposed the estimation of volumetric strains to predict the deformation occurrence due to cyclic loading.

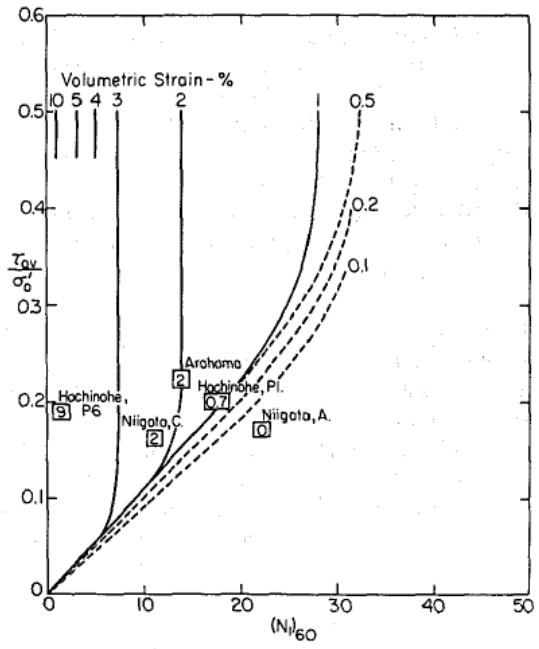

Figure 2.14 Chart for determining cyclic deformations as a function of N-SPT data and volumetric strain (Tokimatsu and Seed, 1987)

Chapter 3

Permeability Characteristics of Soil Layer Remediated with Gravel Drain

3.1 Introduction

The permeability of a soil is defined as the ability of the water to flow through it. The flow of water through soil specimens is governed by Darcy's law which is depending on the permeability coefficient and the difference of pressure head as follows:

$$v = k.i \quad (3.1)$$

$$q = k.i.A \quad (3.2)$$

where v is the velocity of the water flow (cm/s), k is the coefficient of soil permeability (cm/s) and i is hydraulic gradient (head loss/flow length), q is the flow rate of water (cm^3/s), and A is the cross-sectional area of specimen perpendicular to the flow direction (cm^2).

Soil permeability test that commonly used in soil mechanics based on Darcy's law assumed as laminar flow. The linear relationship between hydraulic gradient and the velocity of the water flow only hold true when the flow is laminar based on Hagen-Poiseuille theory. This linear relationship between v and i is valid when the flow is laminar, which is characterized by a Reynolds number, lower than some value between 1 and 10 (Freeze and Cherry, 1979). When the flow is turbulent, the velocity of the water is no longer proportional to the hydraulic gradient. The characteristic of the flow can be defined based on Reynolds Number which is well established in hydraulic engineering. In the flow of water through soil, it has been found that the flow is laminar if the Reynolds Number is less than unity. The Reynolds Number (R_e) is given by,

$$R_e = (\rho . v . D_{50}) / \eta \quad (3.3)$$

Where ρ = density of the fluid (g/cm^3)

v = velocity of the water flow (cm/s)

D_{50} = average diameter of the soil particles (cm)

η = viscosity of the fluid (g/cm.s)

In this chapter, understanding of permeability characteristic mobilized in the soil remediated with gravel drain is described further. The permeability coefficient is one of the important parameters that dominates the behavior of liquefiable soil improved with gravel drain during earthquake. The objective of this study is to determine the permeability coefficient for both sand and gravel in the centrifuge test condition.

3.2 Permeability characteristic of the sand

Sand particles tend to demonstrate a horizontal alignment which results in higher permeability for horizontal flow than that for vertical and thus, a ratio of horizontal to vertical permeability of several to ten is common. Therefore, in this study, not only vertical but also horizontal constant head permeability tests were conducted on sand. Ube Keisa no 7 was used in the test to obtain the sand permeability. The model for this test was made in the same way of making the model for centrifuge test. Ube Keisa no 7 was drained to the acrylic container at a relative density 64%. The characteristic permeability of the soil in the anisotropy condition was depended on its deposition. The direction of soil natural deposition was one of dominant parameters that controlling the maximum value of the permeability. In the centrifuge test condition, the flow of the water in the sand layer is in the horizontal direction, which generally larger than the vertical permeability. In order to achieve this condition, the tap was installed in the wide side of the container to allow only the horizontal flow. Aluminum plate with hole was installed to provide a space at each side to accumulate water before it flows to the soil. The constant head method of the permeability test was adopted in this model. The water tank was placed to keep the head constant. When the sample was built and the box was sealed so that there is no leakage can occur at any point, the sample was saturated with the water by applying vacuum pressure -98 kPa to expel all of the air

bubble that still exist inside the sand layer. After the saturation process finished, the pipe was connected to the tap, the hydraulic gradient was set, and the water was allowed to flow in the soil. During this process, the head of the water tank was maintained constant. When the water flow was stable, the amount of the water discharged from the soil was measured at every 1 minute. This process was repeated by varying the hydraulic gradient from 1, 1.5 and 2.

The sand was prepared in a box in the same way as the centrifuge model construction. The box was fully saturated in the vacuum chamber and sealed with a lid on it. The sand was prepared in two different ways to simulate the water flow in the directions that are parallel and normal to the sedimentation plane as schematically illustrated in Figure 3.1.

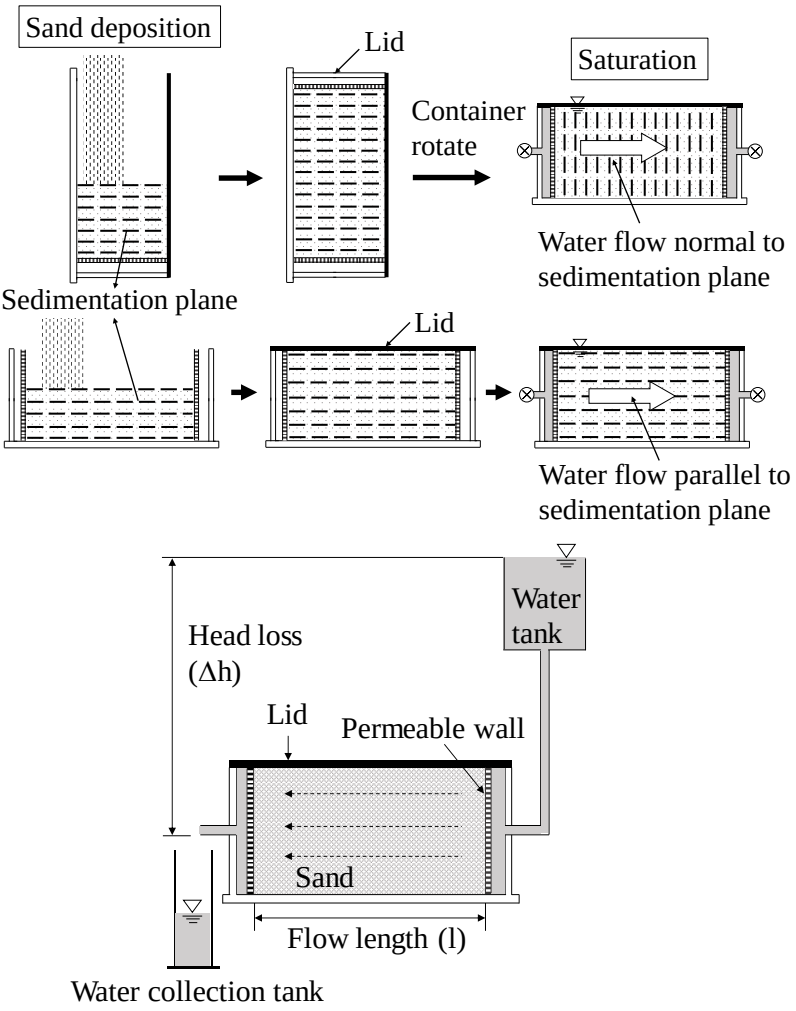

Figure 3.1 Schematic illustration of model preparation and procedure of permeability tests on silty sand

The results of the laboratory permeability test were analyzed, velocity, the Reynolds Number, the pressure different, and the coefficient of the permeability were calculated. The pressure different due to the differential of flow length was calculated by,

$$\frac{dP}{dx} = \frac{P_{in} - P_{out}}{dx} \tag{3.4}$$

Where *dP* is the different pressure at the point of the input flow to the point of the output flow in the specimen (kN/cm^3). Meanwhile *dx* is the flow length (cm). The permeability test result in the sand are presented in Figure 3.2.

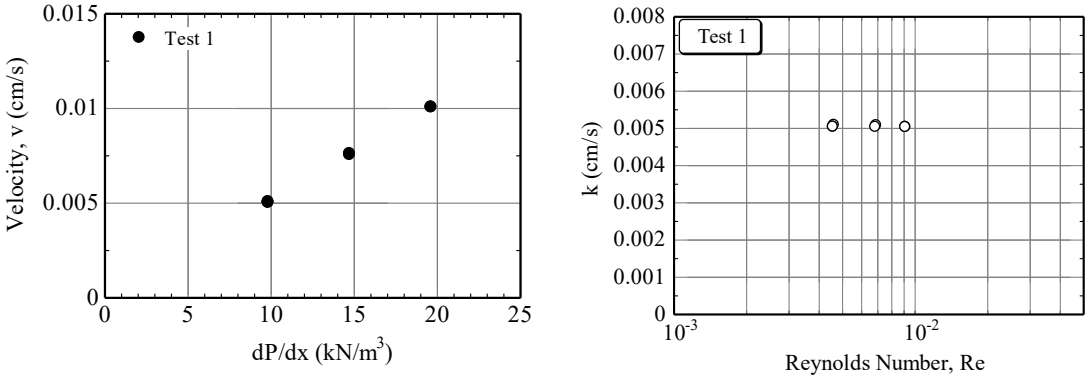

Figure 3.2 Permeability test results for sand

The results of the laboratory permeability test for the sand was calculated by using Eq. (3.1) and the coefficient of permeability of the sand in the vertical (perpendicular to the bedding plane) and horizontal (parallel to the bedding plane) directions, were k_{sv}= 4.8×10^{-6} m/s and k_{sh}= 4.0×10^{-5} m/s, respectively.

3.3 Permeability characteristic of the gravel

In order to obtained the permeability characteristic of the gravel used in the centrifuge test, Ube Keisa no 1 was used in this laboratory test. In the centrifuge test, the flow inside the drain was happened to be flow in the pipe, so that the same type of pipe has been used in this

laboratory test to completely reassemble the centrifuge test condition. The material that used for the permeability test is summarized in Table 3.1.

Table 3.1 Summary of permeability test conditions

Test	Soil	Type of container	Dimension (cm)
1	Ube Keisa no 1	Aluminium Pipe	Ø 2, length 10.6
2	Ube Keisa no 1	Aluminium Pipe	Ø 2, length 136

The sample was made by pouring the gravel into the pipe vertically, and the pipe was shaking to achieve a very dense gravel layer. After the pipe was fully filled with gravel, the pipe was closed by using the aluminum lid then was placed horizontally. The pipe then was connected to the water tank with adjusted hydraulic gradient that allowed the water to flow in a high pressure to the pipe. The tests objective was to reproduce the turbulent flow in the pipe. Thus, the shorter length of the pipe was used. The Reynolds Number has to be large enough so the larger hydraulic gradient was set. Whenever the hydraulic gradient was set, the amount of water discharged from the output pipe was measured at every 30 s. Furthermore, in the similar way, the test has been conducted by using the different length of the aluminum pipe to reproduce the laminar flow in the pipe, so that the hydraulic gradient was set to the minimum value that water still can be flow in the pipe. In the same manner, the water discharged was measured at several time interval, 5 minutes, 3 minutes, and 1 minute. Schematic of the laboratory permeability tests for gravel is shown in Figure 3.3.

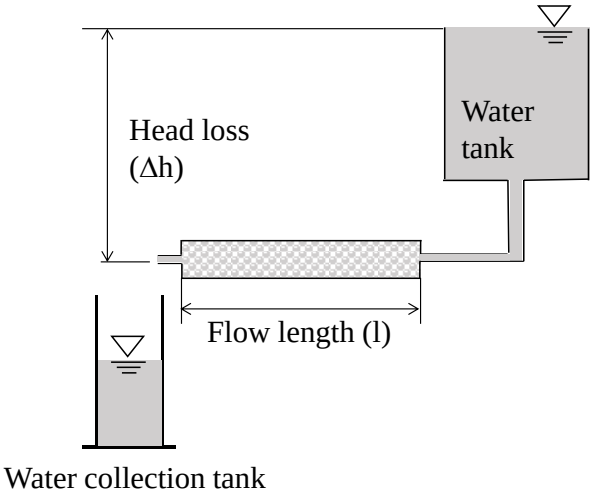

Figure 3.3 Schematic illustration of model preparation and procedure of permeability tests on gravel

Reynolds Number was calculated using Eq. (3.3) and the results of the laboratory permeability test for gravel are shown in Figure 3.4. The coefficient of permeability of the gravel, k_w, was constant when R_e was lower than 5, and decreased with increasing R_e when R_e >5. Note that k_w shown in the figure, which was obtained through tests on the laboratory floor (1g condition) must be scaled up by a factor of 40 when considering the water-saturated centrifuge models.

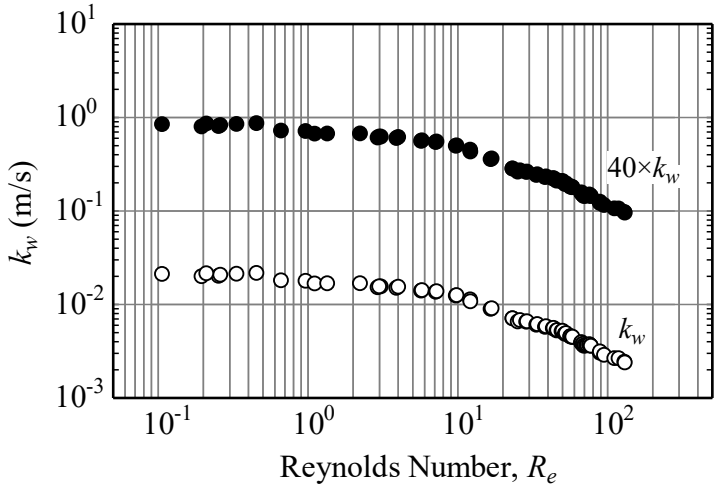

Figure 3.4 Variation in the coefficient of permeability of the gravel in a wide range of Reynolds number at 1g as well as that scaled up for 40G environment

3.4 Conclusions

The soil permeability characteristic for both sand and gravel in the centrifuge test has been established. Based on the results, the usual permeability test may not be appropriated to reproduce the mobilization of the water flow in the soil and gravel in the centrifuge test. The laboratory permeability tests have to follow all of the aspect that occurred in the centrifuge test. In the sand permeability case, the flow direction considering the bedding plane is play an important role due to the difference between horizontal and vertical permeability of the soil. Meanwhile in the gravel case, flow water in the pipe or coarse material has to be taking into account since the Reynolds Number happened to be larger than 1 and the turbulent flow occurrence change the gravel permeability significantly. Since in the design procedure, the soil permeability is one of the substantial parameters that can affect the pore pressure dissipation behavior, obtaining the appropriate soil permeability is necessary.

Chapter 4

Coefficient of Volume Compressibility Characteristics Assessment through Triaxial Cyclic Test

4.1 Introduction

Volume change characteristics have been studied by many researchers to asses both the stability of saturated soil and the potential settlement due to the ground shaking. Volume change behavior that causes change in pore pressure resulting stability problems in deposit saturated cohesionless soils (Silver and Seed, 1971). For given density and number of cycles, volumetric strains are independent of the vertical stress for a given cyclic shear strain amplitude. Lee and Albaisa (1974) found that reconsolidation volumetric strain for non-liquefaction condition increase with increasing grain size of the soil, decreasing relative density, increasing excess pore pressure generated during undrained cyclic loading. However, the volumetric strain almost independent of how excess pore pressure was generated. Volume change of the soil was investigated through a series of triaxial testing to estimate the settlement. Expected settlement when the soil is not liquefied is less than 0.5%, meanwhile when the soil liquefied it was expected to be in the range of 5%. Volume change of the soil with similar relative density and confining pressure was found consistently dependent only on the excess pore pressure build up and was independent of the type of cyclic loading. The important finding is that when the soil subjected to cyclic loading with different CSR, volume change is always same as the other parameter keep constant.

The coefficient of volume compressibility (m_v) is one of the substantial parameters which has been used in gravel drain design procedure to determine the drain spacing (Seed and Booker, 1977). A constant m_v was commonly used and in the current practice, the value is generally decided based on soil density (Baez and Martin, 1992). The behavior of ground improved with gravel drain had been investigated by Okamura et al. (2019) through laboratory tests and numerical simulation. Liquefaction occurrence was observed at a shallower depth of the soil which in the design it was not supposed to liquefy. The use of constant m_v in the design procedure irrespective of the depth has been reported as the cause. Volumetric strain characteristics in saturated sands under cyclic loading had been studied by Lee and Albaisa (1974). It was found that the relationship between volumetric strain and generated excess pore pressure did not significantly depend on confining pressure. Based on these evidences, m_v is likely varied not only by the influence of soil density, but also factors including stress level and generated excess pore pressure. This chapter describes the results of cyclic triaxial tests aimed to provide a better understanding of m_v characteristics of the sand under undrained cyclic shearing.

4.2 Test conditions

Ube Keisa no. 7 sand (e_{max} = 1.138 and e_{min} = 0.657) was used for the triaxial tests. All of the specimens were prepared by air-pluviating the sand to the mold on the pedestal with an internal dimension of 50 mm in diameter and 100 mm in height to a target relative density 60%. The specimens were saturated under a vacuum pressure -95 kPa with the aid of the CO_2 replacement technique to achieve the Skempton's B-value higher than 0.96. The specimens were subjected to cyclic shearing in the undrained condition. When the excess pore pressure ratio ($r_u = \Delta u/\sigma_{c0}'$) of either 0.3, 0.5 or 0.7 was attained, the cyclic shearing

was halted and the drainage valve was opened to measure the drained water volume. Volumetric strain and thus, the coefficient of volumetric compression m_v ($=\varepsilon_v/\Delta u$) was tested for several initial effective confining pressures (σ_{c0}'). Corresponding to the prior tests, additional tests with constant σ_{c0}'= 100 kPa and $r_u \approx$ 0.3 were also carried out with three different cyclic stress ratios to examine its effect on the m_v separately. Test conditions for m_v test are summarized in Table 4.1.

Table 4.1 Triaxial test conditions

σ_{c0}' kPa	r_u					
	≈0.3		≈0.5		≈0.7	
	Dr (%)	CSR	Dr (%)	CSR	Dr (%)	CSR
25	58	0.1	58	0.13	58	0.12
50	59	0.13	59	0.13	58	0.13
100	60	0.1	61	0.13	60	0.13
200	61	0.13	61	0.13	61	0.13
100	59	0.1	-	-	-	-
100	58	0.13	-	-	-	-
100	59	0.132	-	-	-	-

4.3 Effect of confining pressure on volumetric strain behavior of soil

The volumetric compressibility of the sand was investigated through triaxial testing, where the initial confining stress (σ_{c0}'), and target excess pore pressure ratio ($\Delta u_t/\sigma_{c0}$') were varied

among tests while keeping the relative density of the specimens to be fixed to 60%. The specimens were subjected to cyclic shearing in the undrained condition until a target excess pore pressure ratio of 0.3, 0.5 or 0.7 was attained. The cyclic shearing was then halted and the drainage valve was opened to reconsolidate the specimen.

Figure 4.1 shows the time histories of excess pore pressure ratio obtain from three tests at σ'_{c0}= 50 kPa. Pore pressure generated in the same manner under the same cyclic stress ratio, confirming reproducibility of the tests. Excess pore pressure ratio, r_u is determined from the residual excess pore pressure, Δu.

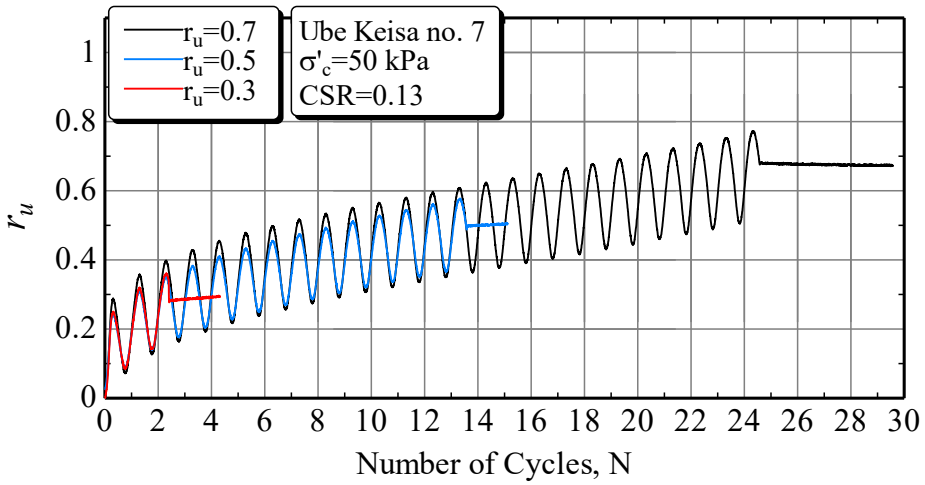

Figure 4.1 Time histories of excess pore pressure ratio during cyclic loading at 50 kPa confining pressure

The relationship between the reconsolidation volumetric stain (ε_v) and the actual excess pore pressure ratio, $\Delta u/\sigma_{c0}$', attained before this reconsolidation is illustrated in Figure 4.2. Volumetric strain increases linearly as $\Delta u/\sigma_{c0}$' increases, with ε_v being practically the same irrespective of σ_{c0}' for the range $\Delta u/\sigma_{c0}' \leq 0.75$. Lee and Albaisa (1974) reported similar test results on several sands that volumetric strain was almost the same irrespective of the

effective confining pressure for the range of $\Delta u/\sigma_{c0}$' lower than 0.6. They also found that CSR in cyclic shearing to generate a certain $\Delta u/\sigma_{c0}$' did not affect the reconsolidation volumetric strain. Hence the coefficient of volumetric strain, m_v (= $\varepsilon_v/\Delta u_t = \varepsilon_v r_u / \sigma_{c0}$') is considered to be inversely proportional to the initial effective confining pressure. The relationship between m_v and σ_{c0}', as demonstrated in Figure 4.3 clearly supports the analogy.

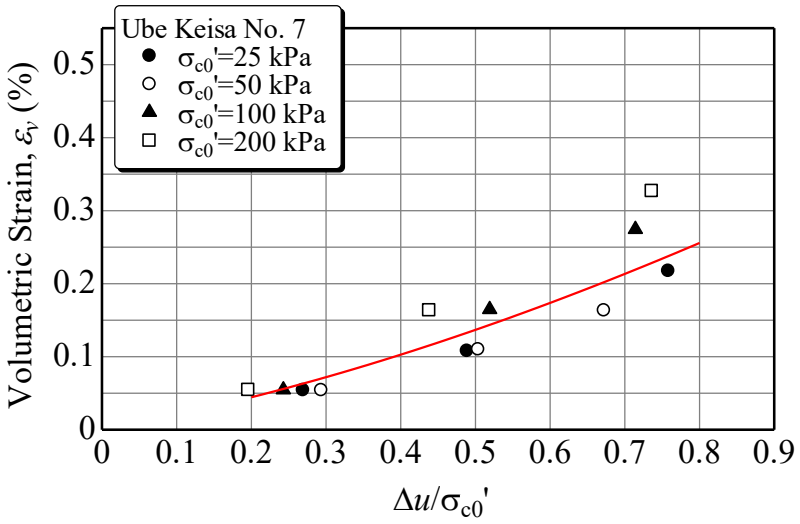

Figure 4.2 Relationship between reconsolidation volumetric strain (ε_v) and excess pore pressure ratio before reconsolidation.

4.4 Effect of excess pore pressure ratio on coefficient of volume compressibility behavior

Considering the linear relationship of the swelling-reconsolidation line with a slope κ on the e – ln p' plane, where e indicates the void ratio and p' represents the mean effective stress, m_v can be expressed as;

$$m_v = -\frac{\kappa}{1+e}\frac{1}{\sigma_{c0}'}\frac{ln(1-r_u)}{r_u} \tag{4.1}$$

The curves indicated in Figure 4.3 are empirical relations to best fit the test results as follows,

which will be used in the numerical simulation described in Chapter 5.

$$m_v = -\frac{0.0016}{\sigma_{c0'}} \frac{ln(1-r_u)}{r_u} \tag{4.2}$$

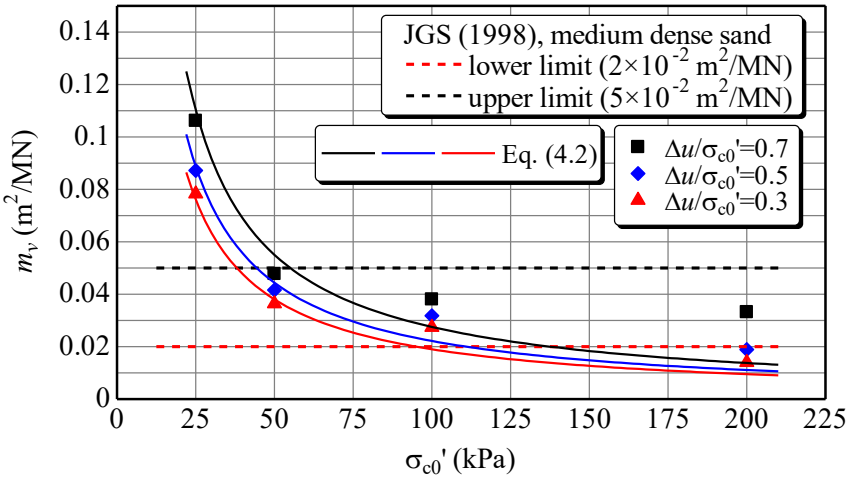

Figure 4.3 Relationship between m_v and effective confining pressure

Furthermore, the tests were also performed to examine cyclic stress ratio influence on the m_v. The tests with variation of cyclic stress ratio were conducted under the same confining pressure to minimize the stress level effect. The test result is presented in Figure 4.4 and it shows m_v is nearly constant at slightly different r_u. It is indicated either the loading was a very small cycles or a few intense cycles, the m_v consistently be in a narrow range as the other parameters were remained constant.

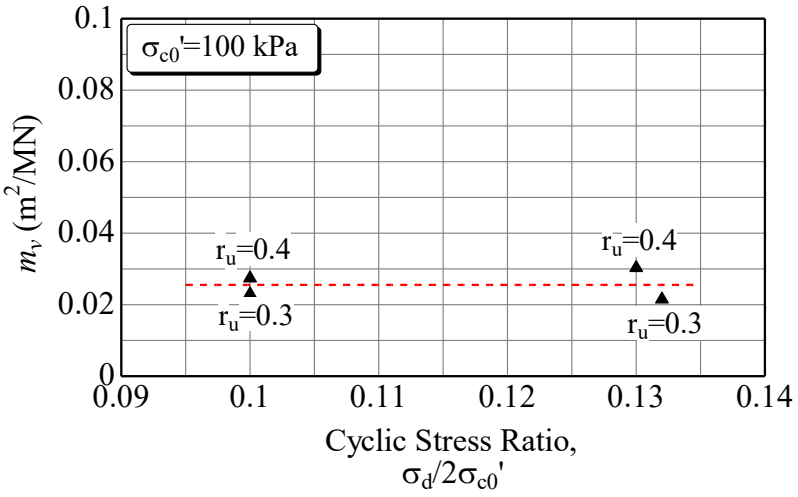

Figure 4.4 Relationship between m_v and cyclic stress ratio

4.5 Conclusions

In this chapter, a series of cyclic triaxial tests were performed to determine m_v value of the saturated sands under cyclic loading. All the m_v tests were conducted in undrained conditions, and after the target excess pore pressure ratio was attained, drainage was allowed to measure the volume change. Volumetric strain and m_v behavior within a different confining pressure have been examined. The results showed that m_v value increases with increasing excess pore pressure ratio. Cyclic stress ratio influence on the m_v was also observed, and m_v was found independent of the cyclic stress ratio. The confining pressure effect on the m_v was found more significant. It was observed that m_v is inversely proportional to the initial effective confining pressure. Therefore, it can be concluded that m_v characteristics have been influenced by both r_u and σ'_c at the same time. These facts proposed that stress-dependent m_v should be considered on the gravel drain design procedure.

Chapter 5

Effect of Permeability and Diameter of the Drain on Pore Pressure Behavior of Sand Remediated with Gravel Drain

5.1 Introduction

Loose saturated sand is susceptible to large excess pore water pressure generation when subjected to earthquake shaking if it unable to drain, leading to loss of stiffness and strength known as liquefaction phenomena (Seed & Idriss, 1982). There were several ground improvement methods have been proposed to mitigate the risk of liquefaction including reinforcement, grouting, densification, and drainage. The gravel drain installation is one of the common methods to mitigate liquefaction due to an earthquake in non-cohesive soil. The installation of gravel drains can increase the soil density, lateral effective stress of the soil, and allow excess pore water pressure gets dissipated almost as fast as it is generated (Adalier & Elgamal, 2004). If pore pressure can be dissipated as they created, then danger of liquefaction may be averted. Seed & Booker (1977) were originally proposed a design procedure of the gravel drain by assuming an infinitely permeable column as a drain material. The behavior of generation and dissipation of pore water pressure was analyzed by considering the soil permeability and coefficient of volume compressibility. The significant influence of drainage resistance on the performance of the drain has been founded by Onoue et al. (1987) by performed large-scale in situ experiments. The drain permeability was used as design criteria to evaluate drainage capability. The results showed that coefficient of permeability of the drainage plays an important role, if the drain permeability value is not

significantly larger than the soil, it reduced the draining capability to dissipate the pore water pressure. The response of drainage in liquefiable soil has been investigated by Brennan & Madabhusi (2002), the generation of pore water pressure induced by the earthquake created vertical hydraulics gradient. Water flow from the deeper soil upwards to the surface causing excess pore water pressure remains high compared to the greater depth. The presence of gravel drain provides the drainage path through horizontal flow which allows the pore pressure to dissipate faster significantly.

This study focuses on the assessment of the gravel drain performance and the pore water pressure response during strong shaking situations by taking into account the permeability changing of the sand layer and variation of gravel drain number. Using the dynamic centrifuge testing machine, nine model tests were performed including the benchmark test without the drain, and the sand layer remediated with gravel drain.

5.2 Design of models

The model ground tested in this study was an 8m deep uniform sand deposit subjected to base shaking. Medium dense silty sand was used and the base input acceleration was determined so that the whole deposit liquefies in a short duration of 4 seconds after the excess pore pressure starts to accumulate. This severe seismic condition may often be valid in practice corresponding to strong design earthquakes or low soil resistance to liquefaction. The soil parameters employed in the design of the gravel drains were determined first based on the conventional laboratory tests and the practical method as summarized in Table 5.1, but later in this paper, subjected to detailed examination. The coefficient of permeability for the sand and the gravel were $k_s = 4.8\times10^{-6}$m/s and $k_w = 2.0\times10^{-2}$m/s, respectively, obtained from the conventional laboratory tests. The coefficient of volumetric compressibility of the sand is $m_v = 0.03$m^2/MN recommended in JGS (1998) for medium-dense sand. The diameter

of gravel drains implemented in the models was d_w= 0.8m and 1.6m. The group of gravel drains in this study was placed in a square pattern as indicated in Figure 5.2. Center-to-center spacing of the gravel drains, b= 2.4m for d_w = 0.8m and 4.8m for d_w= 1.6 m (b/d_w= 3 for both d_w), were decided. The zone of influence of each drain can be approximated by a cylinder with an equivalent diameter of $b_e = b\sqrt{4/\pi} \approx 1.13b$.

5.3 Test conditions

The centrifuge models corresponding to 8m deep uniform prototype sands with and without gravel drains were implemented. Testing parameters, including the permeability of soils, the drain diameter, and the groundwater level, were varied among tests to investigate their effects. A rectangular laminar container was used in all the centrifuge tests, which was designed to shake a plane strain geotechnical model in the long direction of the box. This box is comprised a stack of up to 20 rectangular rings of duralumin alloy separated by linear roller bearings, and has internal dimensions of 12cm width, 40cm length and 22cm depth.

Ube-Keisa No. 7 sand deposited at a relative density D_r= 60% was used in all tests reported in this paper. The grain size distributions of the sand and gravel used in the tests are indicated in Figure 5.1. This sand is a silty sand with fine contents FC= 21%, a specific gravity of 2.63, and the minimum and the maximum void ratios of e_{min}= 0.657 and e_{max}= 1.138, respectively. Ube-Keisa No. 1 gravel was used as the material for gravel drains.

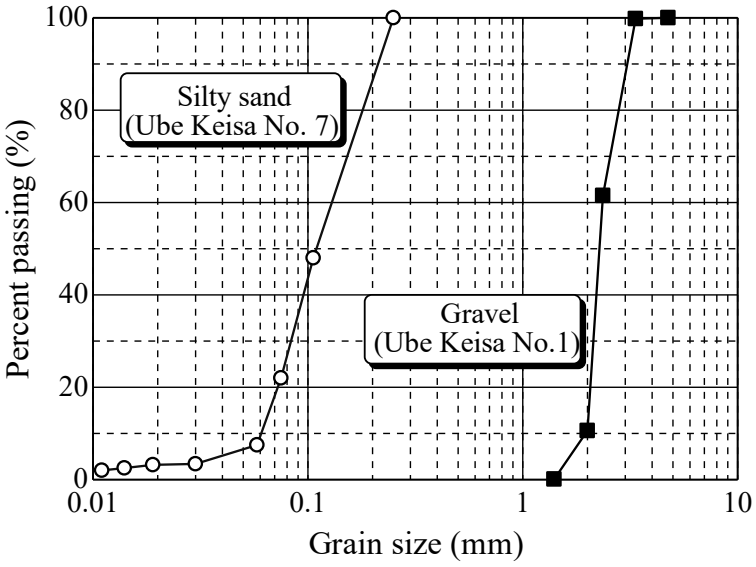

Figure 5.1 Grain size distribution of soils used in the tests

Depending on the test, gravel drains were prepared using aluminum pipes with an internal diameter of 20 or 40mm. A flexible stainless mesh filter of 0.1mm thickness with a 0.05mm aperture opening was placed inside the pipe that the gravel was poured into. The pipe was hit repeatedly to make the gravel as dense as possible (dry unit weight of 13.4kN/m^3). The gravel drains wrapped with the stainless mesh were extracted from the piles and placed in the laminar box. The stainless mesh was selected to prevent soil particles from migrating to the gravel and clogging the filter. Dry sand was poured into the laminar box to a depth of 20cm through a funnel. During sample preparation, pore pressure transducers were installed in the sand and drains to closely monitor the pore pressure variations in the radial and vertical directions, as illustrated in Figure 5.2.

The test conditions are summarized in Table 5.2. Although most of the models were saturated with water, a viscous fluid was used as a substituted pore fluid in two models (Models V and GD-V); this viscous fluid was a Metolose solution prepared by dissolving 1.8% Metolose by weight in water, to achieve a viscosity 40 times the viscosity of water. The use of a Metolose solution instead of water as a pore fluid in sand does not change the mechanical properties

of water-saturated sand except its permeability. A comparison between similar centrifuge tests saturated with water and Metolose allows direct investigation of the effect of permeability alone. Using water in a centrifuge test at 40G to model the seismic liquefaction of water-saturated prototype soil in the field could lead to the simulated actual prototype permeability to be 40 times larger than that of the model. In this case, the prototype permeability would be $4.8 \times 10^{-6} \times 40 = 1.9 \times 10^{-4}$m/s for the sand and $2.0 \times 10^{-2} \times 40 = 8.0 \times 10^{-1}$m/s for the gravel, respectively; this corresponds to the permeability of a clean fine sand in the field rather than that of the silty sand used in the centrifuge experiment. Moreover, if the model is saturated with a viscous fluid 40 times the viscosity of water, corresponding prototype soil permeability is 4.8×10^{-6}m/s for the sand and 2.0×10^{-2}m/s for the gravel.

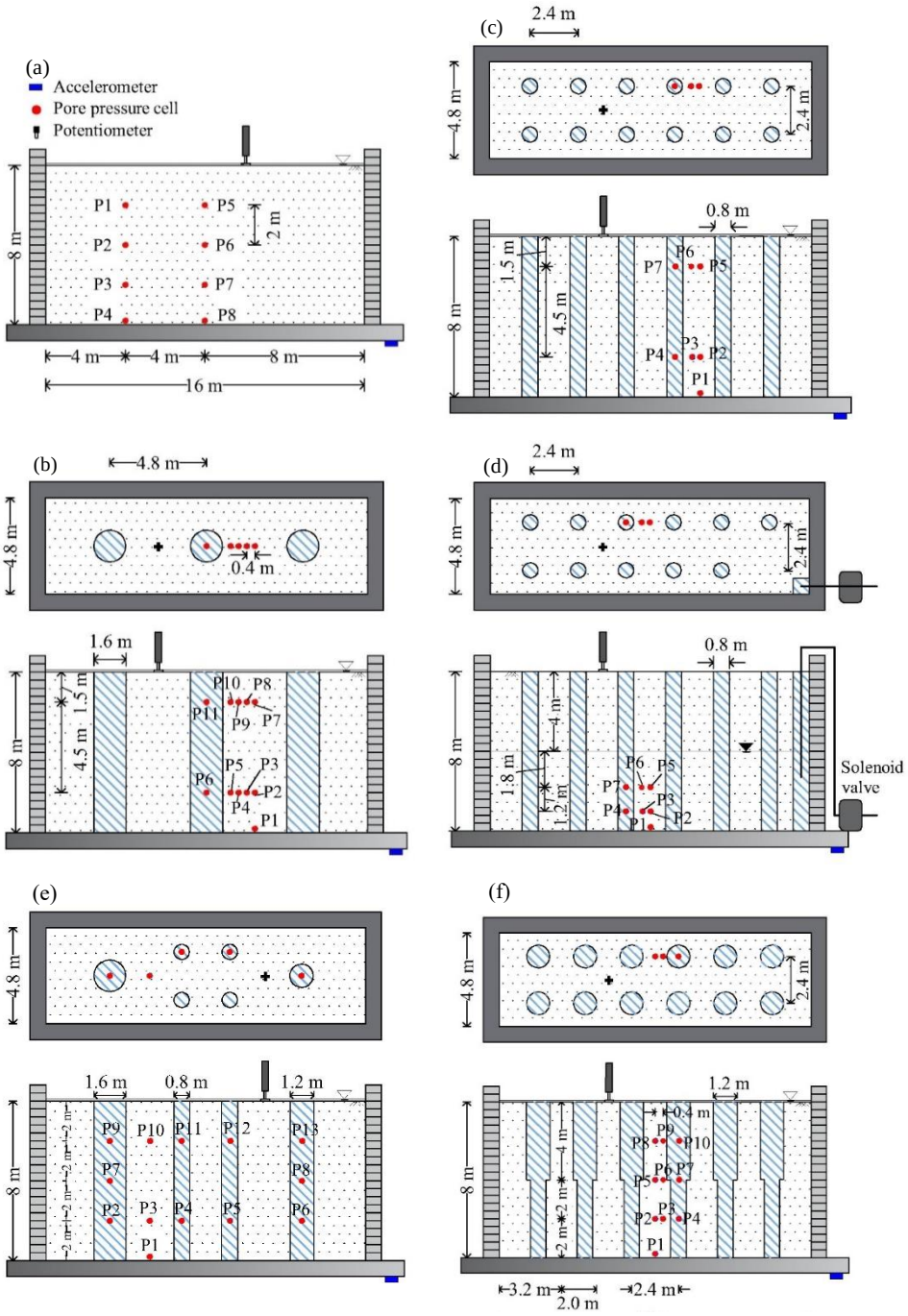

Figure 5.2 Schematic illustrations of centrifuge models and location of the sensors

(a) model without gravel drain (BM, V), (b) model with gravel drains of 1.6m diameter (GD-BM), (c) model with gravel drains of a smaller diameter (GD-SD), (d) model with gravel drain of smaller diameter and lowered groundwater level (GD-WL), (e) model with variation of drain covered with teflon sheet (GD-C), and (f) model with different size of drain along with the depth (GD-LD).

Table 5.1 Design parameters for the current design procedure to determine drain spacing

Parameter		
H	Depth of liquefiable layer and drain length	8 m
d_w	Diameter of gravel drain	0.8 m and 1.6 m
k_s	Coefficient of permeability of sand	1.9×10^{-4} m/s
k_w	Coefficient of permeability of gravel	8.0×10^{-1} m/s
m_v	Coefficient of volumetric compressibility of sand	0.03 m^2/MN (JGS)
t_l	time to liquefaction	4 s
-	Threshold excess pore pressure level	0.3 (JGS)
T_d/r_N	Time factor for radial flow	$4k_st_l/(m_v\gamma_w d_w^2)$
$L_w = 32k_sH^2/(\pi^2k_wd_w^2)$	Coefficient of well-resistance	0.08 for d_w = 0.8 m 0.02 for d_w = 1.6 m
b_t/d_w	Equivalent drain spacing ratio	0.34 for d_w = 1.6 m 0.23 for d_w = 0.8 m

Subsequently, the laminar box was set in a vacuum chamber whereas the air in the model was replaced with carbon dioxide gas to achieve a high degree of saturation after the saturation process. The de-aired pore fluid was introduced through the top of the model under a vacuum pressure of 97kPa until the fluid level in the laminar box exceeded the soil surface. Degree of saturation of the models was confirmed to be higher than 99.7%. The laminar box was then moved on the centrifuge platform and the centrifuge was spun up gradually to 40G. Finally, one-dimensional lateral shaking was imparted along the model long axis using a mechanical shaker. For models with lower groundwater table (WL and GD-WL) an attention was paid to maintain the liquefiable layer fully saturated. This was achieved by draining the groundwater from the initially fully saturated model through a siphon at 40G in-flight.

A total of seven centrifuge tests were carried out as listed in Table 5.2. Two models, BM and GD-BM were benchmark models fully saturated with water. Gravel drains with d_w= 1.6m were installed at a spacing ratio of b/d_w= 3 in GD-BM. GD-SD was a model in which gravel drains with a smaller diameter (d_w= 0.8m) were implemented with fixed spacing ratio and other testing parameters unchanged. Models V and GD-V were saturated with viscous fluid. Except for the soil permeability, all the testing parameters including the gravel drain diameter (d_w= 1.6m) and the spacing ratio were the same as GD-BM. Furthermore, two models, WL and GD-WL, with and without gravel drains, respectively, were examined with the groundwater table 4m below the ground surface. In these tests, except the input acceleration, all other testing parameters and conditions remained the same as that of models BM and GD-SD. The base shaking input to models WL and, GD-WL was scaled up so that the cyclic stress ratio at the mid-depth of the liquefiable layer was the same throughout the tests in this study. The acceleration amplitude of 1.7m/s^2, which was 1.5 times higher than that of other tests, were imparted to these models with lower groundwater table.

Table 5.2 Summary of centrifuge models (in prototype scale) and estimates of permeability based on the conventional permeability test, time factor T_l, well resistance L_w and maximum excess pore pressure ratio, r_{u_max}

Model	Relative Density *Dr* (%)	Coeff. Permeability* k_s (m/s)	k_w (m/s)	Pore fluid viscosity ν (cSt)	Drain diameter d_w (m)	Drain spacing *b* (m)	Groundwater Level GL –(m)	Time factor** T_l	Well resistance coefficient L_w	Estimated r_{u_max}
Benchmark model										
BM	61.7	1.9×10^{-4}	-	1	-	-	0	-	-	-
GD-BM	59.3	1.9×10^{-4}	8.0×10^{-1}	1	1.6	4.8	0	4.03	0.02	0.9
Smaller drain diameter model										
GD-SD	57.2	1.9×10^{-4}	8.0×10^{-1}	1	0.8	2.4	0	16.15	0.08	0.35

Lower permeability model										
V	63.2	4.8×10^{-6}	-	40	-	-	0	-	-	-
GD-V	57.3	4.8×10^{-6}	2.0×10^{-2}	40	1.6	4.8	0	0.10	0.02	1.0
Lower groundwater table										
WL	57.0	1.9×10^{-4}	-	1	-	-	3.6	-	-	-
GD-WL	61.0	1.9×10^{-4}	8.0×10^{-1}	1	0.8	2.4	4.0	16.15	0.08	0.3
Drains covered with plastic sheet										
GD-C	63.3	1.9×10^{-4}	8.0×10^{-1}	40	1.6, 1.2, 0.8	-	0	-	-	-
Different diameter of drain per depth										
GD-LD	60.7	1.9×10^{-4}	8.0×10^{-1}	40	1.2, 0.8	-	0	-	-	-

*: k_s, k_w in this table were obtained from conventional laboratory tests. The direction of water flow was normal to the soil bedding plane, and the applied hydraulic gradients were lower than 0.5.

**: Coefficient of volumetric compressibility of $m_v = 0.03$ m^2/MN was assumed to estimate the time factor.

In the centrifuge models with gravel drains examined in this study, testing parameters including the diameter of gravel drain, soil permeability and groundwater level, were varied between tests, whereas the spacing ratio was kept constant. The time histories of the lateral input shaking applied to the base of the fully saturated models have the shape indicated in Figure 5.3(a), which consisted of 45cycles of a sinusoidal wave with a dominant frequency of 28Hz and uniform acceleration amplitude of 4.4g except for several cycles of a taper at the beginning. For the tests at 40G centrifugal acceleration, this corresponds to a prototype frequency of 0.7Hz, and acceleration of 1.1m/s^2 applied to the base of a homogeneous fully saturated silty sand layer with a prototype thickness of 8m with and without gravel drains. For the models with a lower groundwater table (WL and GD-WL), the input acceleration amplitude was 1.7m/s^2 as mentioned earlier.

Considering the axisymmetric dissipation and the well resistance, the effectiveness of the gravel drains as a liquefaction countermeasure can be expressed in terms of two non-

dimensional parameters (Onoue, 1987), that is the time factor, T_l, and the well resistance coefficient, L_w , which can be shown as,

$$T_l = \frac{4k_s t_d}{m_v \gamma_w d_w^2} \frac{N_l}{N_{eq}} \tag{5.1}$$

$$L_w = \frac{32k_s H^2}{\pi^2 k_w d_w^2} \tag{5.2}$$

where, H is the length of drains, γ_w is the unit weight of water, t_d is the time duration of the earthquake, N_l is the number of equivalent uniform stress cycles required to cause liquefaction, and N_{eq} is the number of equivalent uniform stress cycles. T_l and L_w for the gravel drain models are summarized in Table 5.2. In the following discussions all results and comparisons are presented in prototype units unless mentioned otherwise.

5.4 Test results

5.4.1 Pore pressure response of uniform sand without drain

The excess pore pressure ratio, r_u (=$\Delta u/\sigma_{v0}$'; Δu is the excess pore pressure and σ_{v0}' is the initial vertical effective stress) time histories observed at depths in models of uniform sand without gravel drains, BM and V, are illustrated in Figure 5.3(b), and (c).

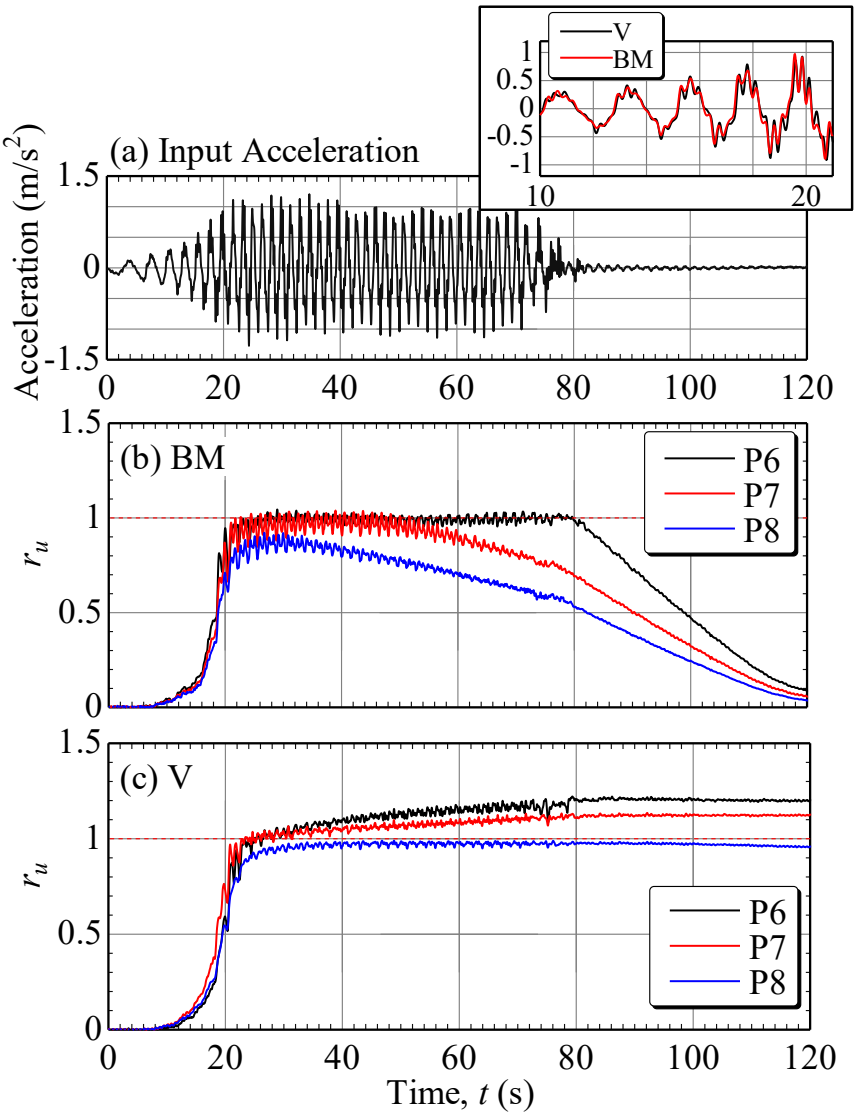

Figure 5.3 Input acceleration and excess pore pressure responses for fully saturated models without gravel drain, BM and V

The inset in Figure 5.3(a) is a close-up view at the beginning of shaking that compares the input accelerations of these tests and confirms a satisfactory reproducibility, which is also the case for all tests conducted in this study. Excess pore pressures were gradually generated during the beginning of the shaking, and started to accumulate significantly at t= 16s when the base acceleration amplitude exceeded approximately 0.5m/s^2, and reached the

liquefaction condition (r_u= 1) at approximately t= 20s throughout the entire depth of the sand. Although the sand permeability was 40 times higher for BM, there was no clear difference in the rate of excess pore pressure generation in these two models, suggesting that sands in these models were practically in undrained condition at the beginning of shaking. Note that the observed r_u significantly overshot the initial effective stress at the shallower depth in V; this is due to the subsidence of pore pressure cells installed at shallower depths after surrounding soil liquefied and lost its stiffness. Differences in pore pressure response between these models are distinctly observed after t= 30s. Excess pore pressures started to dissipate during shaking in BM indicating that sand solidified swiftly from the bottom up, whereas the sand continued to liquefy much longer in V.

5.4.2 Effect of permeability on pore pressures in models with gravel drain

The time histories of r_u for fully saturated models with gravel drains are demonstrated in Figure 5.4. Note that all excess pore pressures, not only pressures in the sand but also in the gravel drains, were normalized with respect to the initial vertical effective stresses in the sand. In the test GD-BM, r_u in sand at a greater depth (z= 6m) attained its maximum value of r_u= 0.4-0.7 at around t= 21s, then leveled off for some time from 21 to 25s, indicating dissipation balanced generation, which was followed by swift dissipation even during shaking. It can be observed that the gravel drains effectively prevented the soil from liquefaction triggering at the depth. Conversely, r_u at the shallower depth (z= 1.5m) at any radial locations (P7–P10) reached the liquefaction condition, although the effects of gravel drains can be observed on the timing of dissipation initiation, as well as in the form of dilative responses during shaking.

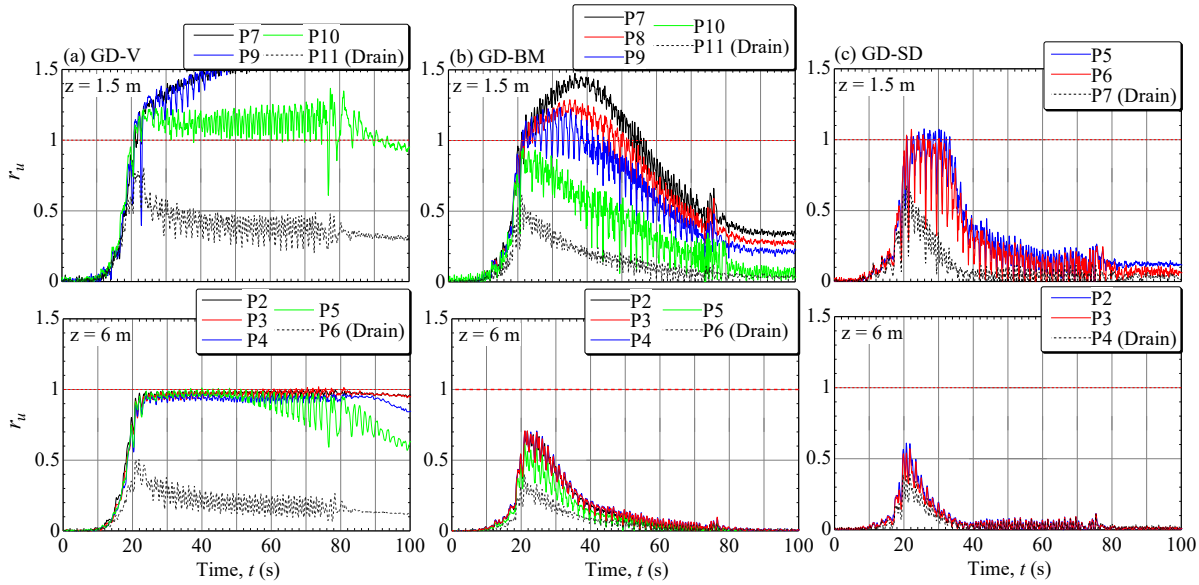

Figure 5.4 Excess pore pressure responses for fully saturated models with gravel drains

For the model GD-V, with 40 times lower permeability and thus with 40 times smaller T_l, excess pore pressure generation in the sand was quite similar to that in the companion model without drain (model V). r_u in sand at both shallower and deeper depths started to increase significantly at approximately t= 16s; the sand reached initial liquefaction at t= 20s and continued to liquefy throughout the shaking event. In this test, the gravel drains were not able to prevent the liquefaction triggering even at a location closest to the drain (P5 and P10). The evolution of the radial distribution in r_u is depicted in Figure 5.5.

r_u in GD-V increased with time and was nearly uniformly distributed in the sand at any time. The effects of the gravel drains to reduce the excess pore pressure in the sand cannot be observed. For GD-BM at a depth of z= 6m, r_u was lower than that in the benchmark model at the same depth (P7 in BM); it decreased from the midpoint of two adjacent drains (r= 2.4 m) towards the drain. This holds true at the shallower depth (z= 1.5 m) at t= 16s and 18s but r_u reached unity at approximately t= 21s.

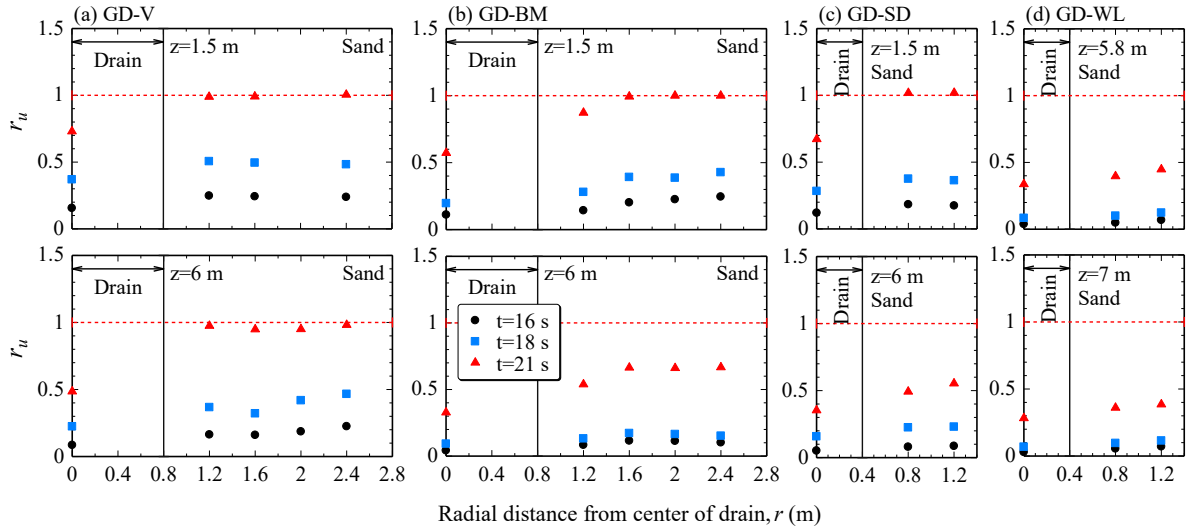

Figure 5.5 Radial distribution of excess pore pressure ratio at two depths

To simultaneously examine the horizontal and vertical flow of the pore fluid, contours of the maximum excess pore pressure, Δu_{max}, attained at t= 21–22s are presented in Figure 5.6. For GD-V, the slopes and intervals of the contour lines at greater depth (z= 6m) demonstrate that the horizontal hydraulic gradient was high only at the perimeter of the gravel drain (r= 0.8–1.0m from the center of the gravel drain) but low at the zone with r> 1.2m. This clearly indicates that the zone where the pore fluid flowed horizontally in the sand toward the drain was very limited. Except for this zone, Δu_{max} was practically the same as that in model V. At shallower depths, contours in sand were more or less horizontal and sparsely distributed in a similar manner to those in model V, indicating that the drain does not appear to have dissipative effects at shallower depths. For model GD-BM, a distinct difference from GD-V can be observed at a greater depth. A zone with hydraulic gradients heading towards the drain extended radially to the midpoint, 2.4 m from the center of the drain; whereas, the excess pore pressures were kept lower than the companion model (BM). At a shallower depth,

the slopes are gentle suggesting that the pore water did not flow toward the drain but the sand surface.

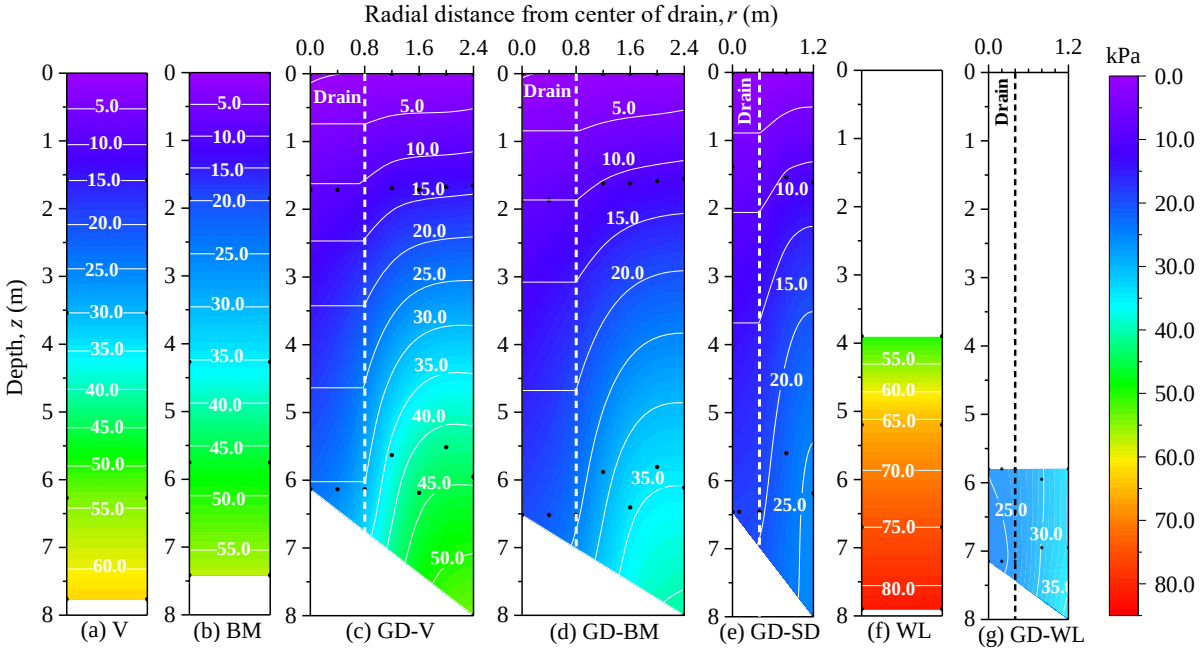

Figure 5.6 Excess pore pressure contours

5.4.3 Effect of diameter of drain

The test conditions of GD-SD were the same as GD-BM in all aspects except for a diameter of the drains (d_w) and a center-to-center spacing (b), keeping the ratio constant to b/d_w= 3. The time histories and radial distributions of r_u observed in GD-SD are presented in Figure 5.4(c) and Figure 5.5(c), respectively. As compared with GD-BM, a lower r_u and faster dissipation in GD-SD at z= 6m can be observed which can be explained by the larger time factor T_l for GD-SD. At the shallower depth of z= 1.5m, sand did liquefy, regardless of the fact that compared to GD-BM, positive effects of the smaller drain diameter in the form of more significant dilative dips in pore pressure responses that appeared from the beginning of shaking, as well as swifter dissipation, can be observed in GD-SD. Contours of Δu_{max} in

Figure 5.6 indicate that, at greater depth, the zone with hydraulic gradients heading towards drains extended radially to the midpoint (r= 1.2m). The contour line slopes are steep, with Δu_{max} lower than that at the corresponding points in GD-BM. However, the drains failed again to prevent the soil from liquefaction triggering at shallower depths. One important point is that contours in sand above 1.5m depth are quite similar in all tests as shown in Figure 5.6. At shallower depths, the initial effective vertical stresses were small and the excess pore pressures likewise, leading to a lower horizontal hydraulic gradient toward the drain.

The test with different drain diameter along with the depth (GD-LD) was conducted not only to examine the diameter effect but the purpose also to accommodate m_v assumption. The larger diameter of the drain at shallower depth meant to simulate faster pore pressure dissipation and resulted in larger volumetric strain of the sand. Two different diameter drain is installed as one column and arranged with the same aspect as GD-SD. The time histories of acceleration and pore pressure ratio are presented in Figure 5.7. The input acceleration time history is designed similar to the previous tests. Pore pressure ratio is measured at three different depths, 2 m, 4 m, and 6 m, respectively. In general, there is no liquefaction occurrence at all depths. r_u observed at 6 m shows similar response as GD-SD after 40 s all of the excess pore pressure are fully dissipated. r_u at 2 m depth reached 0.9 as measured at the farthest distance of the drain and gradually dissipated right after the peak. After t = 40 s, there is residual r_u observed due to the subsidence of the pore water pressure sensors. GD-LD tests has been found can prevent the liquefaction occurrence.

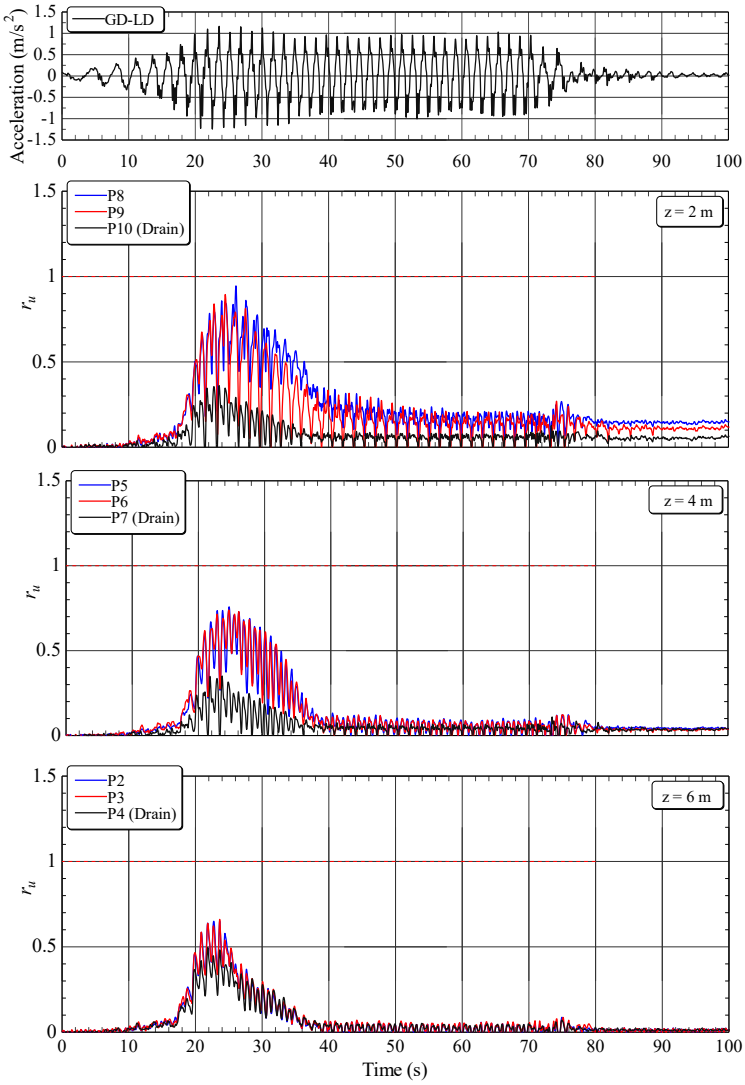

Figure 5.7 GD-LD time histories of input acceleration and excess pore pressure ratio

5.4.4 Effect of depth liquefiable layer

The time histories of input acceleration and excess pore pressure responses are presented in Figure 5.8(a); these time histories are for two companion models with the groundwater table 4m below the ground surface (WL and GD-WL) at two different depths. The acceleration amplitude was higher than that of the other tests, but the sand without gravel drain (WL) liquefied at around t= 20s (4s after starting to generate excess pore pressures), which was

quite similar to the fully saturated models, BM and V. Excess pore pressure ratio in the sand with gravel drains (GD-WL) reached a plateau of r_u approximately 0.4 at around t= 21s. Thereafter, r_u started to increase again at t= 26s, which was mostly due to the input acceleration amplitude being significantly larger than that designed during a period from t= 25 to 40s. Therefore, the radial distribution and contours of r_{u_max} shown in Figure 5.5(d), are the maximum values of r_u while staying at the plateau (t= 21–25s). The comparison of the results with those from GD-SD, for which the testing parameters are the same as GD-WL except the groundwater level is important. Looking at the radial distribution, r_{u_max} in sand of GD-WL is considerably lower than GD-SD. The difference in r_{u_max} between the sand and drains is only about 0.1 in GD-WL which is less than half of GD-SD at a similar depth of z= 6 m. The fact that the dissipation in sand is more rapid for GD-WL than GD-SD could be explained by the difference in the dissipation time factor; however, T_l for these models are the same. A possible explanation for this is that m_v is a stress level dependent soil parameter, and could be smaller for GD-WL than GD-SD. It is also observed that r_{u_max} in the drain of GD-WL is lower than that in GD-SD, which is believed to be due to the difference in well resistance. Drains in GD-SD are longer than those in GD-SD and have to run more water than GD-WL.

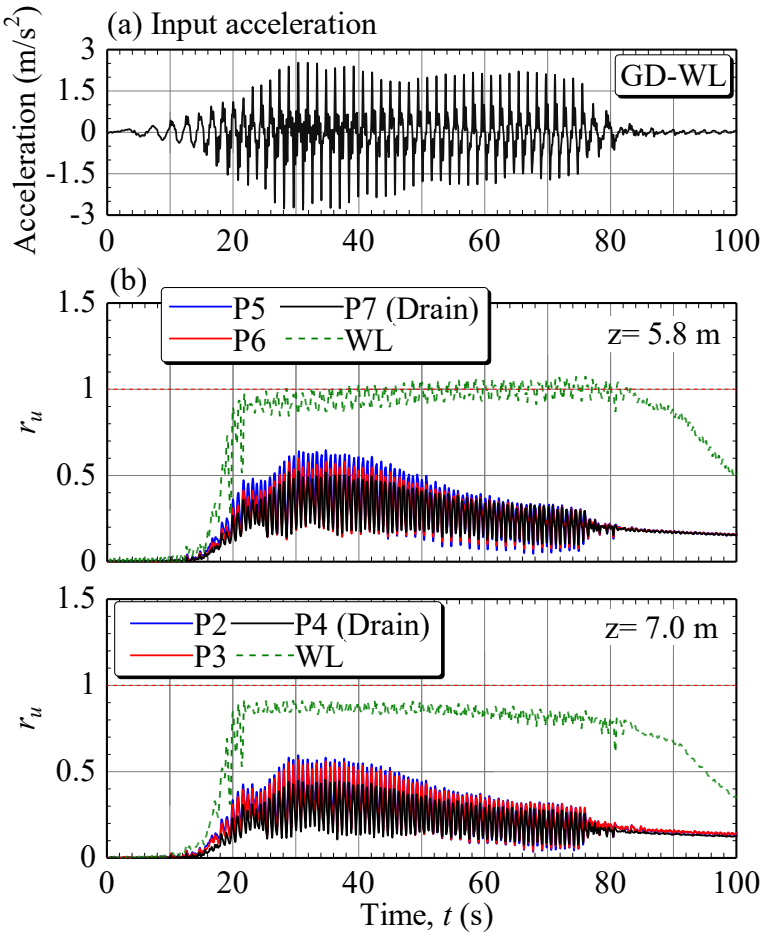

Figure 5.8 Time histories of input acceleration and excess pore pressure in the models with lowered groundwater table (WL, GD-WL)

The relationship between r_{u_max} and time factor, T_l is depicted in Figure 5.9. The other dominant non-dimensional number, L_w, for the models are either 0.02 or 0.08 for the models investigated in this study. Therefore, the estimated r_{u_max} derived from the procedure in the current practice (Onoue, 1988) for L_w= 0.02 and 0.08 are indicated by broken lines in the figure for better comparison. Note that the procedure solves with the equation mentioned in Chapter 1, Eq. (1.1) with consideration of the well resistance. The soil parameters used are summarized in Table 5.1. The overall trend in r_{u_max} from the procedure, which decreases as

T_l increases, agrees with the test results. However, significant differences in r_{u_max} between tests with different groundwater levels, that is, GD-SD and GD-WL, cannot be represented by the procedure. Another important observation in this figure is the depth variation in r_{u_max}. Onoue (1987) examined this variation through numerical simulations and found that differences in the excess pore pressure ratio with depth were mostly less than approximately 0.05, which is the case for the lines in the figure. r_{u_max} derived from the procedure for the two different depth level are practically identical. By contrast, for the tests of GD-BM and GD-SD, r_{u_max} at z= 1.5 m is more than 0.4 higher than that at z= 6 m. The difference in r_{u_max} with depth observed in the tests becomes larger as T_l increases, because r_{u_max} at greater depth decreases with increasing T_l whereas r_{u_max} at the surface stays as unity regardless of T_l. It is concluded that a significantly large variation in r_{u_max} exists with depth in a sand improved with gravel drains, and the height of the groundwater table affects r_{u_max}, both of whose elicitation from the current design procedure are challenging.

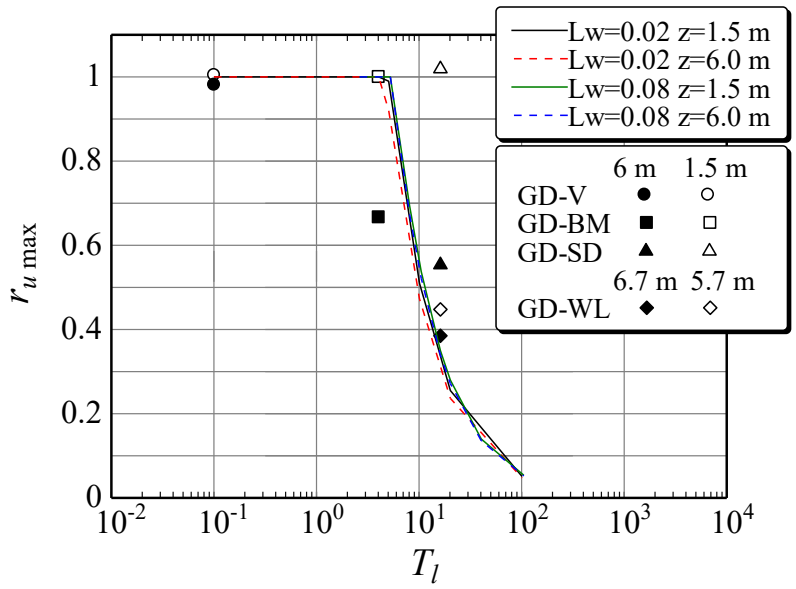

Figure 5.9 Relationships between maximum excess pore pressure ratio and time factor for radial dissipation, T_l

5.4.5 Excess pore pressures in the drain

One of the basic principles of gravel drain design is that gravel does not exhibit volumetric contraction and generate excess pore pressures. To confirm this for the centrifuge tests in this study, an additional centrifuge test, namely GD-C, was conducted. The model was similar to GD-BM (water saturated model with drains of d_w = 1.6 m) in all aspects, except the gravel drains; the gravel drains in GD-C were wrapped with an impermeable flexible plastic sheet to prevent any water inflow from the surrounding sand. The input acceleration time history had the same basic shape as GD-BM.

Time histories of the excess pore pressure in a drain are presented in Figure 5.10. Although fluctuating to some extent, on the order of 0.1, r_u generated in the drain remained quite low. Hence the premise is confirmed for all the tests in this study.

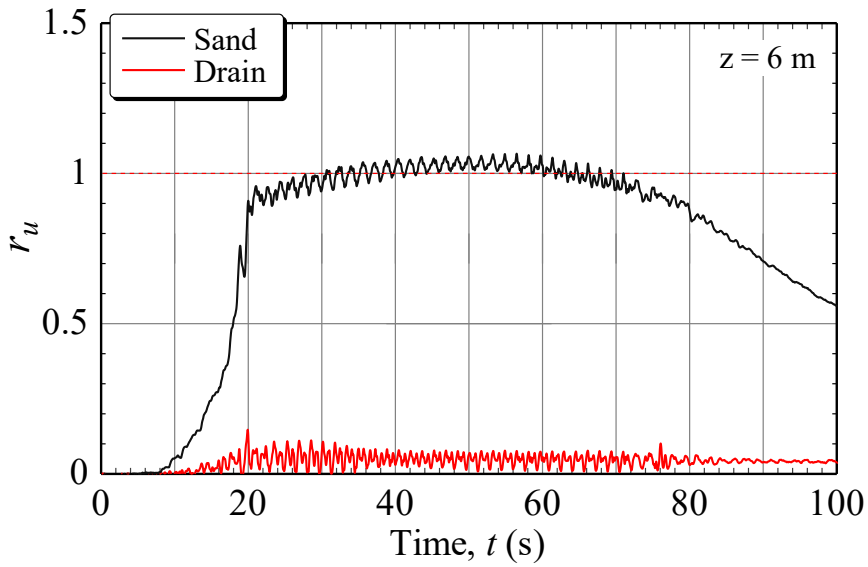

Figure 5.10 Excess pore pressure ratio time history of GD-C

5.4.6 Groundwater level during shaking

It was observed through on-board video cameras that when testing the fully saturated models with drains, pore water flowed out through drains during shaking. Overflowing water during shaking was also observed in a preliminary test with groundwater level 2m below the ground surface. The sand surface was dry prior to shaking, whereas its color around the drains began to darken due to the spilled water wetting the sand sometime after the initiation of shaking. For GD-WL, the sand surface was kept dry throughout the shaking, indicating that the water level rose up but did not reach the surface. Because the rise in water level and thus the pore pressure in the drain obstructs the dissipation of generated excess pore pressure in sand, the water level in the drain during shaking for GD-WL is estimated in this section.

Two cycles moving average of the excess pore pressures (Δu) is illustrated in Figure 5.11, which includes all the pore pressure transducers in the GD-WL together with the settlement of sand surface. The deeper in the model and the farther from the drain, the higher the

generated Δu was at the beginning of the shaking event. Transducers set on the base, P1, show a residual excess pore pressure of 6.8kPa suggesting that the groundwater level rose by approximately 0.7m. Some sensors installed in the sand and drains exhibited slightly higher residual pressure than 6.8kPa due to subsidence of sand and/or transducers, but the readings of all Δu fell within a small range between 6.8 and 8.2kPa. Meanwhile, the differences in Δu among the transducers decreased with time, and when t= 53s, Δu was approximately 22 kPa with small variations.

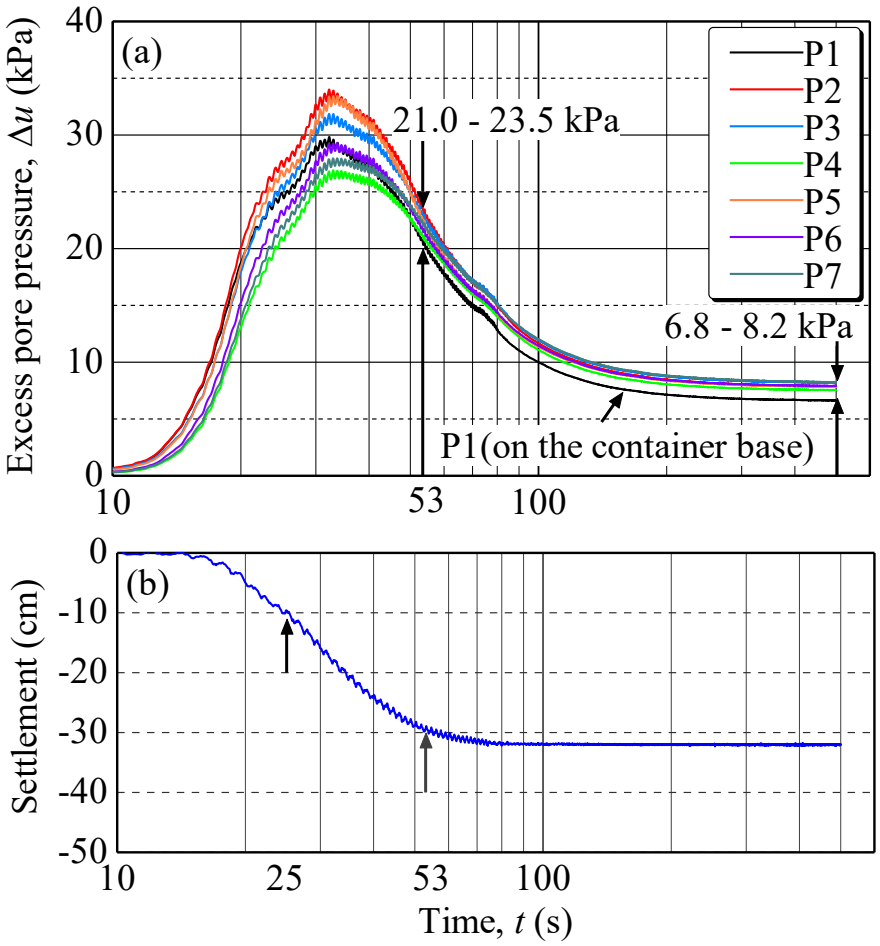

Figure 5.11 Excess pore pressure time histories (a) and settlement of GD-WL (b)

Figure 5.12 schematically illustrates change in the water table during shaking and the

following dissipation phase. During the early shaking stage, the water table in the drain rose due to water that is squeezing out from the sand (evidenced by the settlement), but the water table in the sand remained unchanged because the less permeable unsaturated overlying sand (Figure 5.12(b)). Thereafter, the water level increased further in the drain, allowing some water in the drain and sand to seep into unsaturated sand, which gradually increased the water table of sand. At t= 53s, Δu in the sand and gravel was approximately the same with the minor variations, indicating that the pressures of sand and gravel in the drain in its entirely were almost equalized at Δu= 22kPa (Figure 5.12(c)). After a sufficient amount of time, Δu in sand and gravel fully dissipated; the water table stabilized at GWL -3.25m (Figure 5.12(d)). The settlement behavior of sand surface shown in Figure 5.11(b) is consistent with the Δu observations; surface settlement accumulated in the early stage of shaking and after approximately t= 53s the rate significantly slowed down, indicating that the contraction of sand and generation of excess pore pressure almost ceased. The settlement at t= 21–25s was 10cm which was one-third that at t= 53s. Assuming that the water expelled from sand stayed in the drain, and its volume was proportional to the settlement, the rise in water level in the drain at t= 21–25s was estimated to be 0.75m. This assumption presumably provides the estimated water level conservatively, because water pressure at t= 53s could have been higher than 22kPa if water did not seep into the unsaturated sand.

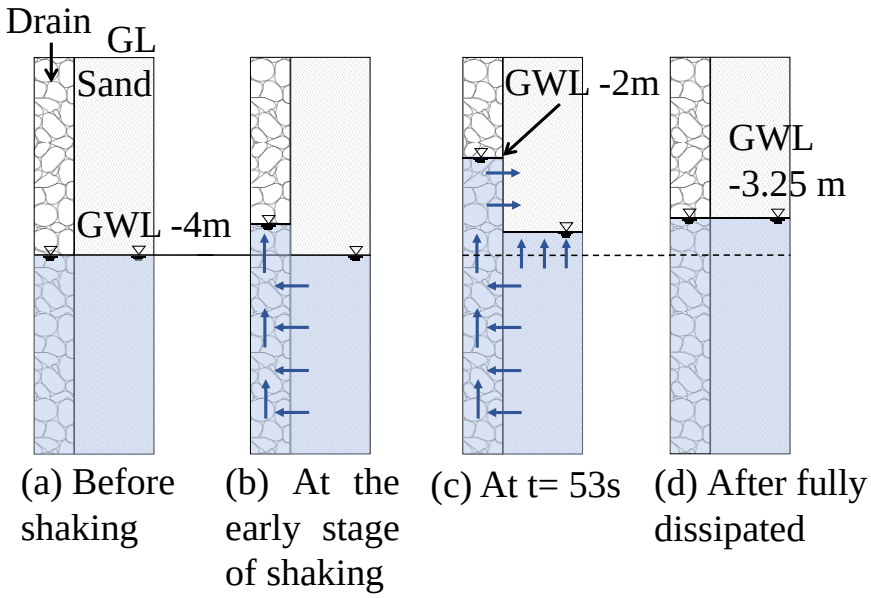

Figure 5.12 Schematic of water level in the drain during shaking for GD-WL

5.5 Numerical simulation

The generation and dissipation of the excess pore pressure of sand as described in Chapter 1 by Eq. (1.1), while the continuity condition along with the periphery of the drain is;

$$\left(\frac{\partial \Delta u}{\partial r}\right)_{r=d_w/2} + \frac{d_w}{4}\frac{k_w}{k_s}\left(\frac{\partial^2 \Delta u}{\partial z^2}\right)_{r=d_w/2} = 0 \qquad (5.3)$$

The generation term in Eq. (1.1), $\partial \Delta u_g / \partial t$, is often expressed by an arcsine function to closely approximate the generation curves observed in triaxial tests (Seed and Booker, 1977; JGS, 2004). In this study, however, a simple linear function was employed to simulate the centrifuge tests. The sand in the models without drains, BM, V and WL, generated r_u almost linearly with time and reached 100% in 4s (see Figure 5.3 and Figure 5.8), therefore, the generation term can be expressed as,

$$\frac{\partial \Delta u_g}{\partial t} = \frac{1}{4}\sigma_{v0}' \quad \text{(kPa/s)} \qquad (5.4)$$

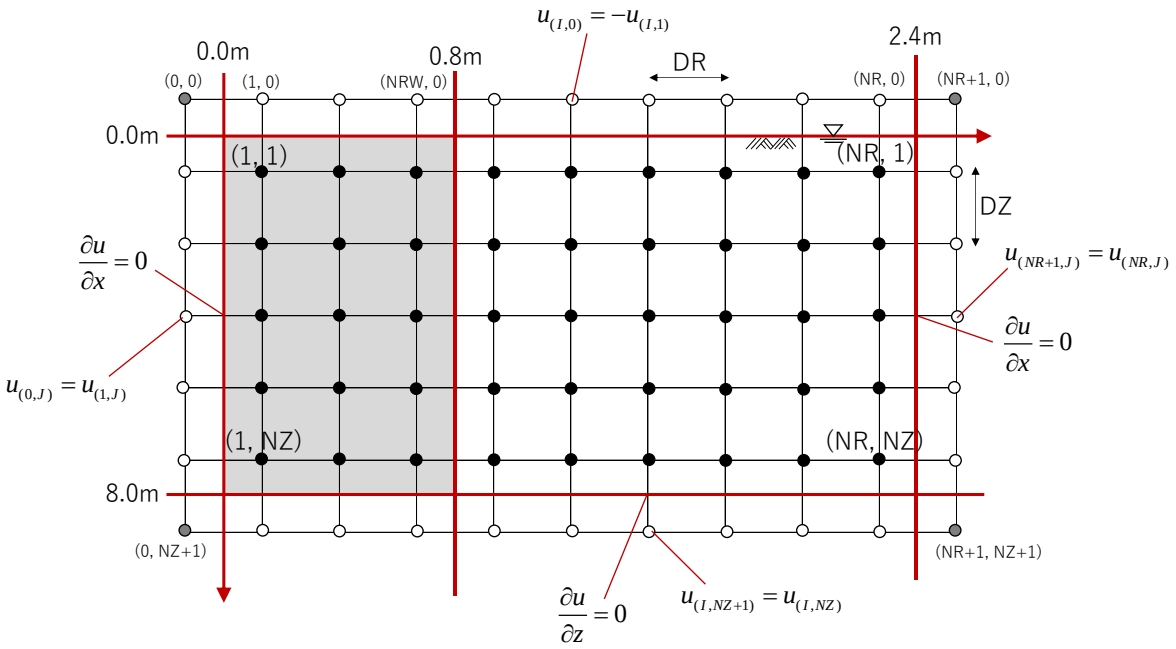

Figure 5.13 Numerical simulation mesh and boundary condition

The Eq. (1.1), (5.3), and (5.4) were solved in a finite difference scheme with the soil parameters obtained from the above-mentioned laboratory tests. The analysis domain was a cylinder with an equivalent diameter, b_e= 2.7m or 5.4m. Coefficients of permeability of sand for vertical and horizontal directions were set independently. Regarding the gravel, since k_w in the simulation is dependent on R_e, several time iterations were needed to reach convergence. Allowing for the anisotropic stress condition in the level ground for K_0= 0.5 and assuming r_u= 0.7, m_v was determined as follows.

$$m_v = -\frac{0.0024}{\sigma_{v0'}}\frac{ln(0.3)}{0.7} \tag{5.5}$$

The boundary condition for numerical simulation is presented in Figure 5.13. The hydraulic gradient across the boundaries is set to be zero at the bottom and the circumference of the domain to represent the no-flow boundary condition. The pore pressure at the ground surface for fully saturated models (GD-BM and GD-SD) is set at zero, while for GD-WL the pore pressure at the surface of the groundwater in the drain (4 m below the ground surface before shaking) was set at 7.5 kPa to account for the conservative estimate of water level in the

drain, as discussed in Sub Chapter 5.4.6.

5.6 Comparison between test results and numerical simulation results

The time histories of Δu in both the sand and drain for the benchmark model GD-BM obtained from the numerical simulation are shown in Figure 5.14 together with test observations at corresponding locations. Δu from the simulation starts to accumulate from t= 16s and reaches plateaus at approximately t= 20s. Δu continues to level off after t= 20s indicating that the generation balances dissipation in the domain, while the plateau did not last long and started to dissipate during the shaking for the test. This is because the contractive volume change of actual sand owing to cyclic shearing gradually ceases as the shearing continues while m_v is assumed constant throughout the shaking in the simulations. Except for this difference in the latter part of shaking, Δu from the simulation compares quite well with that observed in the test.

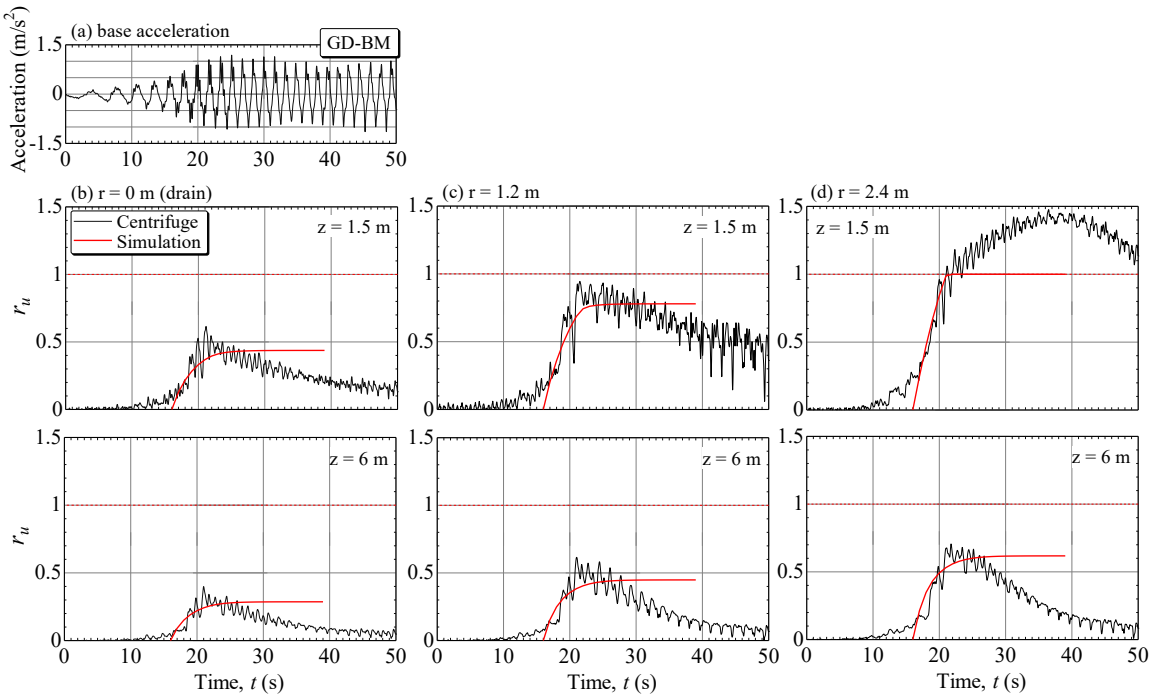

Figure 5.14 Time histories of excess pore pressure ratio for GD-BM

The radial distributions and contours of the maximum excess pore pressure ratio, r_{u_max} are shown in Figure 5.15 and Figure 5.16, respectively. The zone where Δu decreases near the drains and is lower than unity, is limited at the drain perimeter for model GD-V, and extends apart from the drains for water-saturated models, GD-BM and GD-SD, in a similar manner to the tests. Variations in r_{u_max} with depth also agree fairly well with those from the tests. The sand in the fully saturated ground near the ground surface always liquefies irrespective of the drain diameter and the permeability of soils while r_{u_max} at greater depth decreases with increasing soil permeability and drain diameter. Moreover, with regard to the effects of groundwater level, the simulated r_{u_max} for GD-WL compares well with test results. r_{u_max} from the simulation decreases by lowering the ground-water level in a similar way to that observed in the test GD-WL. This is caused by the smaller m_v for GD-WL due to higher effective vertical stress, as well as smaller well resistance due to the shorter length and higher permeability of the drain generated by the lower discharge flow rate.

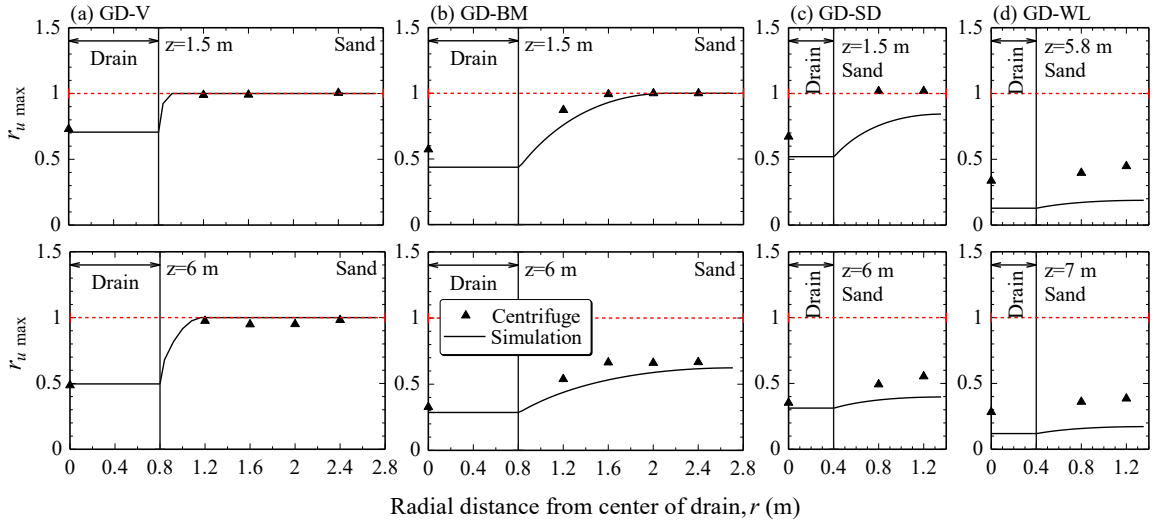

Figure 5.15 Comparisons of radial distributions of r_{u_max} from numerical analysis with those from tests

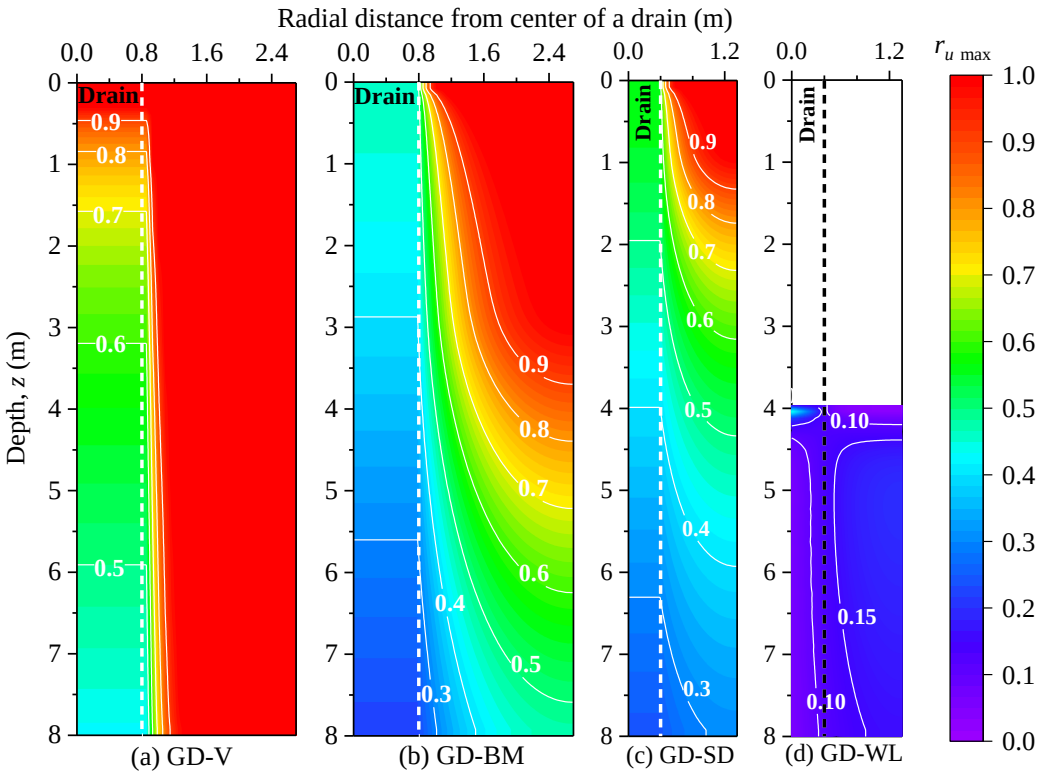

Figure 5.16 Contours of excess pore pressure ratio obtained from numerical simulations

The significant improvement of the numerical simulation for fully saturated models described above is achieved by employing two soil parameters, m_v and k_w. To individually investigate the effects of these parameters, additional numerical simulations were conducted for sets of parameters as follows (summarized in Table 5.3).

Table 5.3 Soils parameters used for numerical simulations

Soil parameter set	Permeability of sand		Permeability of gravel	Coefficient of volume compressibility
	k_{sh} (m/s)	k_{sv} (m/s)	k_w (m/s)	m_v (m^2/MN)
a) Centrifuge Test Condition	1.6×10^{-3}	1.9×10^{-4}	*Re* dependent	Stress level dependent
b) k_{drain} constant	1.6×10^{-3}	1.9×10^{-4}	0.8	Stress level dependent
c) m_v constant	1.6×10^{-3}	1.9×10^{-4}	*Re* dependent	0.03
d) Current design procedure	1.6×10^{-3}	1.9×10^{-4}	0.8	0.03

a) The variations in both k_w and m_v with depth were considered. This was the same parameters set mentioned above.

b) The variation in m_v was considered, while k_w was fixed at $k_w = 8.0\times10^{-1}$m/s.

c) The variation in k_w was considered, while m_v was fixed constant at $m_v = 0.03$m^2/MN.

d) Both k_w and m_v were constant at $k_w = 8.0\times10^{-1}$m/s and $m_v = 0.03$m^2/MN.

Note that the parameter set d) corresponds to the current design procedure.

Profiles of r_{u_max} at the midpoint of drains for the fully saturated model are indicated in Figure 5.17(a) and (b). In the case of d), r_{u_max} increases slightly from the bottom up, because the water volume flow rate as well as the pressure gradient in the drain increase accordingly. When the variation in k_w is considered (type c)), the well resistance effects increased the r_{u_max} slightly over the depth, although r_{u_max} is much lower than the centrifuge test observation.

For type b) simulation where only m_v varied with depth, with m_v being inversely proportional to the depth, r_{u_max} increases significantly and reaches the liquefaction condition near the surface. According to triaxial test results, m_v increases infinitely and the time factor for diffusion, T_l, is zero at the surface of a fully saturated uniform sand. Radial diffusion of excess pore pressure cannot be expected, and liquefaction conditions are inevitable. For type a) simulation, the variation agrees reasonably well with centrifuge tests when the variation of both m_v and k_w are considered. As the water flow rate in the drain increases, the Reynolds number increases accordingly resulting in a decrease in k_w particularly at shallow depths. The influence of the enhanced well resistance due to the turbulent flow in the drain is not limited at shallower depths but extends to the bottom where the flow regime is laminar.

Figure 5.18 depicts the profiles of the Reynolds number and k_w. For GD-BM, the Reynolds number increases from less than unity at the bottom to 140 at the surface. The zone of laminar flow is limited to a depth 0.05 m from the bottom, with k_w degrading to approximately 1/8 at the surface. These observations are also valid for GD-SD, and lead to a conclusion that the significant difference in r_{u_max} with depth is due to the stress level dependency of m_v. Although the degradation in permeability of gravel is significant at shallower depth, its effect on r_{u_max} is not limited to such depth level but extends to all the depth of the domain.

The effects of groundwater level can be observed by comparing GD-SD (Figure 5.17(b)) with GD-WL (Figure 5.17(c)). The simulated r_{u_max} decreases with the lowering of the groundwater level in a similar way to that observed in the tests. The variation in r_{u_max} for GD-WL is largely uniform along the depth. In this case, the hydraulic gradient near the water table is much higher than that of the fully saturated models, which results in a dramatic reduction in the well resistance; excess pore pressure in the drain is kept low. The effects of variations in m_v and k_w on r_{u_max} are less noticeable.

The simulation results for two boundary conditions at the groundwater table are shown in Figure 5.17(c); one is the pore pressure of 7.5 kPa at a depth of z= 4 m, whereas the other is zero. It appears that the pressure set at the boundary pushes the simulated r_{u_max} on the right-hand side in this figure as the same quantity at all depths. It is a common design practice that the pore pressure is assumed to be zero at the boundary of the groundwater table; however, consideration of the rise in water level during shaking is important.

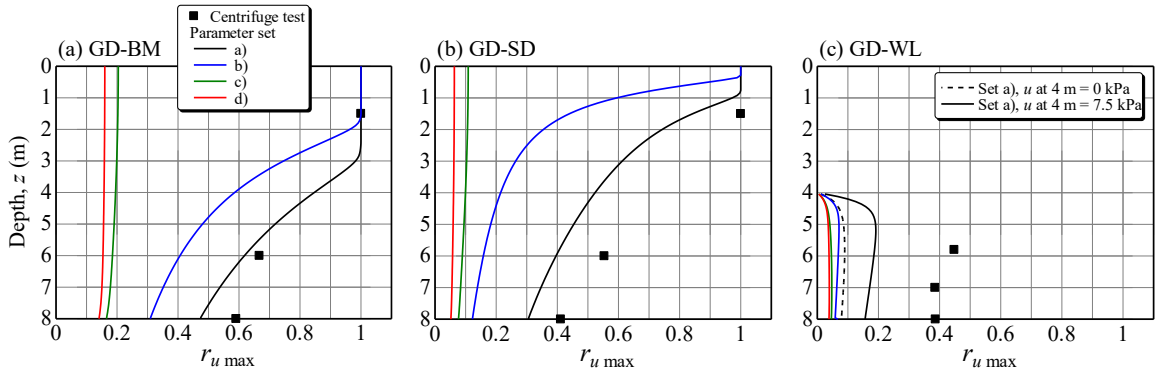

Figure 5.17 Vertical profiles of r_{u_max} for different sets of soil parameters

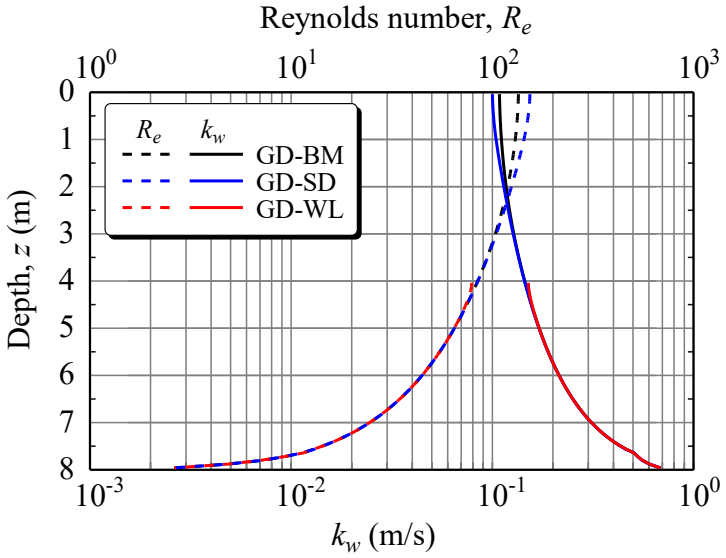

Figure 5.18 Vertical profiles of R_e and k_w in gravel drains

5.7 Conclusions

In this chapter, a series of dynamic centrifuge tests were performed to evaluate the effect of permeability and drain diameter on the performance of gravel drain applied to uniform sand deposits to reduce the excess pore pressure as liquefaction prevention. The permeability effect on the gravel drain performance was analyzed first by varying 40 times different permeability at two tests. Permeability of sand layer concluded to be one of the important

parameters that has a significant influence on gravel drain performance. It could not prevent the liquefaction occurrence when the permeability of the sand is very low. Gravel drains were effective in reducing the excess pore water pressure ratio at greater depths for the test with higher permeability. Further, the effect of the number of gravel drain installed was observed with a constant improvement ratio. The tests with different drain diameter were conducted and the pore pressure response was compared. It was found that the greater number of gravel drains with the smaller diameter of drain, the dissipation time of excess pore water pressure was shortened. Even though at the shallower depth, excess pore pressure ratio still reached 100%. The groundwater level effect was further examined through the test and showed a very significant improvement in lowering the excess pore pressure ratio. Lowering groundwater level was supposed to increase the effective stress of the soil, which was found effective in the process of diffusion of pore water pressure.

The effect of mechanical properties of the soil on the performance of the gravel drain to avert the risk of liquefaction were studied through a numerical simulation based on current design procedure of the gravel drain. Not only the permeability but the flow regime in the drain was considered in the simulation as well as the coefficient of volume compressibility of the soil. The constant m_v assumption that has been adopted in the design procedure, overestimated the effectiveness of the drain. It was found that m_v need to be considered as the stress-dependent function in order to simulate actual behavior of the soil layer. The turbulent flow that was found in the drain, contributed to higher resistance of the drainage to dissipate the excess pore pressure.

Chapter 6

Settlement on the Ground Improved with Gravel Drain

6.1 Introduction

Settlement of ground improved with gravel drains is one of the issues raised by many researchers. Excessive settlement might occur due to dissipation of excess pore pressure generated during earthquakes through vertical drains although the improved ground was considered non-liquefied. The improved ground in Rokko island and Port Island hit by the 1995 Kobe Earthquake (Yasuda et al. 1996), in Shiogama port hit by the 2011 Tohoku earthquake as well as shaking table tests (e.g. Sasaki and Taniguchi. 1982; Unno et al. 2014) were the case. These field case histories and model test observations are, however, contradictory to the accumulated knowledge that volumetric strain of sand after dissipation of excess pore pressure generated by undrained or partially drained cyclic shearing is very small as long as the sand does not reach the liquefaction condition. The settlement observed in the tests in this study is approximately promotional to the depth of liquefied sand. The excessive settlement was probably caused by liquefaction of soil at shallower depth of improved ground; the vertical drains designed and implemented in the sites were effective to prevented soil to liquefy at greater depth which reduced the depth of liquefied sand but could not prevent triggering at shallower depth. In fact, Yasuda et al. (1996) reported that settlement in the zone with vertical drain implemented, typically ranging between 0 and 40 cm, was considerably smaller than that in the adjacent non-improved zone, 0 - 95cm. Tokimatsu and Seed (1987) were also estimated the settlement of the soil based on CSR and proposed a simplified method for saturated and unsaturated sands.

6.2 Observed settlements in centrifuge tests

Settlements of the sand surface in the centrifuge test were observed based on surface measurement at several locations after the tests. The average values of measured height of the sand surface after the tests at more than 10 locations are used in this chapter to discuss the settlement behavior. The locations of measurement did not include the drain. Settlement during increasing centrifuge acceleration from 1g to 40g is being considered so that the settlement data is derived only due to the earthquake shaking.

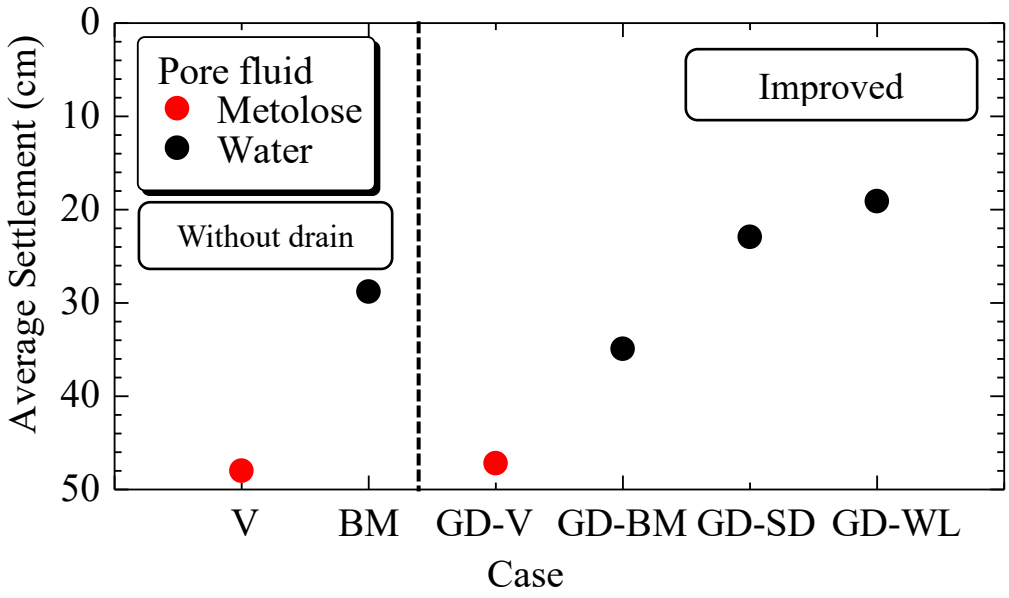

Figure 6.1 Settlement observed from each model of centrifuge tests

Figure 6.1 shows the average settlement for each model due to the shaking event. The model with lower permeability (saturated with viscous fluid) indicated with red dots implemented significant settlement occurrence compare with the other models. The large settlement was inevitable even in the case improved with gravel drain. Settlement was observed 48 cm and 30 cm in the case without drain, V and BM, respectively. In the models improved with larger

diameter drain (GD-BM), which conducted in the same manner with benchmark model BM, the settlement is not improved. The settlement was measured 35 cm, even at the liquefaction did not occurred in the entire sand layer as discussed in the previous chapter. For the model with smaller diameter, settlement was found reduced to 22 cm. Furthermore, the smallest settlement was observed in the model with lower groundwater level, as measured 19 cm. In this case, the liquefaction did not occur and the excess pore pressure in the shallower depth has maintained low. However, it did not prevent the settlement occurrence.

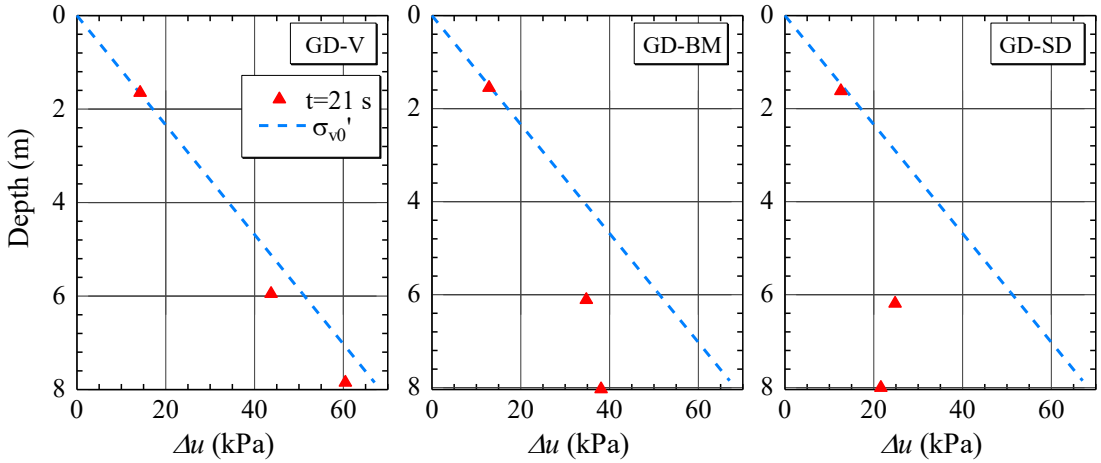

Figure 6.2 Vertical distribution of maximum *Δu*

Vertical distribution of maximum excess pore pressure of the fully saturated model was shown in Figure 6.2. The distribution was obtained along the midpoints between drains at t= 20 – 21 s when the excess pore pressure attained the maximum value. It is observed that *Δu* is higher at the deeper depth which should propagated upward and make the overlying soil liquefy. To estimate the depth of liquefied layer, *Δu* observed at depth of 6 m is extended vertically upward and the depth of the intersection with the initial effective stress line is regarded as the bottom of liquefied sand.

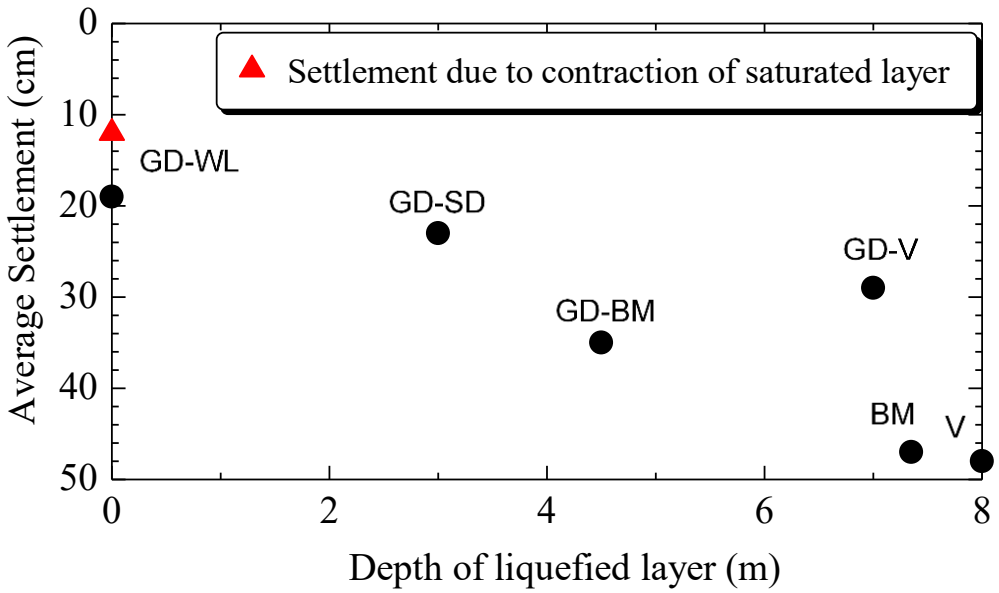

Figure 6.3 Relationship between depth of liquefied layer with settlement

The relationship between the depth of liquefied sand and the settlement is presented in Figure 6.3. The settlement was found approximately proportional to the depth of liquefied sand. This behavior may associated with the volumetric change characteristics of sand. Volumetric strain of sand during cyclic loading is limited if the maximum generated excess pore pressure is lower than approximately 80% and suddenly increase if the sand liquefies and rearrangement of soil fabric occurs (Ohno et al. 1983). It is evident from the figure that settlement is dominated by the thickness of the liquefaction layer.

6.3 Drained triaxial test for the settlement prediction

An attempt has been made to understand the volume change characteristic of the liquefiable sand. The test was conducted in the similar manner with the undrained triaxial testing as mentioned in Chapter 4 except during the cyclic loading the drain valve is open to allow the

water drain from the sample. Drained triaxial cyclic test results comparison is presented in Figure 6.4 below.

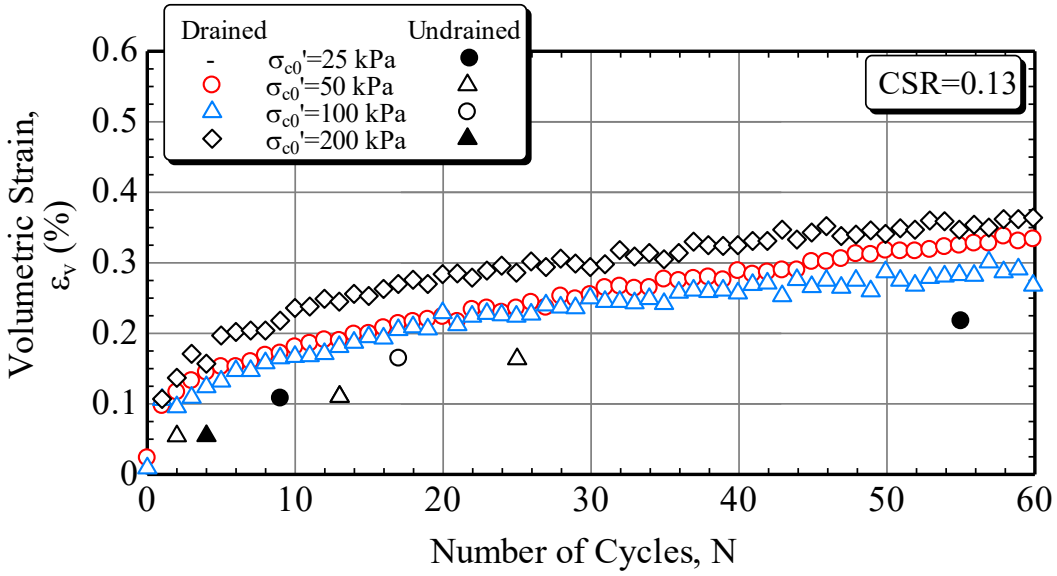

Figure 6.4 Volumetric strain comparison between undrained and drained triaxial cyclic test results

In the test with the same cyclic stress ratio, volumetric strain results obtained from drained and undrained triaxial cyclic test are independent from confining stress. Volumetric strain behaviour of undrained and drained test is happened to be in a narrow difference for the non-liquefied soil case (volumetric strain less than 1%).

Figure 6.5 shows the results of volumetric strain obtained from drained cyclic triaxial tests at different cyclic stress ratio. These tests are aimed to observe the volume change characteristic of the soil under strong shaking. Volumetric strain is increase as higher cyclic stress ratio is applied. Volumetric strain is significantly rise at the small number of cycles and level out when the number of cycles is large. This behavior shows the condition when the soil initiated the liquefaction within a very small cycles and continue to liquefy due to a higher cyclic stress ratio which correspond to strong earthquake imparted.

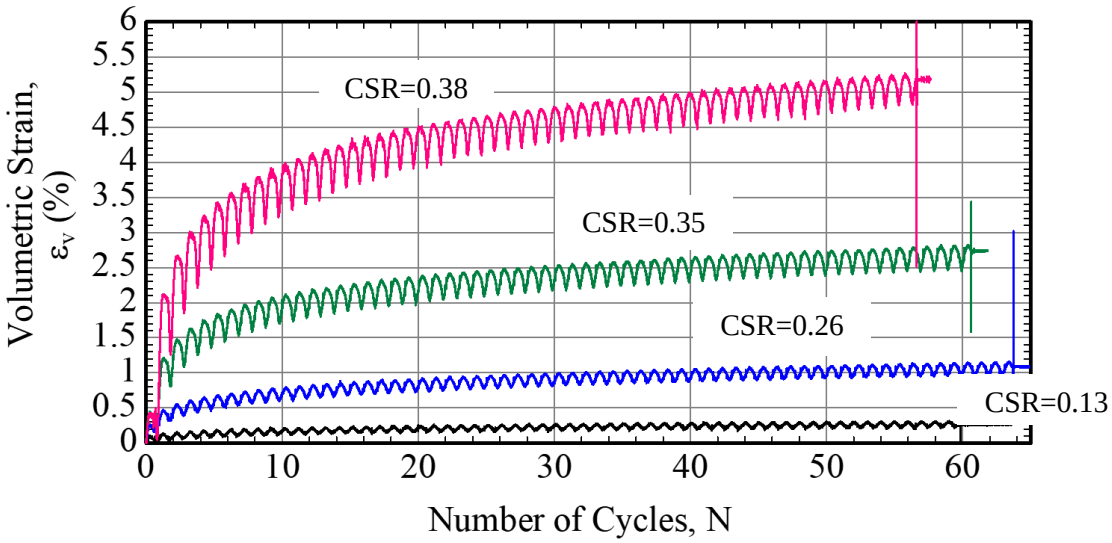

Figure 6.5 Volumetric strain of drained cyclic triaxial test at different CSR

Comparison of volumetric strain measured from drained cyclic triaxial test and centrifuge test as well as measured settlement in the centrifuge tests are shown in Figure 6.6. Cylic stress ratio in the centrifuge test is obtained based on Finn (2002), then volumetric strain and settlement were plotted. Volumetric strain results from cyclic triaxial tests are higher than the centrifuge test results at the same cyclic stress ratio. Note that the measured settlements in the centrifuge test were obtained from the average subsidence of ground surface after the shaking end. However, the settlement occurred is around 20 – 50 cm corresponding to 3 – 4 % volumetric strain. Lee and Albaisa (1974) have found that expected settlement of non-liquefied soil is less than 0.5% and for liquefied soil is 1-4%. The results found in this research shows the similar behavior. Even though the

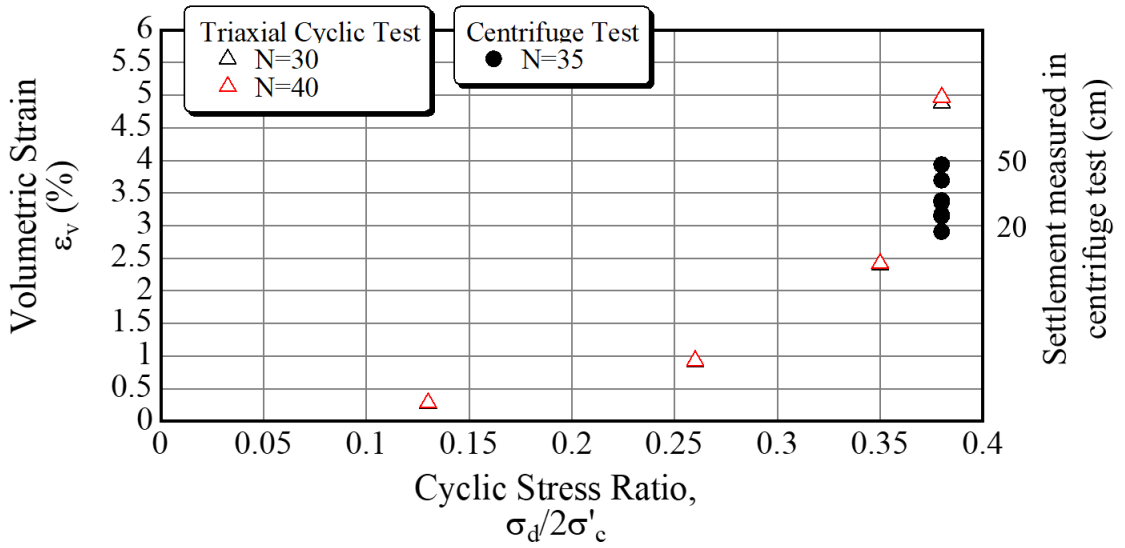

Figure 6.6 Volumetric strain and measured settlement relationship with cyclic stress ratio

6.4 Conclusion

In this chapter, analysis of settlement occurrence in the centrifuge test was presented. Drained cyclic triaxial tests were also conducted to study the behavior of volumetric strain in high cyclic stress ratio. It was found that there is always ground settlement occurred even the excess pore pressure ratio is kept low due to the effect of the drainage. These centrifuge results partly support the hypothesis that excessive settlement observed in the ground improved with vertical drains such as that in Kobe earthquake in 1995, Tohoku earthquake in 2011 and shaking table tests may be owing to the liquefaction of soil at shallower depth, which was supposed not to be liquefied in the design with the used of constant m_v irrespective of depth. It also confirms that non-negligible settlement may occur even though the excess pore pressure ratio is maintained at lower level by the gravel drains.

Chapter 7

Summary and Conclusions

7.1 Summary

In this dissertation, an attempt was made to investigate the effectiveness of gravel drain to prevent liquefaction and to validate the current design procedure of the gravel drain through a series of element tests and centrifuge tests. Several factors affecting the performance of the drain were analyzed. The effects of gravel drains on suppressing excess pore pressure accumulation in liquefiable soils during earthquakes was investigated with a focus on the remediated sand behavior dependent on the stress level. Because the current design procedure of drains has not been sufficiently verified, a series of centrifuge tests were conducted to gain insight into the stress-dependent behavior of loose sand deposits with level surface that was improved with gravel drains. The mechanical properties of the soils used in the tests were also examined and used in numerical simulations for excess pore pressure predictions. Experimental data were used to validate the current design procedures.

Ground settlement in the centrifuge tests were observed based on surface measurement. The depth of liquefaction layer was determined from the vertical profile of maximum excess pore pressure ratio. Drained triaxial cyclic tests were performed to obtain the volumetric strain behavior of sand under strong shaking and relationship between the volumetric strain and settlement was the established to predict the settlement occurrence.

7.2 Conclusions

The major findings of the first part of this study can be summarized as follows.

1. For a fully submerged uniform liquefiable sand deposit, the implementation of gravel drains can suppress the accumulation of excess pore pressure during earthquakes. The effect of the lowering excess pore pressure ratio becomes more significant with depth. By contrast, near the ground surface where effective stress is very small, the effect is minimal and liquefaction is inevitable regardless of the drain spacing.
2. Groundwater level also has significant effects on the dissipation of the excess pore pressure ratio. The lower the groundwater level and thus the higher the initial effective stress is, the faster the excess pore pressure diffusion becomes.
3. The current design procedure fails to appropriately elucidate these responses of soils improved with gravel drains, which includes a significantly large variation in r_{u_max} with depth and effects of the height of groundwater table on r_{u_max}.
4. In current design procedure, m_v is assumed to be constant. This assumption, however, could significantly underestimate the volume of water to be squeezed out from soil at shallower depths, and thus overestimate the effects of drains (on the unsafe side). Conversely, it underestimates the effects of drains at greater depths.
5. Although the water flow regime in soils is usually assumed to be laminar, it can be a turbulent flow in gravel drains, resulting in more significant well resistance than that predicted from the current design procedure.
6. The axisymmetric diffusion equation with consideration of well resistance appropriately predicts the excess pore pressures in sand with gravel drain when the stress level dependent m_v and Reynolds number dependent k_w are utilized for input soil parameters.
7. Water level in the drain during shaking significantly affects r_{u_max} when the groundwater table is lower than the ground surface. The water level rise in the drain appears to degrade the effectiveness of the drainage ability of wells, which should be considered in the design.

8. Excessive settlement observed in the ground improved with vertical drains in past earthquake was partly due to the liquefaction of soil at shallower depth, which was not supposed to liquefy in the design procedure with the assumption of m_v irrespective of the depth.
9. Settlement of ground surface increased with the depth of liquefied layer. Even for the model with lowered groundwater table, which did not liquefy at any depth, still demonstrate noticeable subsidence.

References

Adalier, K., Elgamal, A., 2004. Mitigation of Liquefaction and Associated Ground Deformations by Stone Columns. Eng. Geol. 72, 275–291. doi:10.1016/j.enggeo.2003.11.001

Baez, J. I. and Martin, G. R. 1995. Permeability and shear wave velocity of vibro-replacement stone columns. Soil Improvement for Earthquake Hazard Mitigation. Geotechnical Special Publication No 49, American Society of Civil Engineers ASCE, New York, pp. 66-81.

Brennan, A.J., and Madabhushi, S.P.G., 2002. Effectiveness of vertical drains in mitigation of liquefaction. Soil Dyn. Earthquake Eng. 22, 1059-1065.

Brennan, A.J., and Madabhushi, S.P.G., 2006. Liquefaction remediation by vertical drains with varying penetration depths. Soil Dyn. Earthquake Eng. 26, 469-475.

Bouckovalas G. D., Dimitriadi V., Tsiapas Y., Tsioulou A., (2011a). Numerical simulation of drain performance in liquefiable soils, Proceedings, 5th International Conference on Earthquake Geotechnical Engineering, January 10 –13,Santiago,Chile.

Budhu, M. (2015). Soil mechanics fundamentals. John Wiley & Sons, United Kingdom.

Casagrande, A., 1975. Liquefaction and Cyclic Deformation of Sands: a Critical Review, Harvard Soil Mechanics Series No.88.

Castro, G., Enos, J.L., France, J.W., Poulos, S.J., 1982. Liquefaction Induced by Cyclic Loading, National Science Foundation. Washington, D.C.

Finn, W. 1981. Liquefaction potential: developments since 1976, Proc. Int. Conf. Recent Advances in Geotechnical Earthquake Engineering and Soil Dynamics, 2: 655–681.

Freeze, R.A., and Cherry, J.A., 1979. Groundwater. Prentice-Hall, Inc., Englewood Cliffs. NJ.

Garcia-Torres, S., and Madabhushi, S.P.G., 2018. Earthquake-induced liquefaction mitigation under existing buildings using drains. Proc. Int. Conf. Physical Modelling in Geotechnics. 1181-1186.

Howell, R., Rathje, E., Kamai, R., and Boulanger, R., 2012. Centrifuge modeling of prefabricated vertical drains for liquefaction remediation. J. Geotech. Geoenviron. Eng. 138(3), 262-271.

Iai, S., Koizumi, K., Noda, S., Tsuchida, H., 1988. Large scale model tests and analysis of gravel drains. Proc. 9th WCEE. 261-266.

Ishihara, K., 1996. Soil Behaviour in Earthquake Geotechnics, Oxford Engineering Science Series 46. Clarendo Press, Oxford.

Ishihara, K., Tatsuoka, F., Yasuda, S., 1975. Undrained Deformation and Liquefaction of Sand under Cyclic Stresses. Soils Found. Japanese Soc. Soil Mech. Found. Eng. 15, 29–44.

Ishihara, K. and Yoshimine M. 1992. Evaluation of settlements in sand deposits following liquefaction during earthquakes. Soils and Foundations, 32(1): 173–188.

Japanese Geotechnical Society, 1998. Remedial measures against soil liquefaction, from investigation and design to implementation. A.A. Balkema. Rotterdam. Netherland.

Japanese Geotechnical Society, 2004. Remedial measures against soil liquefaction. Maruzen. Tokyo. Japan. (in Japanese)

Kimura, T., Takemura, J., Hiro-oka, A., Okamura, M., and Matsuda, T., 1996. Countermeasures against liquefaction of sand deposits with structures. Proc. First Int. Conf. Earthquake Geotech. Eng. 1203-1024.

Kokusho, T., 1999. Formation of water film in liquefied sand and its effect on lateral spread, J. Geotech. Geoenviron. Eng. ASCE 125 (10), 817-826.

Kokusho, T. 2015. Liquefaction Research by Laboratory Tests versus In Situ Behavior. Proc. 6th International Conference on Earthquake Geotechnical Engineering, Christchurch, New Zealand. 786-819.

Kramer, S.L., 1996. Geotechnical Earthquake Engineering. Prentice-Hall, Inc., Upper Saddle River, NJ 07458.

Lee, K., and Albaisa, A., 1974. Earthquake induced settlements in saturated sands. J. Geotech. Eng. Div. ASCE. 100(GT4), 387-406.

Onoue, A., Mori, N., and Takano, J., 1987. In-situ experiment and analysis on well resistance of gravel drains. Soils Found. 27(2), 42-60.

Onoue, A., 1988. Diagrams considering well resistance for designing spacing ratio of gravel drains. Soils Found. 28(3), 160-168.

Okamura, M., Noguchi, K., 2009. Liquefaction Resistance of Unsaturated non Plastic Silt. Soils Found. Japanese Geotech. Soc. 49, 221–229.

Okamura, M., Soga, Y., 2006. Effects of Pore Fluid Compressibility on Liquefaction Resistance of Partially Saturated Sand. Soils Found. Japanese Geotech. Soc. 46, 695–700.

Pestana, J.M., Hunt, C.E. and Goughnour, KR. (1997). "FEQDrain: A finite element computer program for the analysis of the earthquake generation and dissipation of pore water pressure in layered sand deposits with vertical drains," Earthquake Engineering Research Center, Report No. \JCB/EERC 97-17

Rasouli, R., Towhata, I., and Akima T., 2016. Experimental evaluation of drainage pipes as a mitigation against liquefaction-induced settlement of structures. J. Geotech. Geoenviron. Eng. 142(9), 04016041-1 – 04016041-11.

Sasaki, Y., and Taniguchi, E., 1982. Shaking table tests on gravel drains to prevent liquefaction of sand deposits. Soils Found. 22(3), 1-14.

Seed, H., and Booker, J., 1977. Stabilization of potentially liquefiable sand deposits using gravel drains. J. Geotech. Eng. Div. ASCE. 103(GT7), 757-768.

Seed, H.B., Idriss, I.M., 1971. Simplified Procedure for Evaluating Soil Liquefaction Potential. J. Soil Mech. Found. Devision, Proocedings Am. Soc. Civ. Eng. 97, 1249–1273.

Silver, M. L., and Seed, H. B. (1971) Volume Changes in Sands during cyclic loading. Journal of Soil Mechanics and Foundations Division. 97(SM9), 1171-1182.

Tanaka, Y., 1987. A method to calculate excess pore pressures and surface settlements of the ground improved by gravel piles. Proc. of JSCE No.288/III-8, 23-32. (in Japanese)

Tomizawa, A., Sasaki, T., Ishihara, M., Sasaki, T., 2018. Dynamic centrifuge tests on countermeasure of gravel drain against liquefaction of river embankment. Proc. 53rd Japan National Conf. Geotech. Eng. 1923-1924. (in Japanese)

Unno, T., Hayashi, K., Oono, Y., Asanuma, T., Sento, N., and Uzuoka, R., 2014. Seismic deformation of improved ground with drainage during larger excess pore water pressure generation than the design value. J. JSCE, Ser C, 70(1), 67-82. (in Japanese)

Yasuda, S., Ishihara, K., Harada, K., and Shinkawa, N., 1996. Effect of soil improvement on ground subsidence due to liquefaction. Special Issue Soils Found. 99-107.

Appendix-A

Record of Cyclic Triaxial Tests

σ_{c0}' kPa	r_u					
	≈0.3		≈0.5		≈0.7	
	Dr (%)	CSR	Dr (%)	CSR	Dr (%)	CSR
25	58	0.1	58	0.13	58	0.12
50	59	0.13	59	0.13	58	0.13
100	60	0.1	61	0.13	60	0.13
200	61	0.13	61	0.13	61	0.13
100	59	0.1	-	-	-	-
100	58	0.13	-	-	-	-
100	59	0.132	-	-	-	-

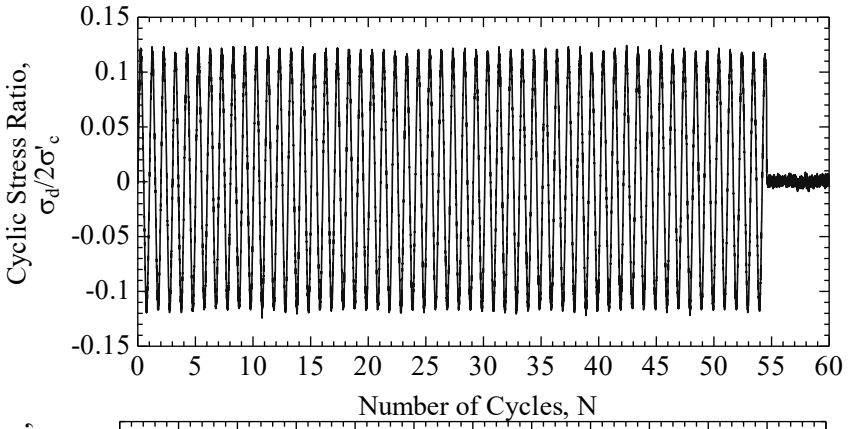

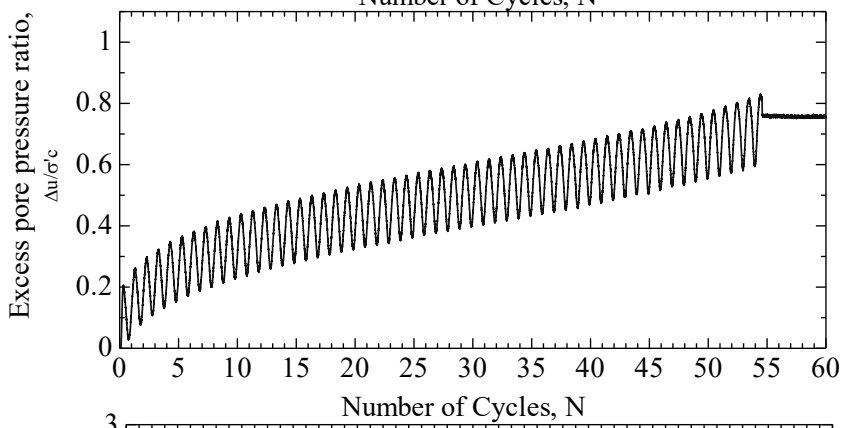

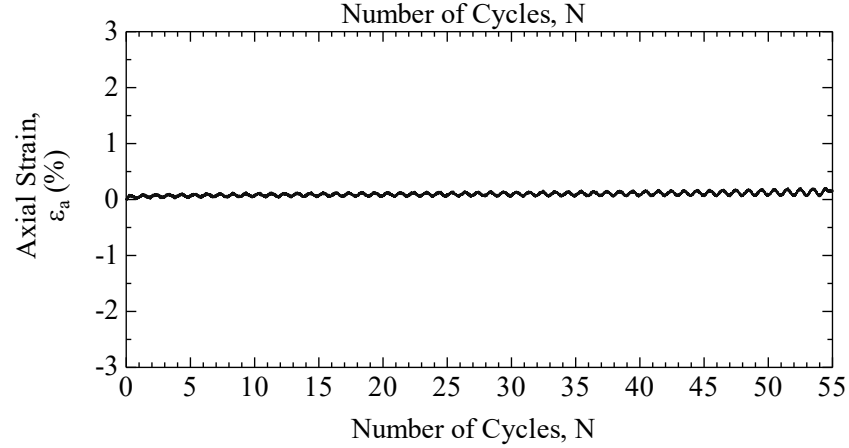

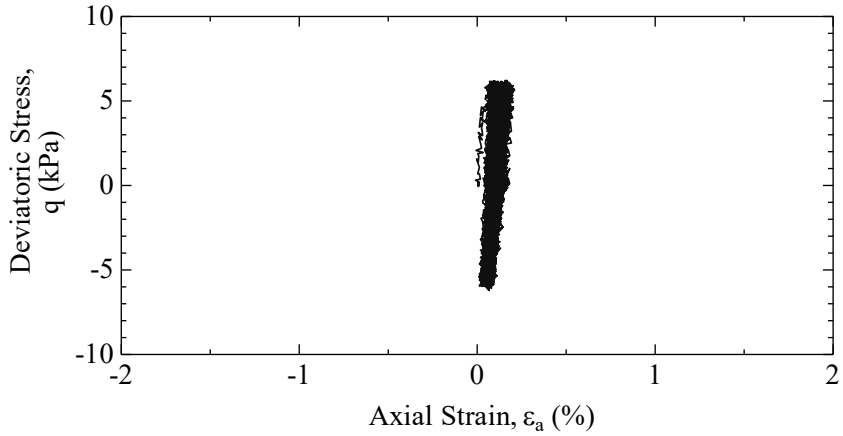

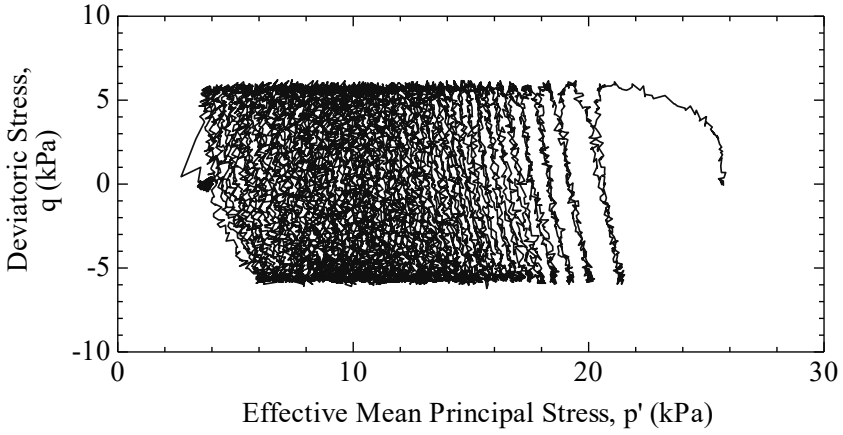

σ'_c=25 kPa

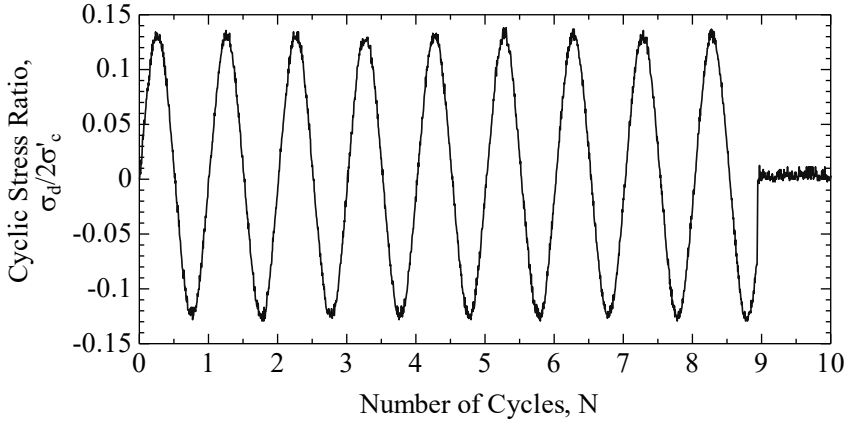

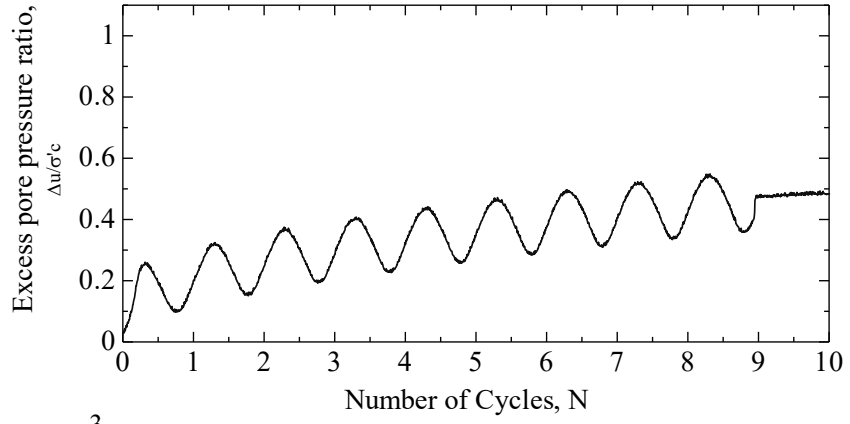

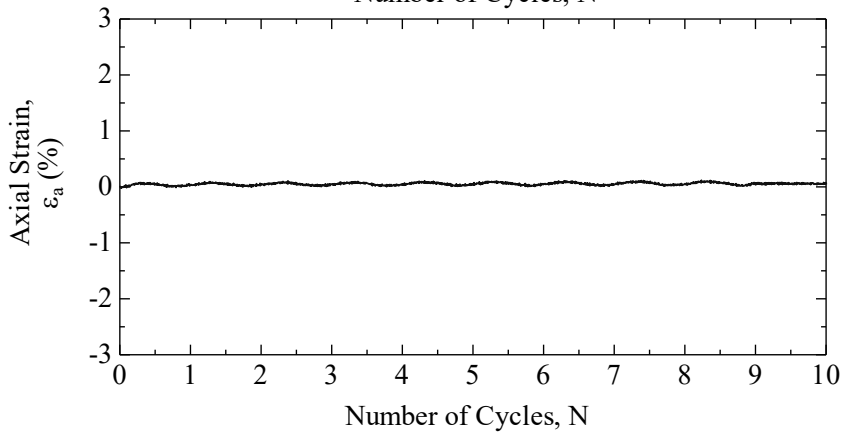

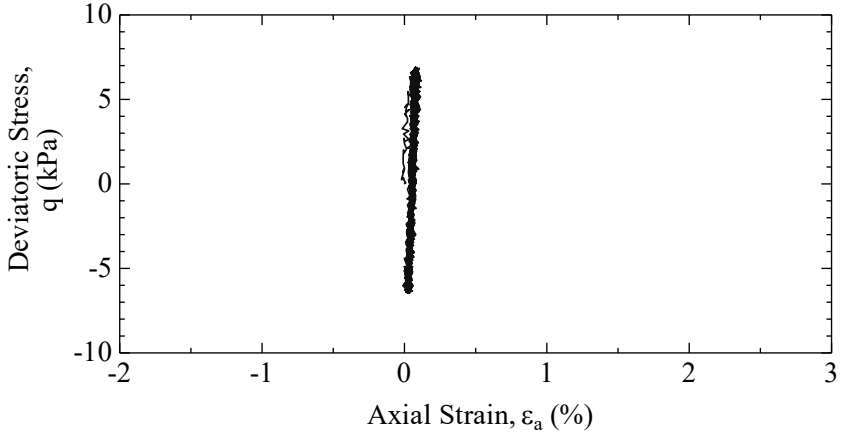

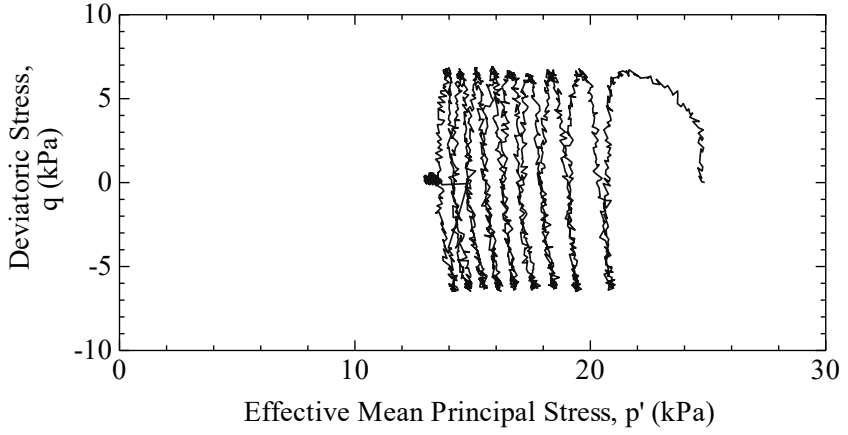

σ'_c=25 kPa

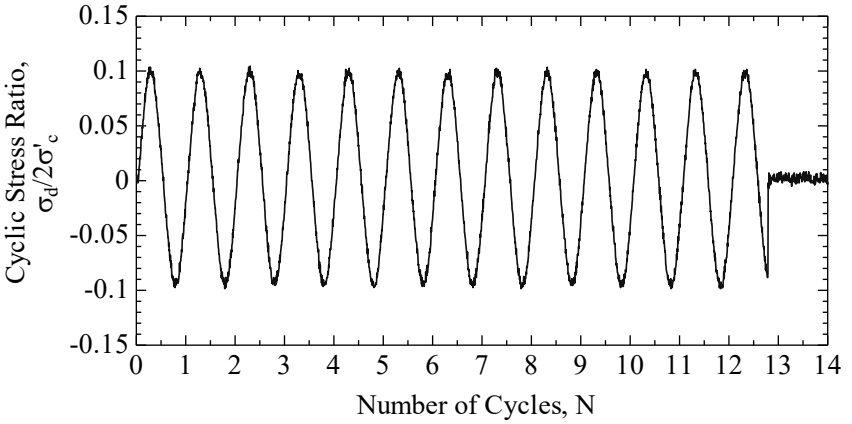

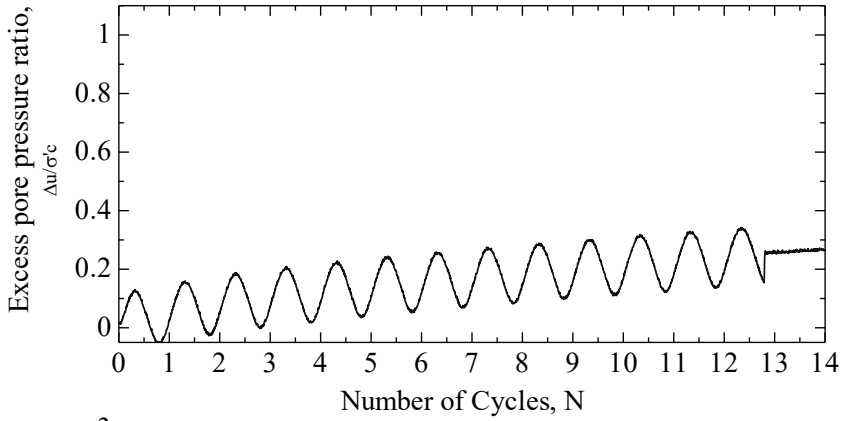

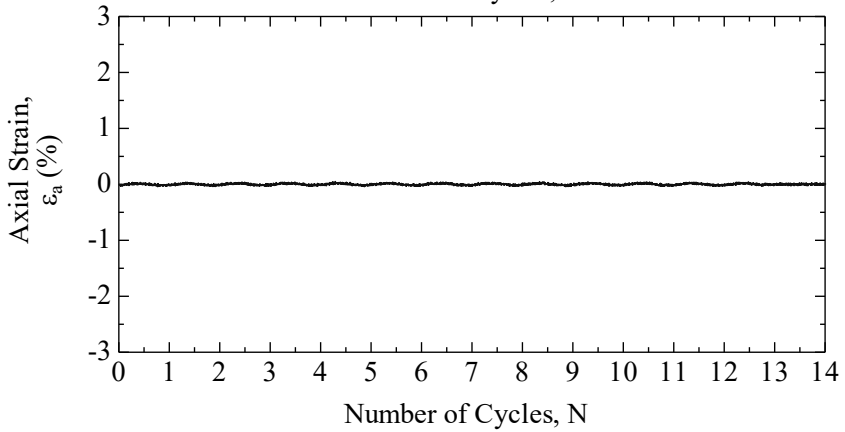

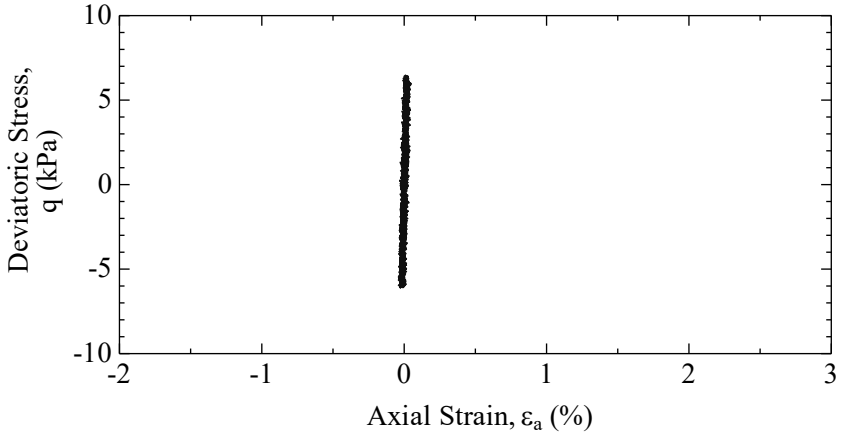

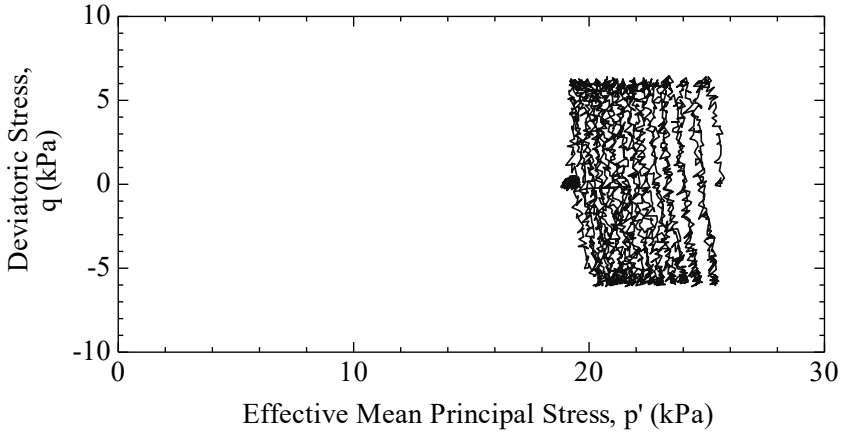

σ'_c=25 kPa

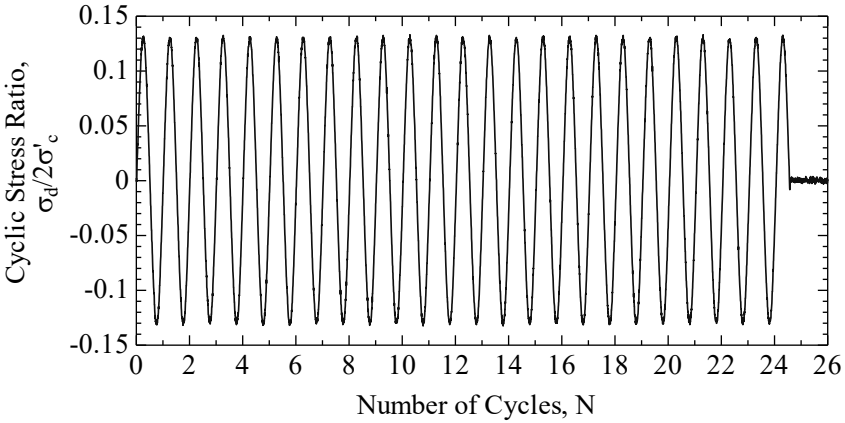

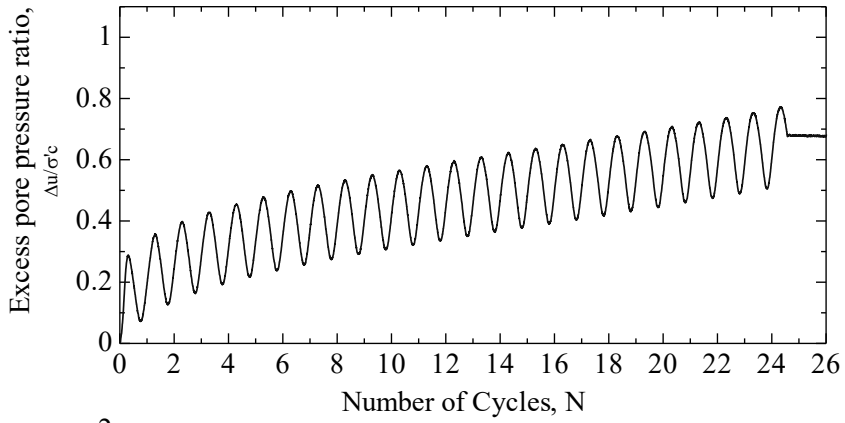

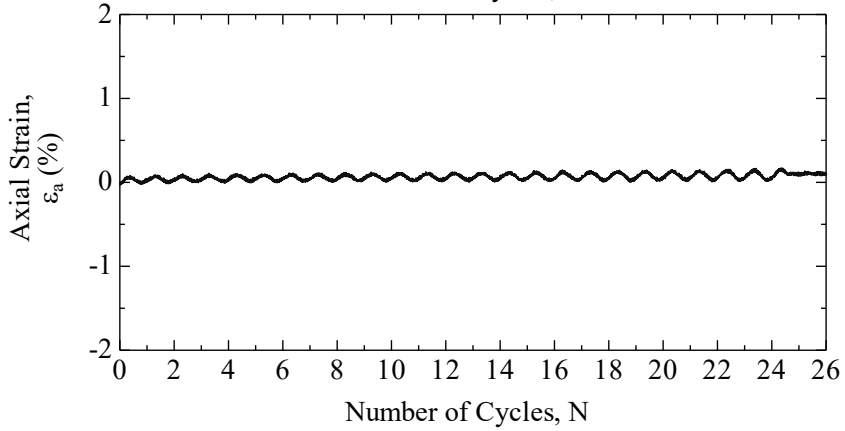

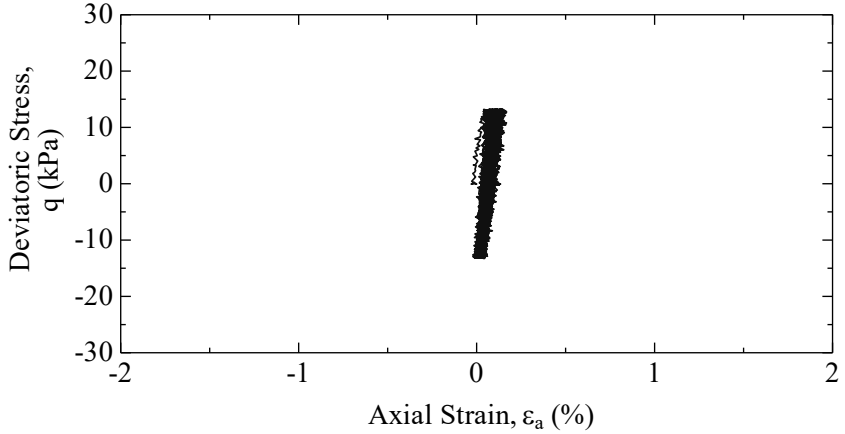

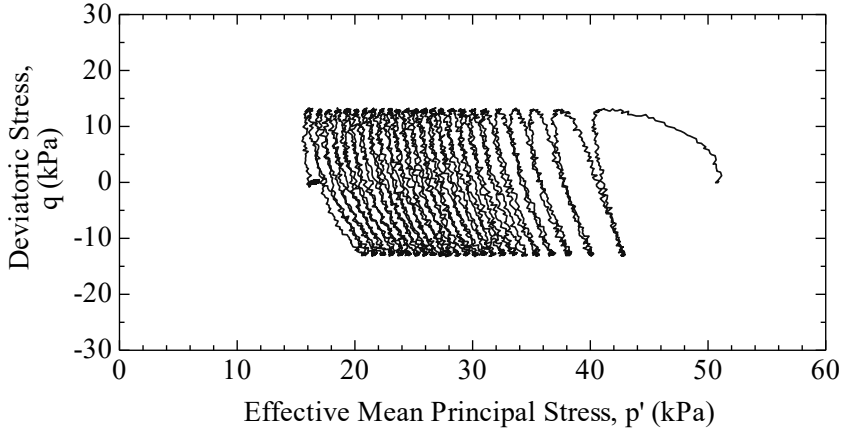

σ'_c=50 kPa

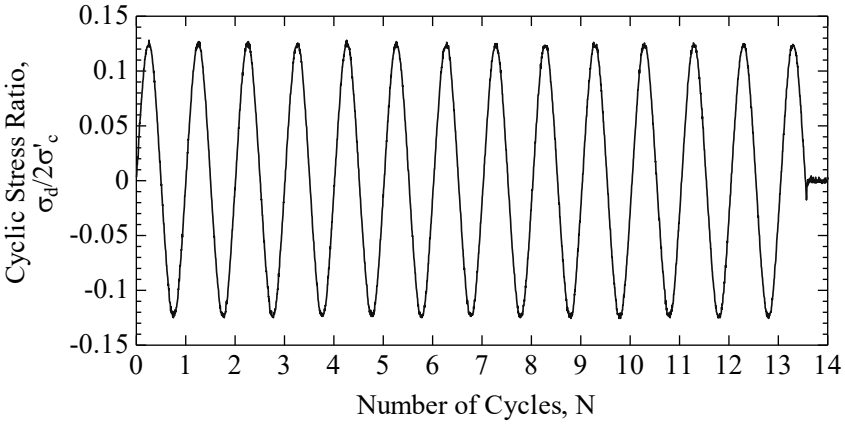
Cyclic Stress Ratio,
$\sigma_d/2\sigma'_c$
0.15
0.1
0.05
0
-0.05
-0.1
-0.15
0 1 2 3 4 5 6 7 8 9 10 11 12 13 14
Number of Cycles, N

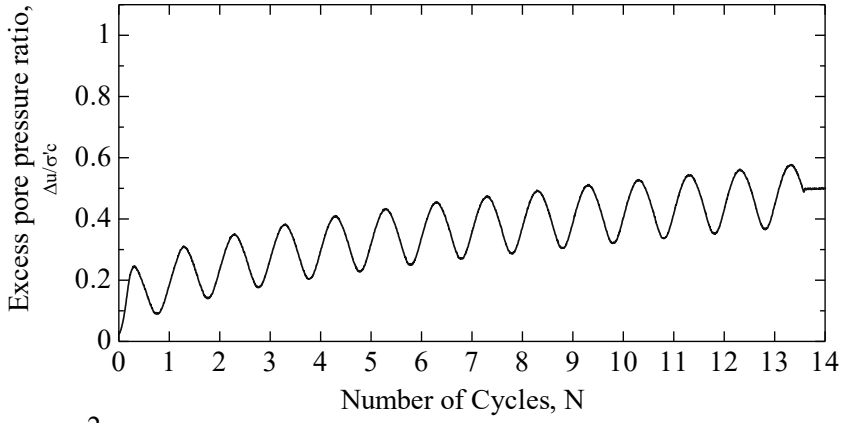
Excess pore pressure ratio,
$\Delta u/\sigma'_c$
1
0.8
0.6
0.4
0.2
0
0 1 2 3 4 5 6 7 8 9 10 11 12 13 14
Number of Cycles, N

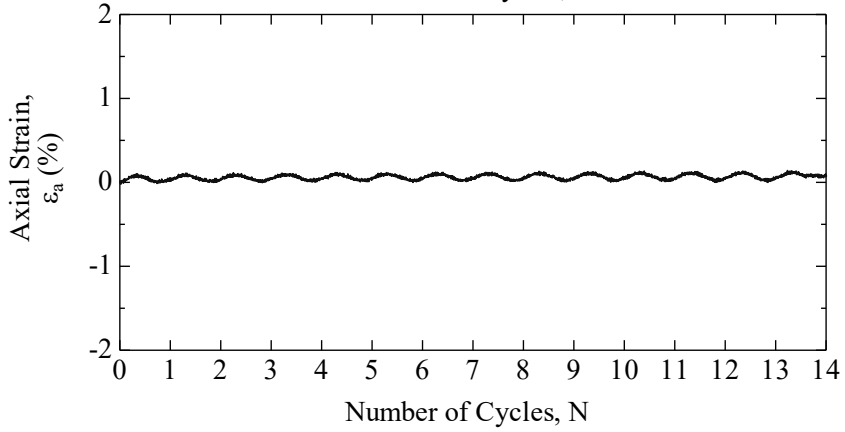
Axial Strain,
ε_a (%)
2
1
0
-1
-2
0 1 2 3 4 5 6 7 8 9 10 11 12 13 14
Number of Cycles, N

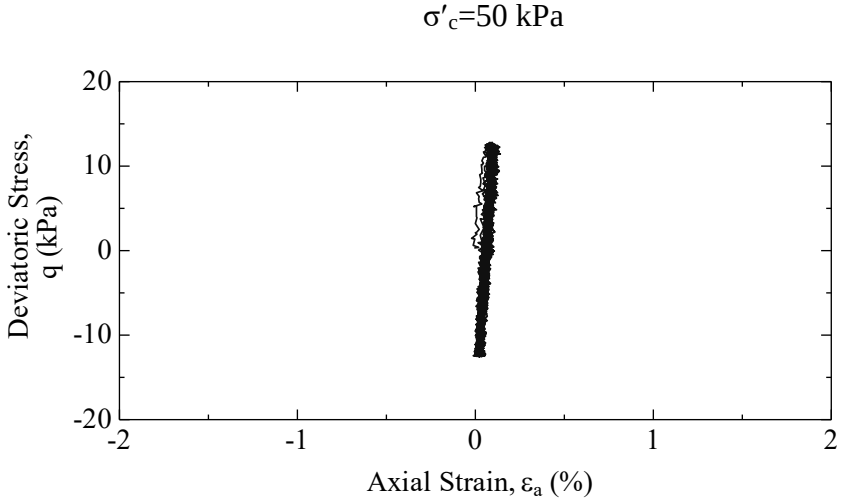
σ'_c=50 kPa
Deviatoric Stress,
q (kPa)
20
10
0
-10
-20
-2 -1 0 1 2
Axial Strain, ε_a (%)

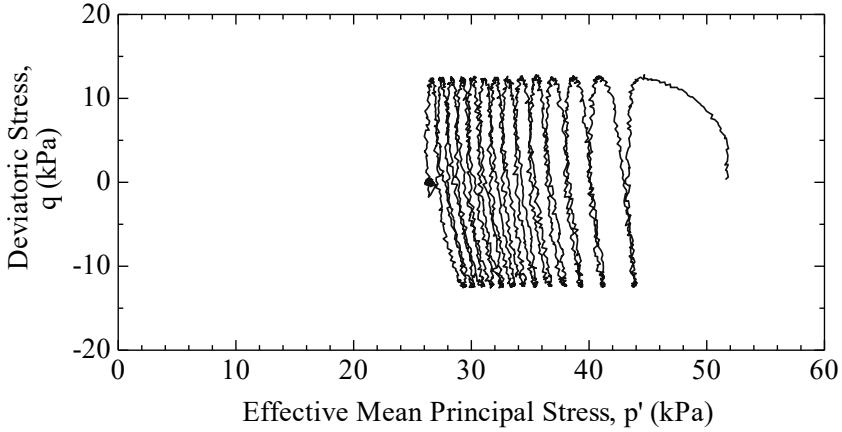
Deviatoric Stress,
q (kPa)
20
10
0
-10
-20
0 10 20 30 40 50 60
Effective Mean Principal Stress, p' (kPa)

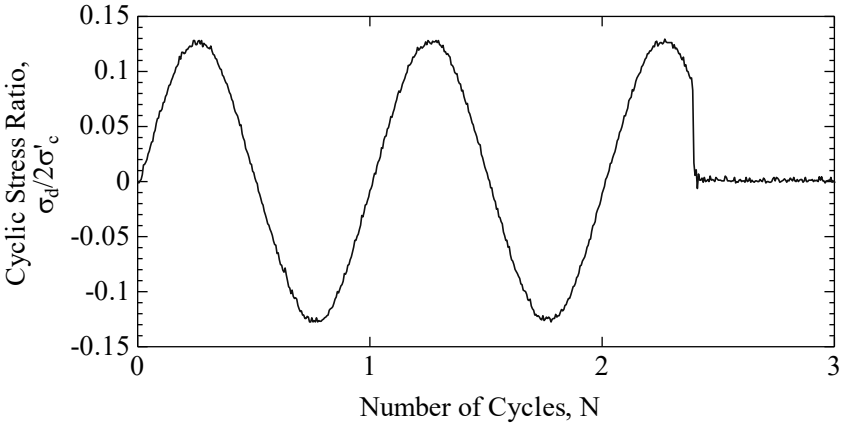
Cyclic Stress Ratio,
$\sigma_d/2\sigma'_c$
0.15
0.1
0.05
0
-0.05
-0.1
-0.15
0
1
2
3
Number of Cycles, N

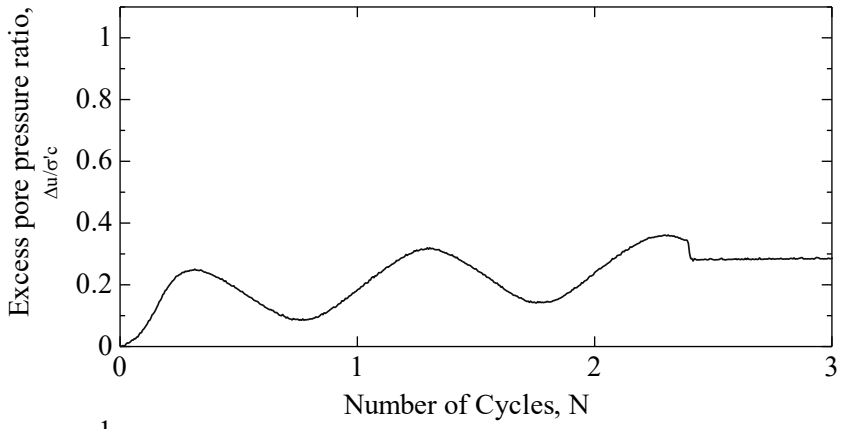
Excess pore pressure ratio,
$\Delta u/\sigma'_c$
1
0.8
0.6
0.4
0.2
0
0
1
2
3
Number of Cycles, N

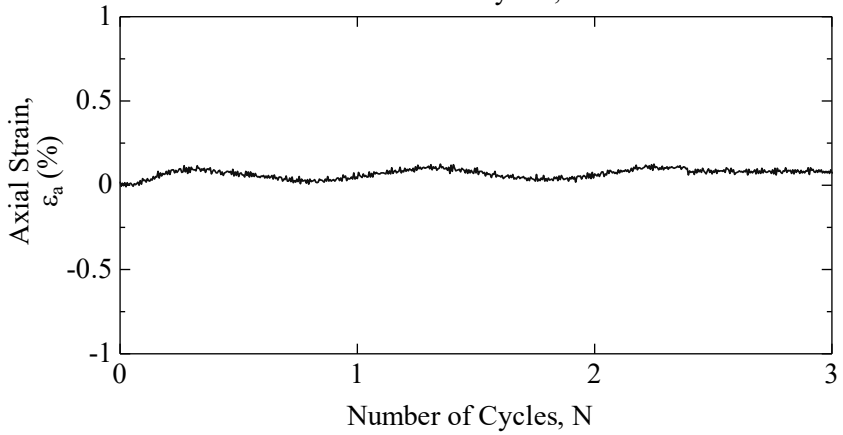
Axial Strain,
ε_a (%)
1
0.5
0
-0.5
-1
0
1
2
3
Number of Cycles, N

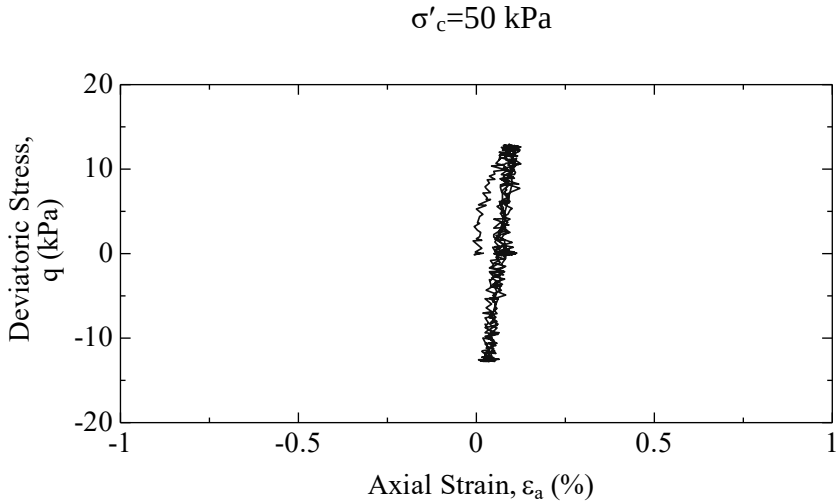
σ'_c=50 kPa
Deviatoric Stress,
q (kPa)
20
10
0
-10
-20
-1
-0.5
0
0.5
1
Axial Strain, ε_a (%)

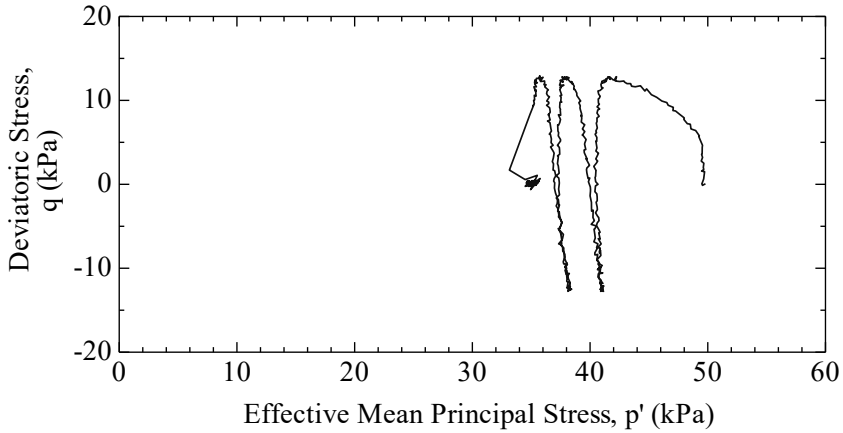
Deviatoric Stress,
q (kPa)
20
10
0
-10
-20
0
10
20
30
40
50
60
Effective Mean Principal Stress, p' (kPa)

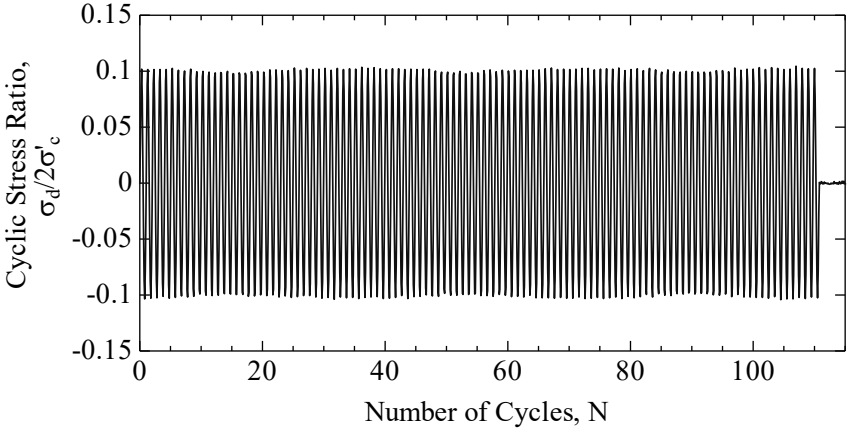

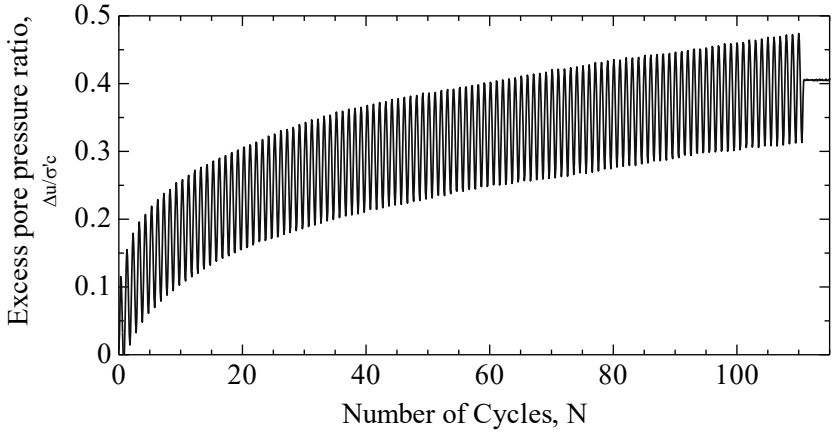

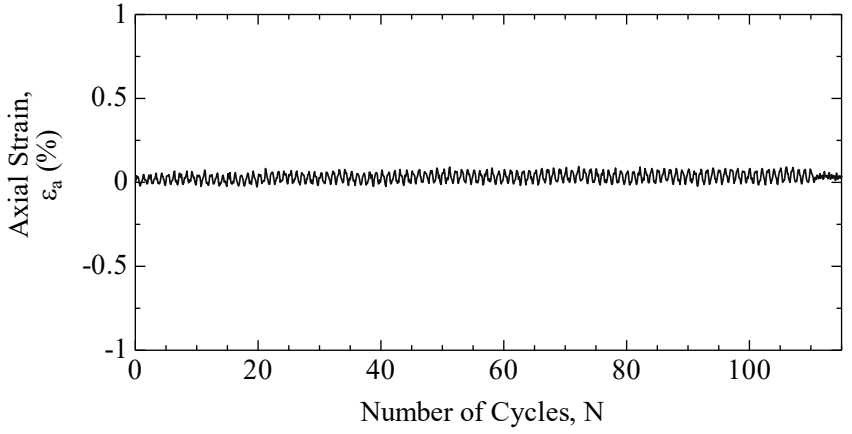

σ'_c=100 kPa

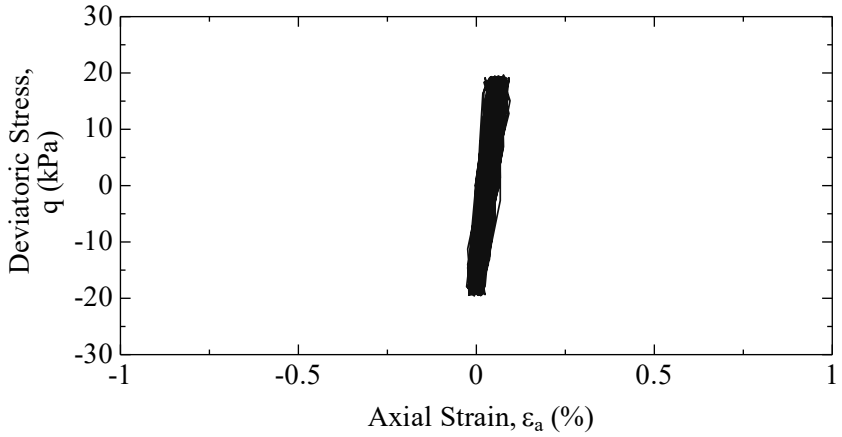

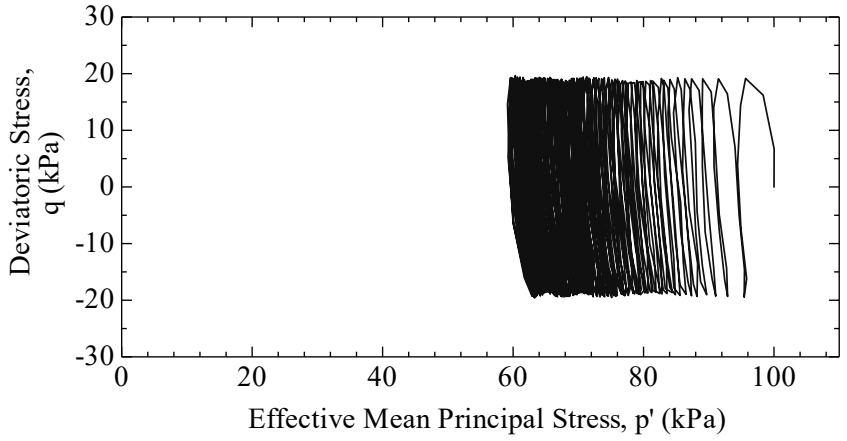

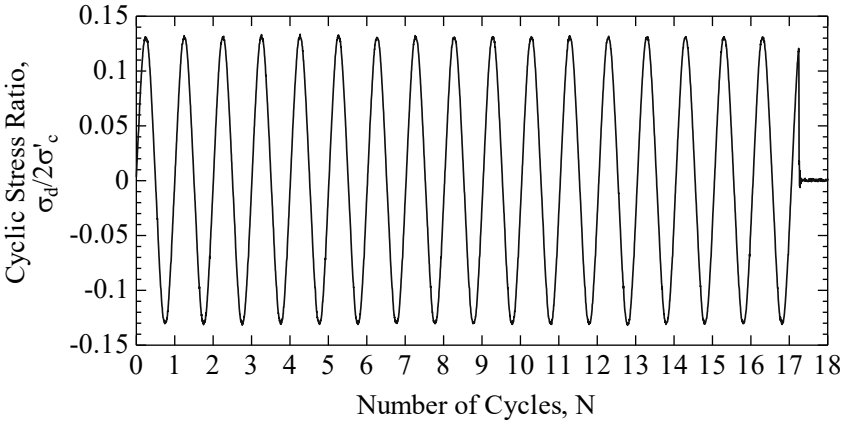

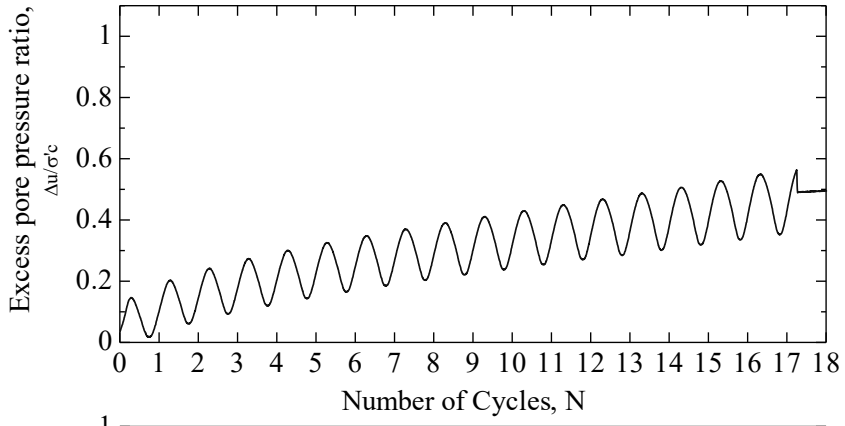

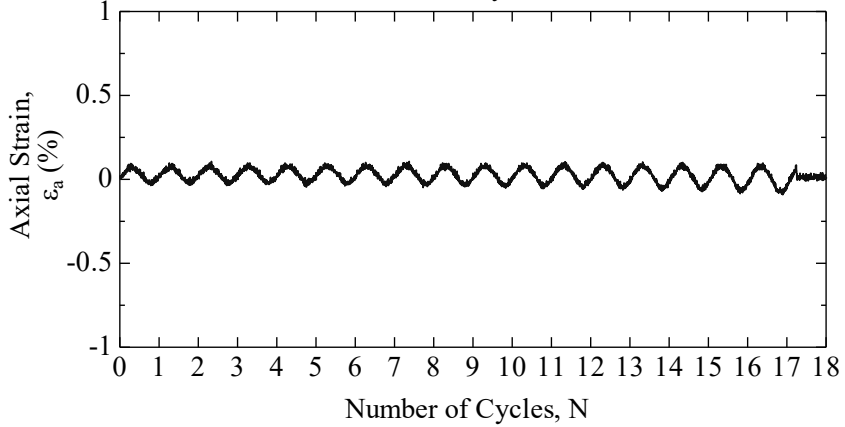

σ'_c=100 kPa

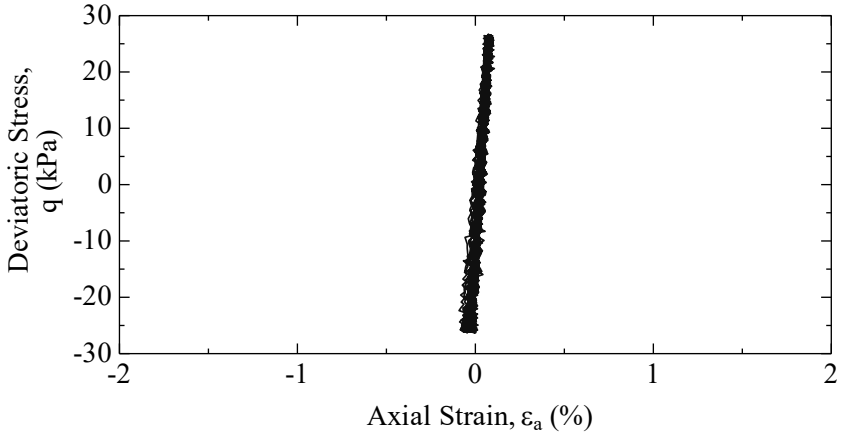

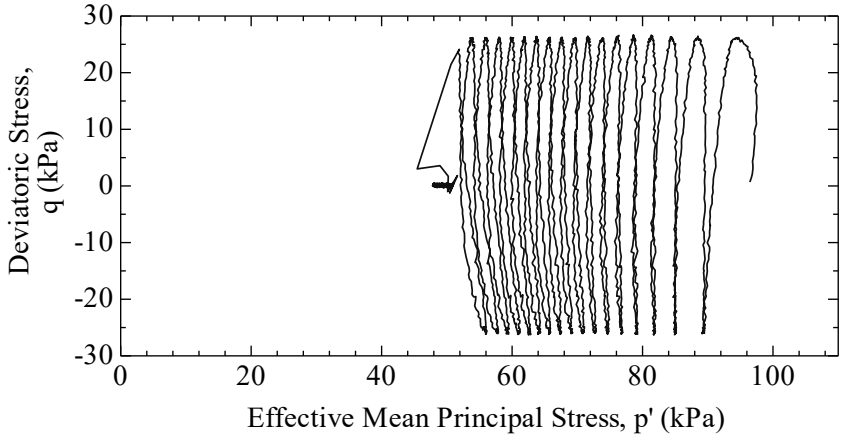

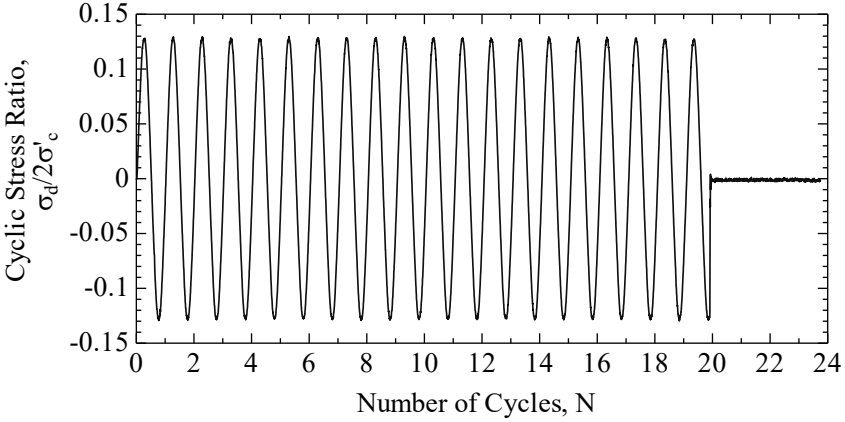

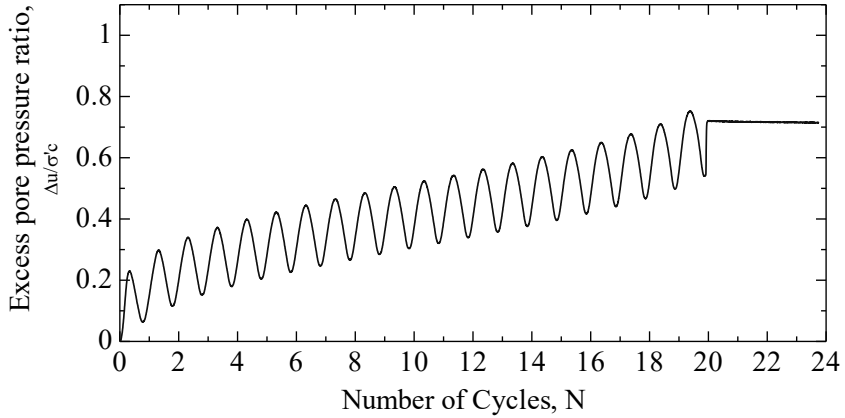

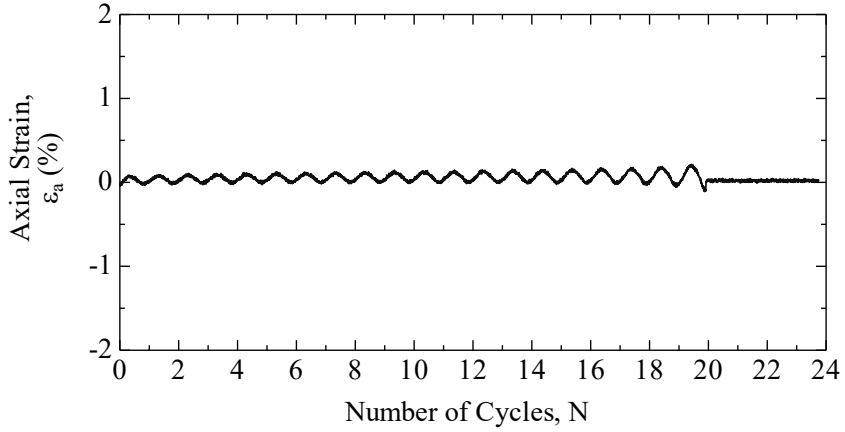

σ'_c=100 kPa

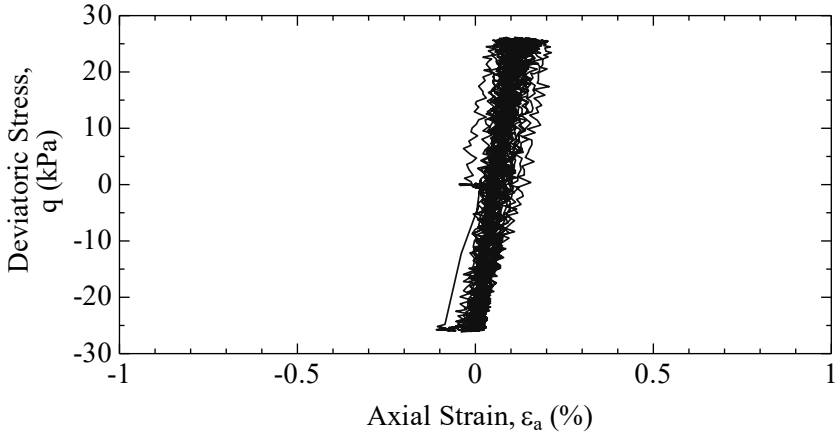

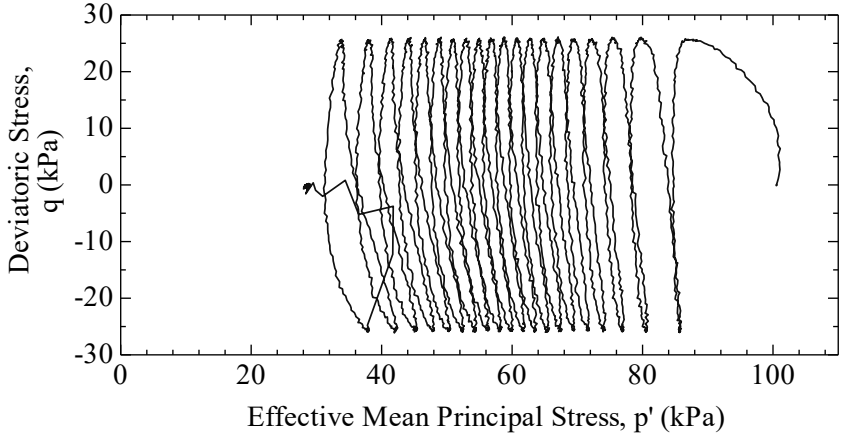

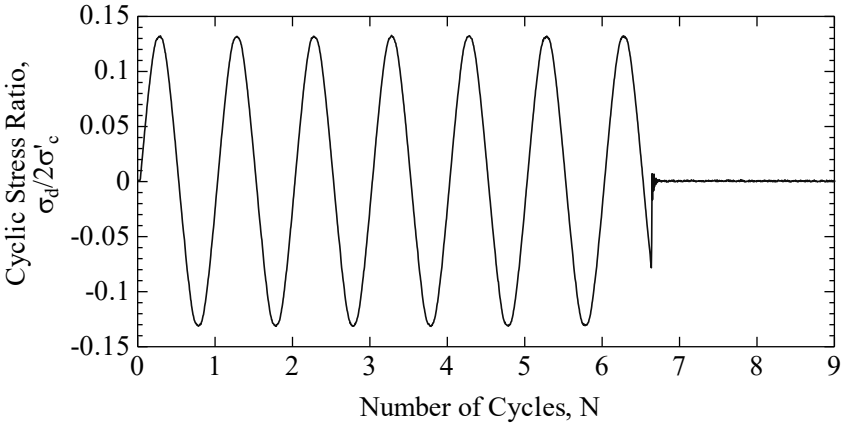
Cyclic Stress Ratio,
$\sigma_d/2\sigma'_c$
0.15
0.1
0.05
0
-0.05
-0.1
-0.15
0 1 2 3 4 5 6 7 8 9
Number of Cycles, N

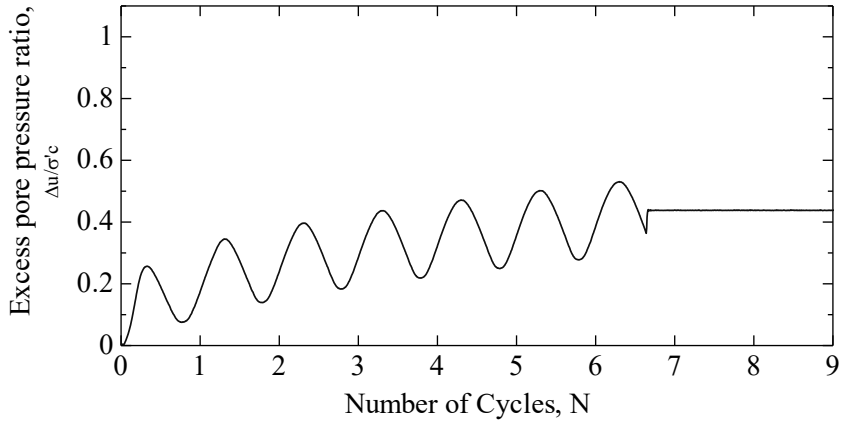
Excess pore pressure ratio,
$\Delta u/\sigma'_c$
1
0.8
0.6
0.4
0.2
0
0 1 2 3 4 5 6 7 8 9
Number of Cycles, N

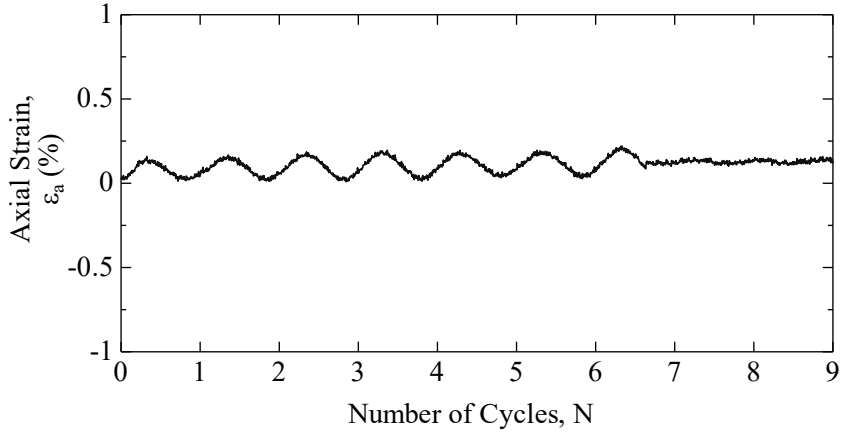
Axial Strain,
ε_a (%)
1
0.5
0
-0.5
-1
0 1 2 3 4 5 6 7 8 9
Number of Cycles, N

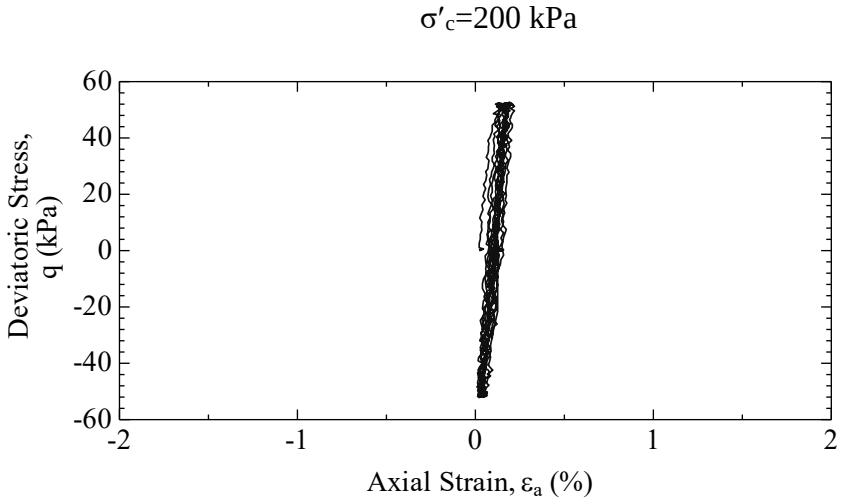
σ'_c=200 kPa
Deviatoric Stress,
q (kPa)
60
40
20
0
-20
-40
-60
-2 -1 0 1 2
Axial Strain, ε_a (%)

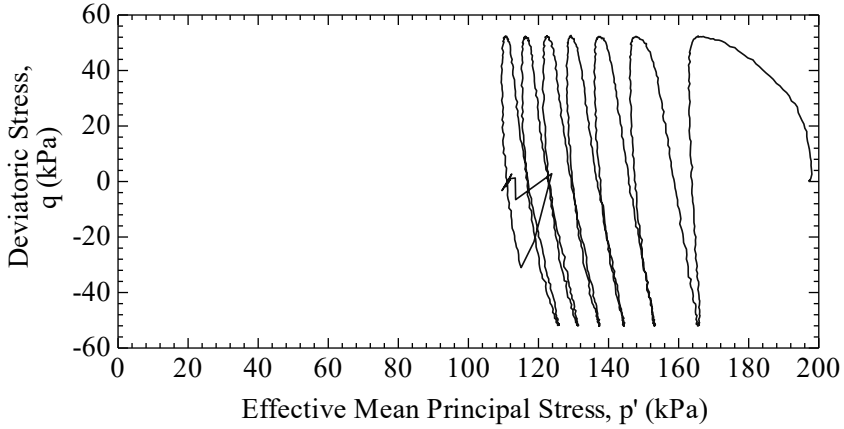
Deviatoric Stress,
q (kPa)
60
40
20
0
-20
-40
-60
0 20 40 60 80 100 120 140 160 180 200
Effective Mean Principal Stress, p' (kPa)

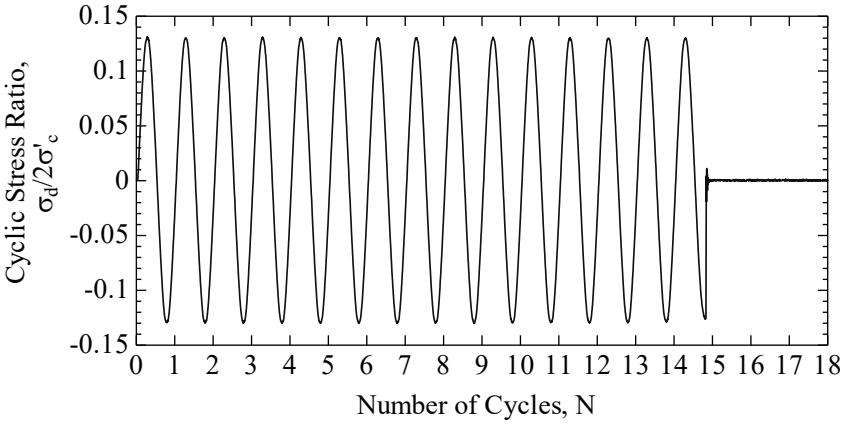

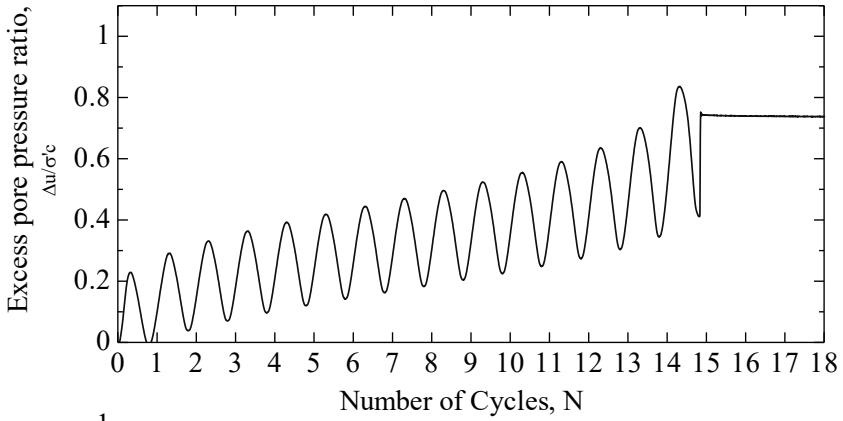

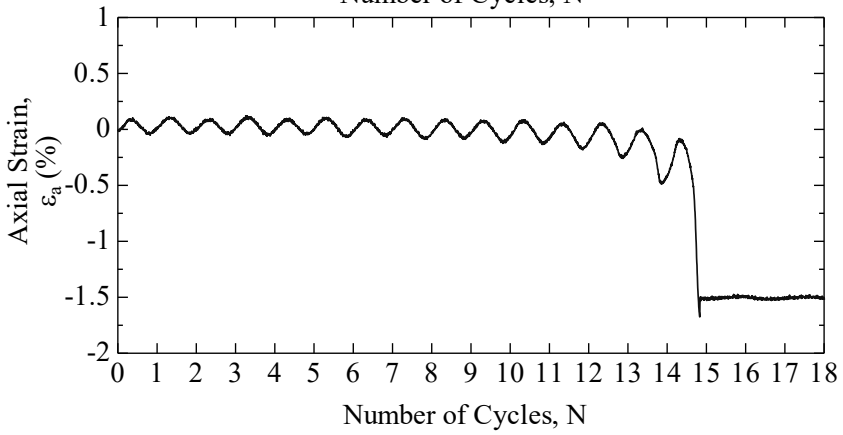

σ'_c=200 kPa

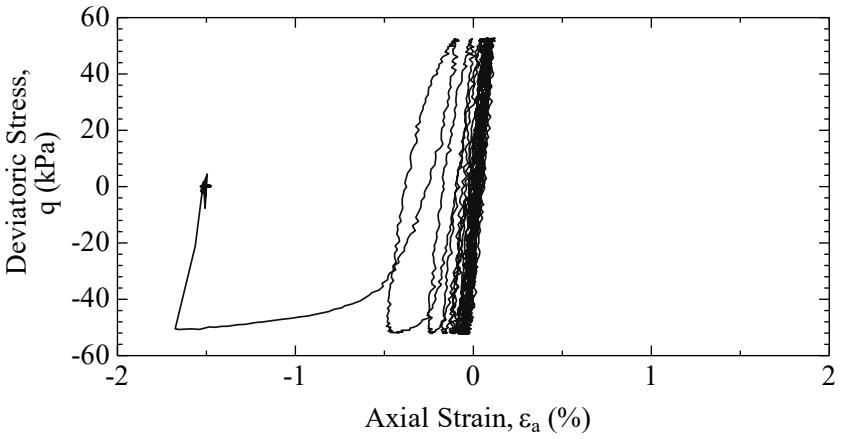

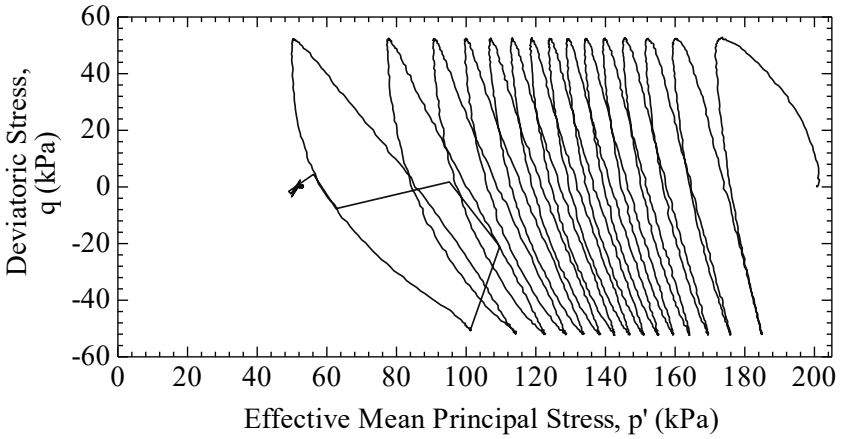

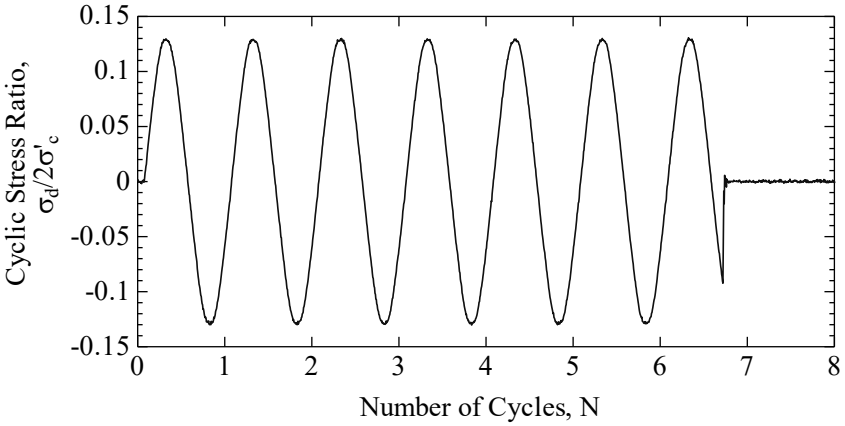
Cyclic Stress Ratio,
$\sigma_d/2\sigma'_c$
0.15
0.1
0.05
0
-0.05
-0.1
-0.15
0
1
2
3
4
5
6
7
8
Number of Cycles, N

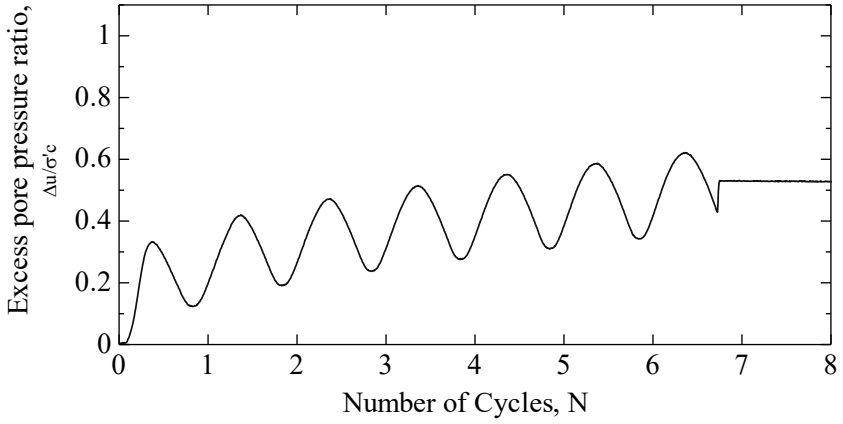
Excess pore pressure ratio,
$\Delta u/\sigma'_c$
1
0.8
0.6
0.4
0.2
0
0
1
2
3
4
5
6
7
8
Number of Cycles, N

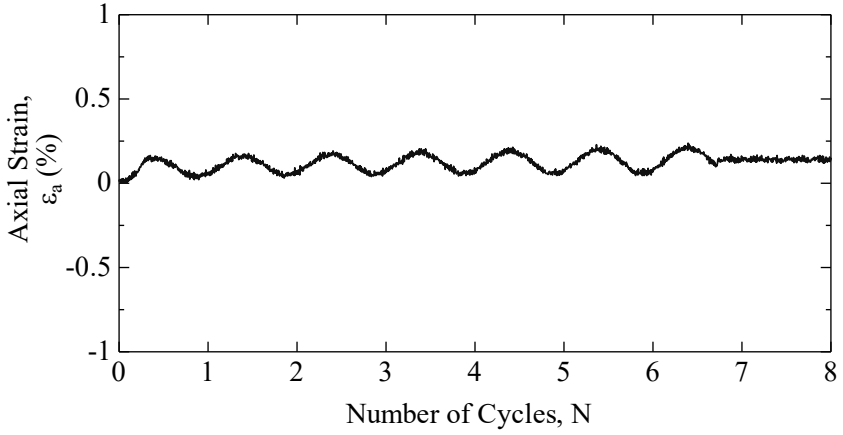
Axial Strain,
ε_a (%)
1
0.5
0
-0.5
-1
0
1
2
3
4
5
6
7
8
Number of Cycles, N

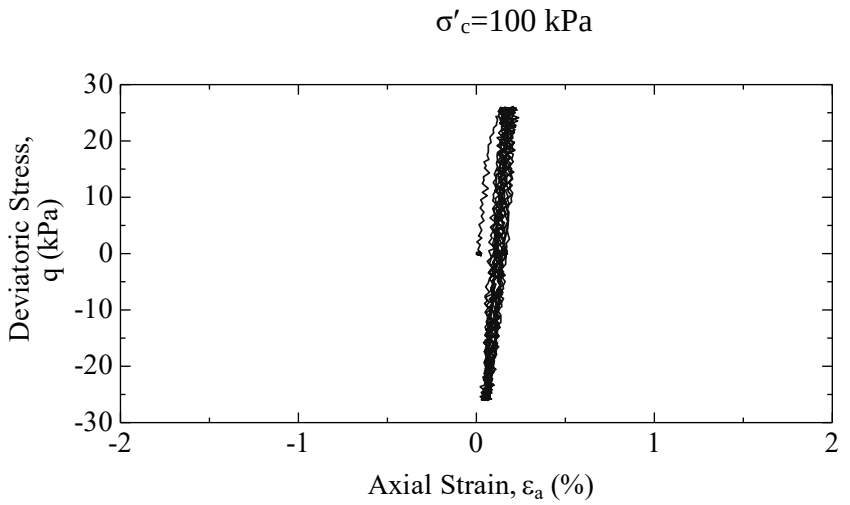
σ'_c=100 kPa
Deviatoric Stress,
q (kPa)
30
20
10
0
-10
-20
-30
-2
-1
0
1
2
Axial Strain, ε_a (%)

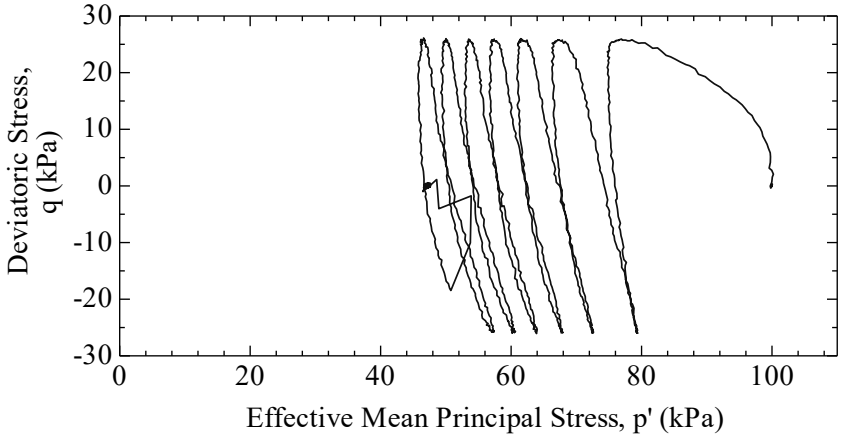
Deviatoric Stress,
q (kPa)
30
20
10
0
-10
-20
-30
0
20
40
60
80
100
Effective Mean Principal Stress, p' (kPa)

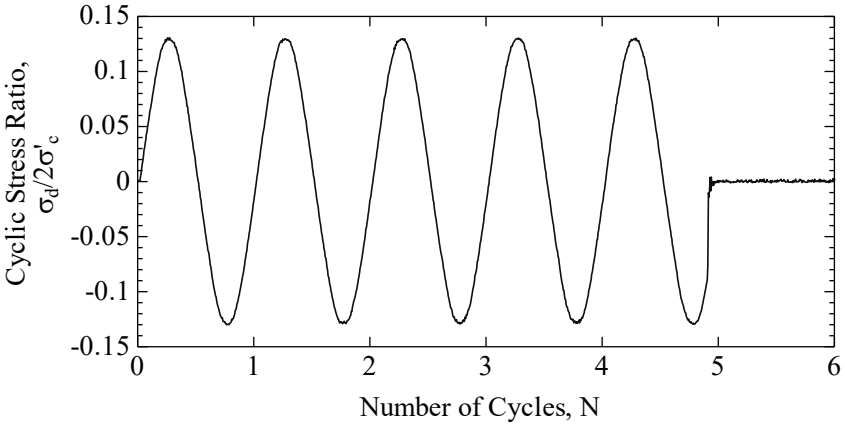

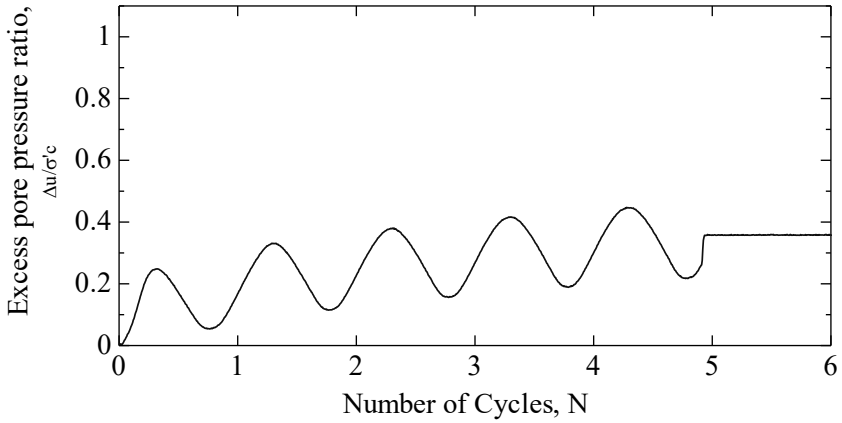

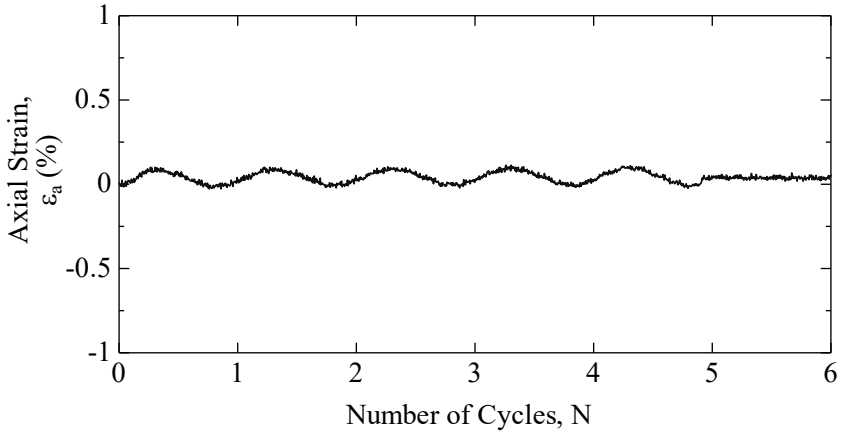

σ'_c=100 kPa

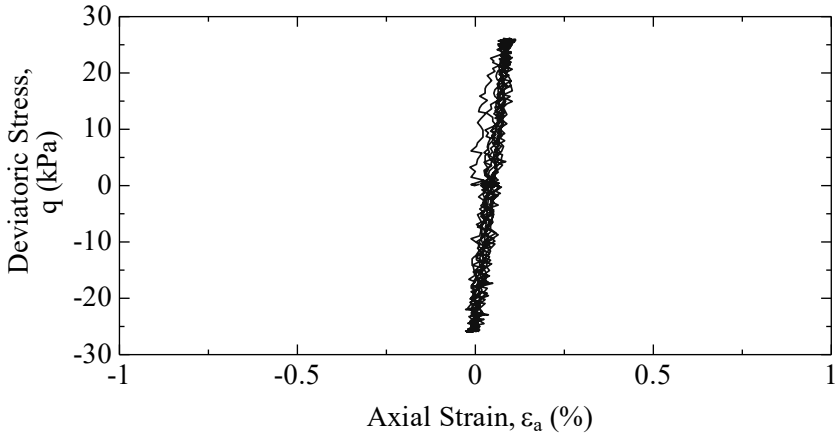

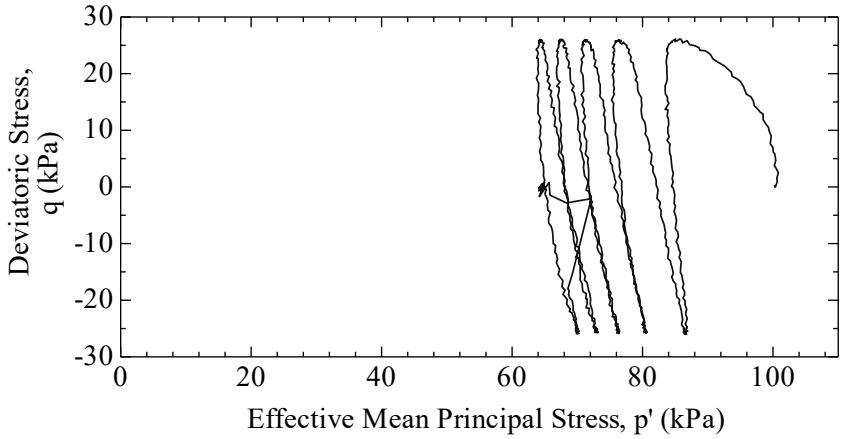

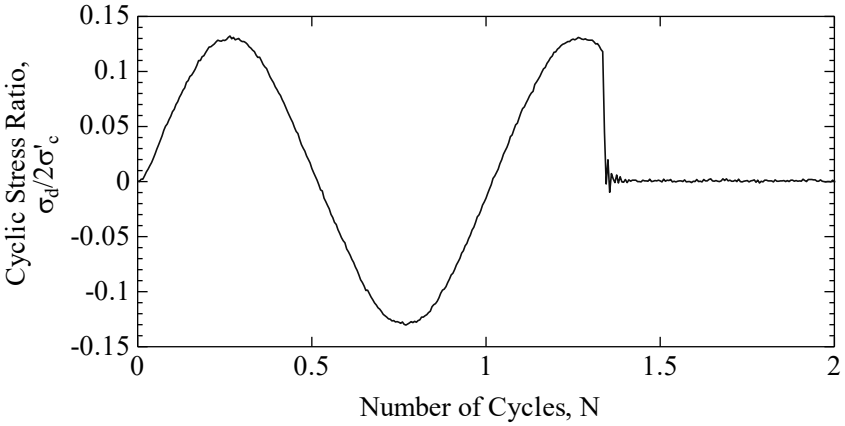
Cyclic Stress Ratio,
σd/2σ'c
0.15
0.1
0.05
0
-0.05
-0.1
-0.15
0
0.5
1
1.5
2
Number of Cycles, N

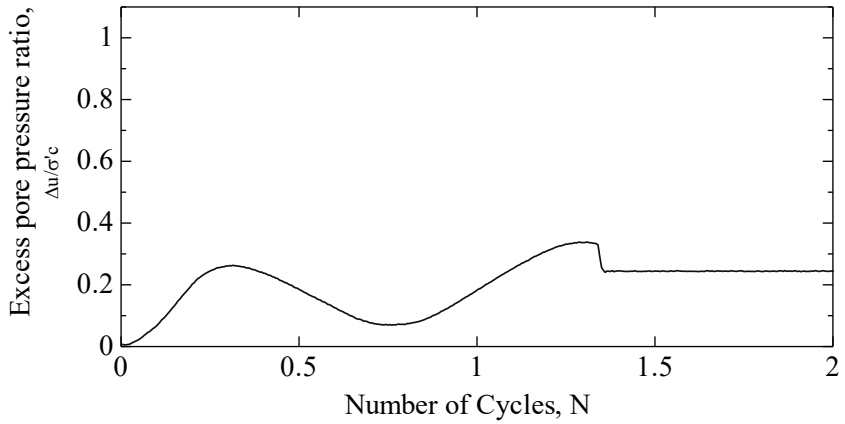
Excess pore pressure ratio,
Δu/σ'c
1
0.8
0.6
0.4
0.2
0
0
0.5
1
1.5
2
Number of Cycles, N

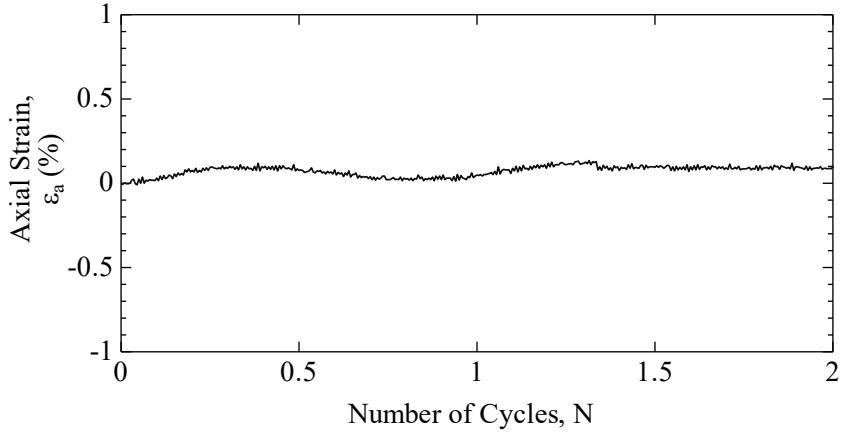
Axial Strain,
εa (%)
1
0.5
0
-0.5
-1
0
0.5
1
1.5
2
Number of Cycles, N

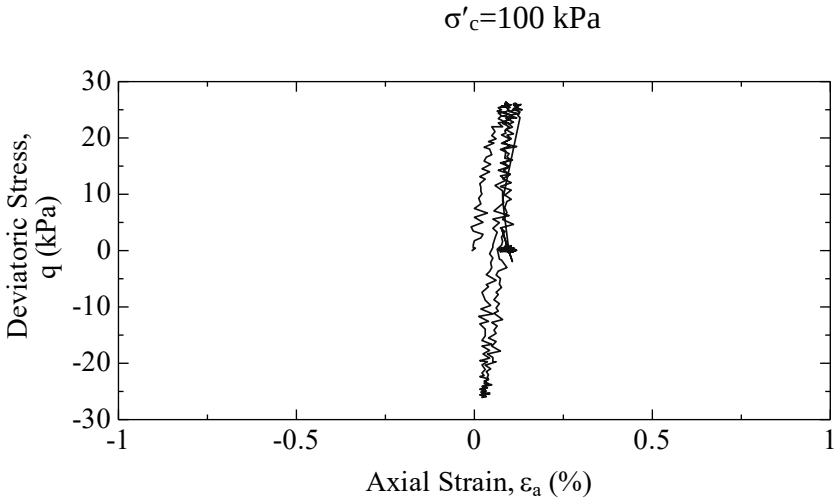
σ'c=100 kPa
Deviatoric Stress,
q (kPa)
30
20
10
0
-10
-20
-30
-1
-0.5
0
0.5
1
Axial Strain, εa (%)

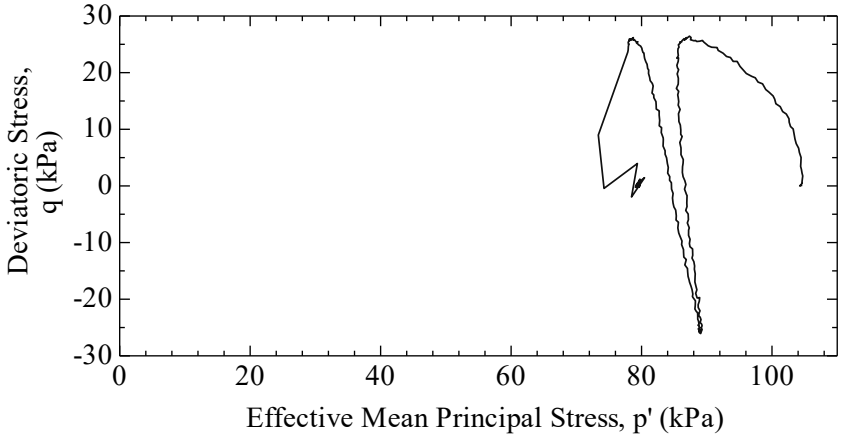
Deviatoric Stress,
q (kPa)
30
20
10
0
-10
-20
-30
0
20
40
60
80
100
Effective Mean Principal Stress, p' (kPa)

Appendix-B

Record of Centrifuge Tests

Model	Relative Density *Dr* (%)	Coeff. Permeability*		Pore fluid viscosity ν (cSt)	Drain diameter d_w (m)	Drain spacing *b* (m)	Groundwater Level GL –(m)
		k_s (m/s)	k_w (m/s)				
Benchmark model							
BM	61.7	1.9×10^{-4}	-	1	-	-	0
GD-BM	59.3	1.9×10^{-4}	8.0×10^{-1}	1	1.6	4.8	0
Smaller drain diameter model							
GD-SD	57.2	1.9×10^{-4}	8.0×10^{-1}	1	0.8	2.4	0
Lower permeability model							
V	63.2	4.8×10^{-6}	-	40	-	-	0
GD-V	57.3	4.8×10^{-6}	2.0×10^{-2}	40	1.6	4.8	0
Lower groundwater table							
WL	57.0	1.9×10^{-4}	-	1	-	-	3.6
GD-WL	61.0	1.9×10^{-4}	8.0×10^{-1}	1	0.8	2.4	4.0
Drains covered with plastic sheet							
GD-C	63.3	1.9×10^{-4}	8.0×10^{-1}	40	1.6, 1.2, 0.8	-	0
Different diameter of drain per depth							
GD-LD	60.7	1.9×10^{-4}	8.0×10^{-1}	40	1.2, 0.8	-	0

Input Acceleration

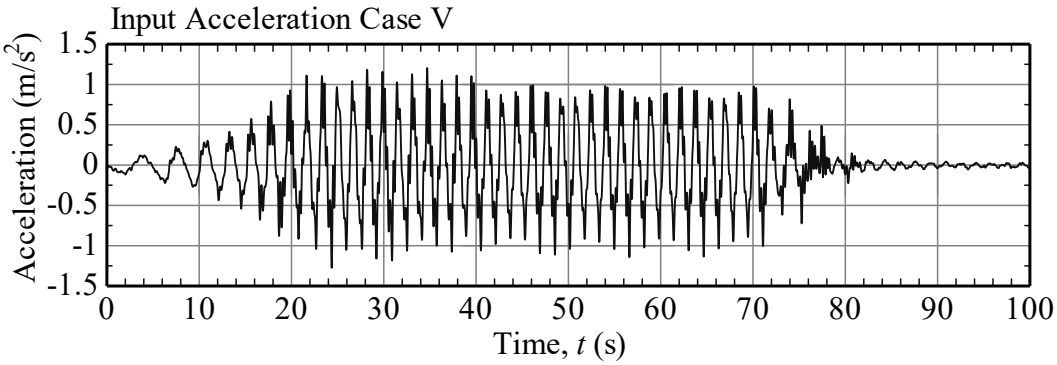

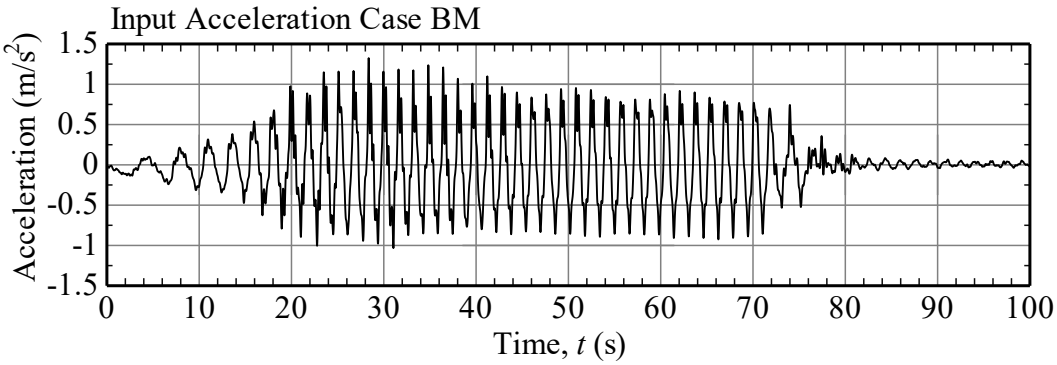

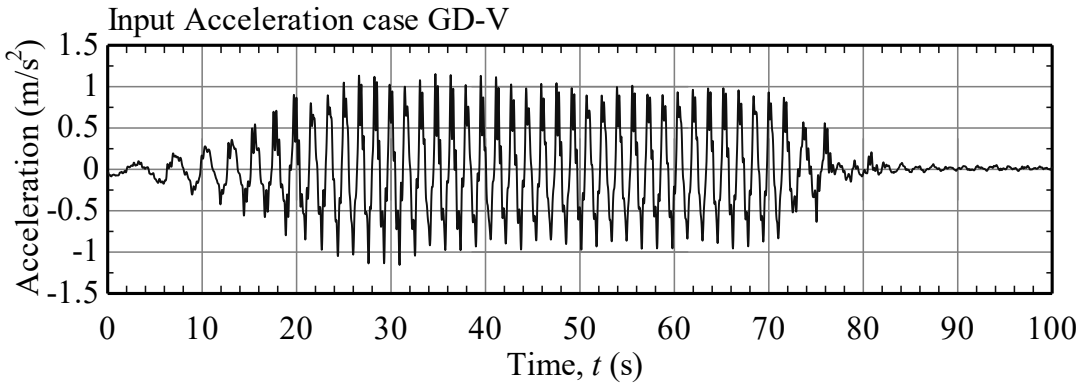

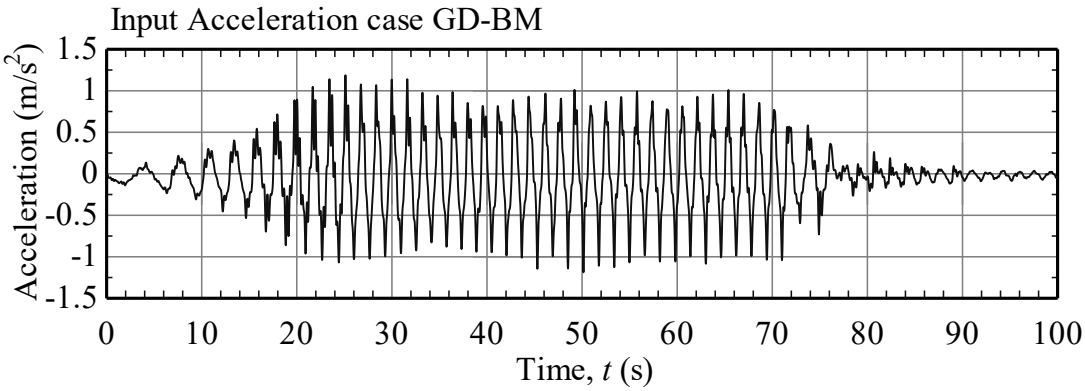

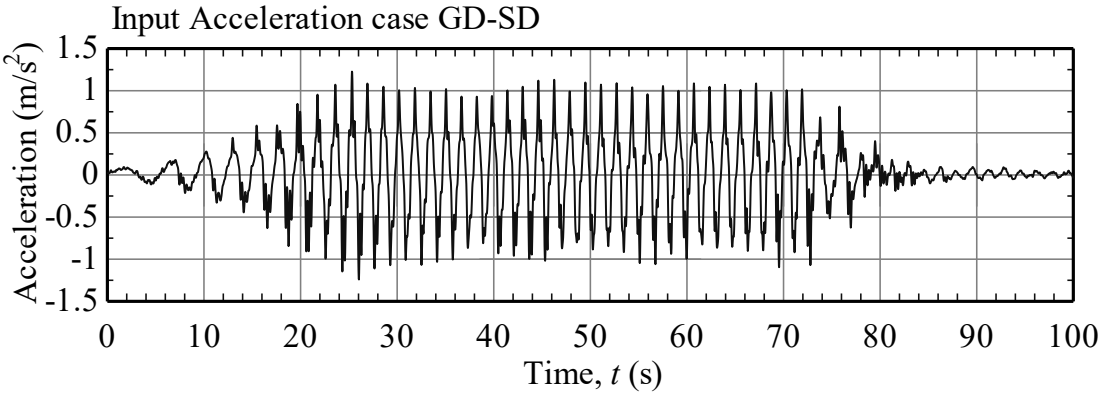
Input Acceleration case GD-SD
Acceleration (m/s^2)
1.5
1
0.5
0
-0.5
-1
-1.5
0
10
20
30
40
50
60
70
80
90
100
Time, t (s)

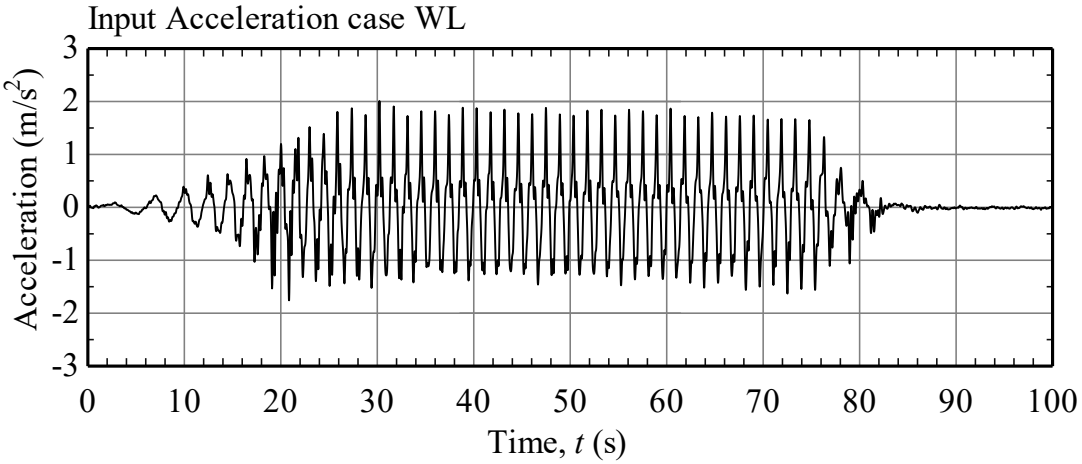
Input Acceleration case WL
Acceleration (m/s^2)
3
2
1
0
-1
-2
-3
0
10
20
30
40
50
60
70
80
90
100
Time, t (s)

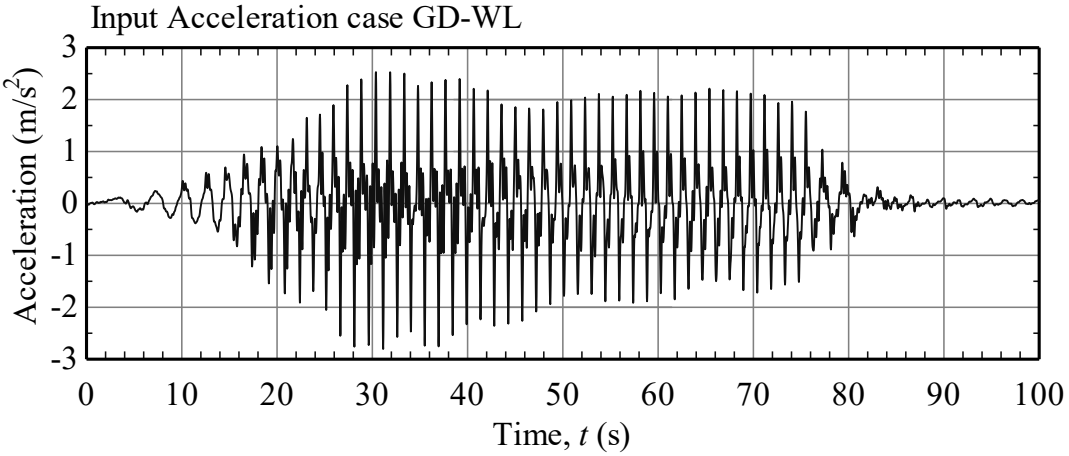
Input Acceleration case GD-WL
Acceleration (m/s^2)
3
2
1
0
-1
-2
-3
0
10
20
30
40
50
60
70
80
90
100
Time, t (s)

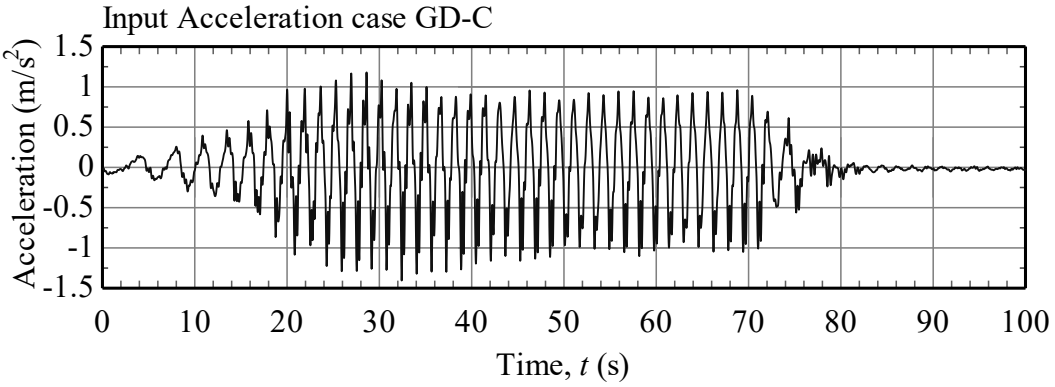
Input Acceleration case GD-C
Acceleration (m/s^2)
1.5
1
0.5
0
-0.5
-1
-1.5
0
10
20
30
40
50
60
70
80
90
100
Time, t (s)

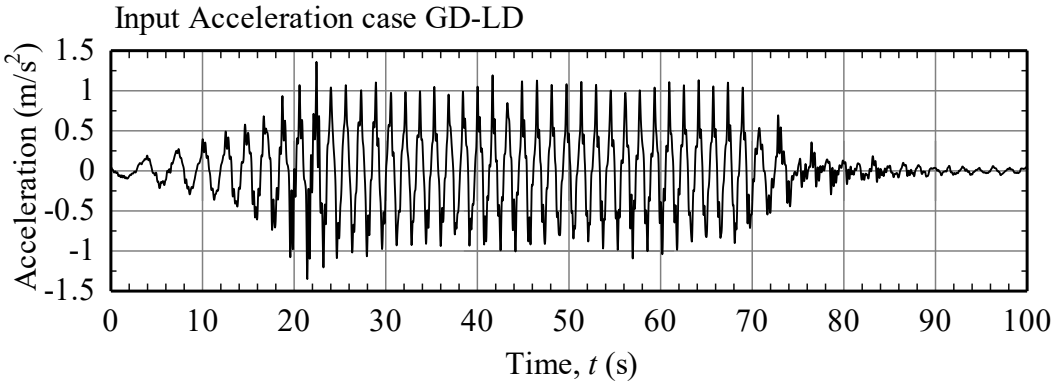
Input Acceleration case GD-LD
Acceleration (m/s^2)
1.5
1
0.5
0
-0.5
-1
-1.5
0
10
20
30
40
50
60
70
80
90
100
Time, t (s)